Surface Modification and Charge Transfer Studies at Silicon and Gallium Arsenide Interfaces

Thesis by

Ashish Bansal

In Partial Fulfillment of the Requirements for

the Degree of Doctor of Philosophy

California Institute of Technology

Pasadena, California

1997

(submitted March 31, 1997)

To My Father and Mother

Acknowledgements

Its been a long journey to the degree, and along the way I have had the pleasure of knowing and working with a lot of smart and brilliant people who I wish to acknowledge before I complete this journey.

First and foremost, I want to thank my advisor Prof. Nathan Lewis, for not only being instrumental in bringing a bewildered IIT undergrad to Caltech, but also for his guidance and support, throughout my stay here. I have always admired his attitude towards science, of proving things "beyond the shadow of doubt" (or as he likes to put it - "driving that last nail in the coffin"), and although this approach to scientific integrity can make for some tough times for a graduate student, I can say by personal experience that the end results are certainly more satisfying.

The Lewis group, past and present, deserves my sincerest gratitude for making significant contributions to my work and for helping me survive graduate school in a sane manner. Ming, Bruce and Amit taught me the tricks of this trade, that have served me well. I want to thank Xiuling Li for being indirectly instrumental in leading my career down the path of surface science which later became a significant part of my graduate work. Working with Marya Lieberman were the most exciting times of my scientific life and I enjoyed every opportunity to pick her brains on matters scientific or otherwise. I am also deeply indebted to Alan Rice for always keeping the XPS machine up and running. Without his help I would still be doing experiments in the lab. The assistance of Sang Yi and Prof. Henry Weinberg in performing many of the experiments described in this thesis is also sincerely acknowledged.

Life outside chemistry would have been very different, if it were not for the International Students' Office. I was fortunate to be a part of the first ISP group formed under the able guidance of chief Parandeh Kia and I learnt A LOT from this opportunity.

Through ISP, I met my "deer" friends: Wayez (Commander), Jean-Yves (Johnny), Mario, Luis, Marianne, Fabienne, Bahadir and others, who introduced me to the wild trips to Grand Canyon, Zion, Bryce and to the concept of repeated "all you can eat" dinners. I want to especially thank Bahadir and Fabienne for being my best friends and sounding boards during some of the very tough times in the graduate school.

Away from home, I want to thank the Wagner family - Ken, Joan, Lon, Lynn and Dan, for opening their hearts, including me in their Thanksgiving dinners and for being my "family in America." I also want to thank my roommates - Neilay, Mohit and Siddhartha for providing me the homely Indian atmosphere and great Indian food, away from home.

Last, but not the least, my sincerest gratitude are due to my family - my wife, my parents, my grandparents and all my family in India, for keeping faith in me and providing me with all the moral and emotional support that were so crucial during the graduate school. Papa, Ma, this work is dedicated to you for being my pillars of strength. Finally, to Rachna, thanks for all your support and sacrifice during my last two years at school. I wouldn't have made it without you.

Abstract

The thesis describes some chemical modifications of Si and GaAs surfaces, as a means of gaining control over the physical, chemical and electrical properties of these surface and of the interfaces formed from these surfaces.

The Current-voltage properties of n-GaAs photoanodes were evaluated in KOH-$Se^{-/2-}$(aq), CH_3CN-ferrocene $(Fc)^{+/0}$, and CH_3CN-methyl viologen $(MV)^{2+/+}$ solutions. Chemisorption of transition-metal ions (Rh^{III}, Rh^{III}, Co^{III}, Os^{III}) onto GaAs has been shown previously to effect improved photoanode behavior for n-GaAs/KOH-$Se^{-/2-}$(aq) contacts, but it is not clear whether the chemisorbed metal forms a buried semiconductor/metal (Schottky) junction or results in a "hybrid" semiconductor/metal/liquid contact. Metal ion treated n-GaAs photoanodes displayed different open circuit voltages in contact with each electrolyte solution investigated. The role of the chemisorbed metal in the n-GaAs/KOH-$Se^{-/2-}$(aq) system is, therefore, best described as catalyzing interfacial charge transfer at the semiconductor/liquid interface, as opposed to forming a semiconductor/metal or semiconductor/insulator/metal contact.

The ability to modify Si surface without partial oxidation or formation of electrical defects is potentially important. However, little is known about the chemistry of these surfaces under ambient temperature and pressure. A two-step halogenation/alkylation route to chemical functionalization of Si(111) surface is described, that allows covalent attachment of alkyl functionalities without concomitant oxidation of the silicon surface. In the first step, a hydrogen terminated silicon surface is chlorinated to obtain a chlorine terminated silicon surface. In the second step, the chlorinated surface is reacted with alkyl lithium or alkyl Grignard to obtain an alkyl terminated surface. The surface of silicon is extensively analyzed using a number of techniques such as XPS, HREELS, IRS, AES, TPD etc. The alkyl terminated surfaces are more resistant to oxidation in air and in contact with wet chemical environments than the H-terminated surface.

Current-voltage and capacitance-voltage measurements of the alkyl terminated surfaces in CH_3OH-$Me_2Fc^{+/0}$ indicate that the electrical properties of these surfaces are very similar to those of a H-terminated surface. The alkyl overlayers provide a small resistance to charge transfer across the Si/liquid interface but do not shift the band edges or induce additional surface recombination. I-V characteristics of n-Si/alkyl/Au MIS devices indicate that these junctions behave largely like n-Si/Au Schottky junctions. The efficacy of alkyl overlayers in preventing photooxidation and photocorrosion of n-silicon surfaces was measured in contact with $Fe(CN)_6^{3-/4-}$(aq) and with CH_3OH-$Me_2Fc^{+/0}$ containing known amounts of water. The alkyl terminated surfaces consistently show better I-V characteristics and lower oxidation than the H-terminated surface, indicating that stability to oxidation had been achieved without any significant compromise in the electrical quality of the silicon surface.

Table of Contents

List of Figures

Chapter 3

Chapter 4

List of Tables

Chapter 1

Introduction

"Today...I propose to tell you of a real two-dimensional world in which phenomena occur that are analogous to those described in 'Flatland.' I plan to tell you about the behavior of molecules and atoms that are held at the surface of solids....."

--- I. Langmuir, Science **1936**,*84*,379

I. INTRODUCTION

Of the three energy conversion systems known to man, for converting light energy into commercially useful forms of energy, viz fuel or electricity, semiconductor/liquid junction photoelectrochemical (PEC) cells occupy a unique position between plants (photosynthesis) and photovoltaic cells.[1] The PEC cells are similar to plants in that both can convert solar energy into stored chemical fuels. The PEC cells can also behave like photovoltaic cells when they convert sunlight directly into electricity. Furthermore the PEC cells are unique in that they can be configured to produce *both* fuel and electricity at the same time.

Figure 1 shows a typical PEC cell which consists of a working semiconductor electrode, a liquid and an inert counter electrode. The semiconductor electrode is the charge separating component of the cell and drives the current through the circuit. The liquid consists of a redox couple and an electrolyte dissolved in a solvent. The redox couple is formed from a molecule which can exist in two (usually adjacent) charged states and can undergo a reduction or an oxidation at an electrode. The redox couple is a critical component of the cell as it determines the energetics of the junction in contact with the semiconductor electrode. An electrolyte is a chemically inert molecule that is usually added to the liquid to increase its conductivity. The inert counter electrode (often Pt) forms the third component of the PEC cell and in a regenerative mode, it performs the reverse of the reaction taking place at the semiconductor electrode.

When a semiconductor electrode is brought in contact with the liquid containing the redox couple, charge transfer takes place between the semiconductor and the liquid to equilibrate the Fermi levels of the two phases. For a non-degenerately doped n-type semiconductor in contact with a liquid, where the electrochemical potential (Fermi level) of the semiconductor is more negative than the electrochemical potential of the liquid phase, electrons are transferred from the semiconductor to the liquid till the electrochemical potentials of the two phases become equal and the junction has reached an equilibrium.

Figure 1. Schematic of a regenerative photoelectrochemical cell. Electron hole pairs created in the semiconductor under illumination are separated by the electric field near the interface. The holes move to the front of the semiconductor and oxidize the reduced form of the redox couple. The electrons move to the back of the semiconductor, traverse the circuit and come out of the metal electrode to reduce to oxidized form of the redox couple

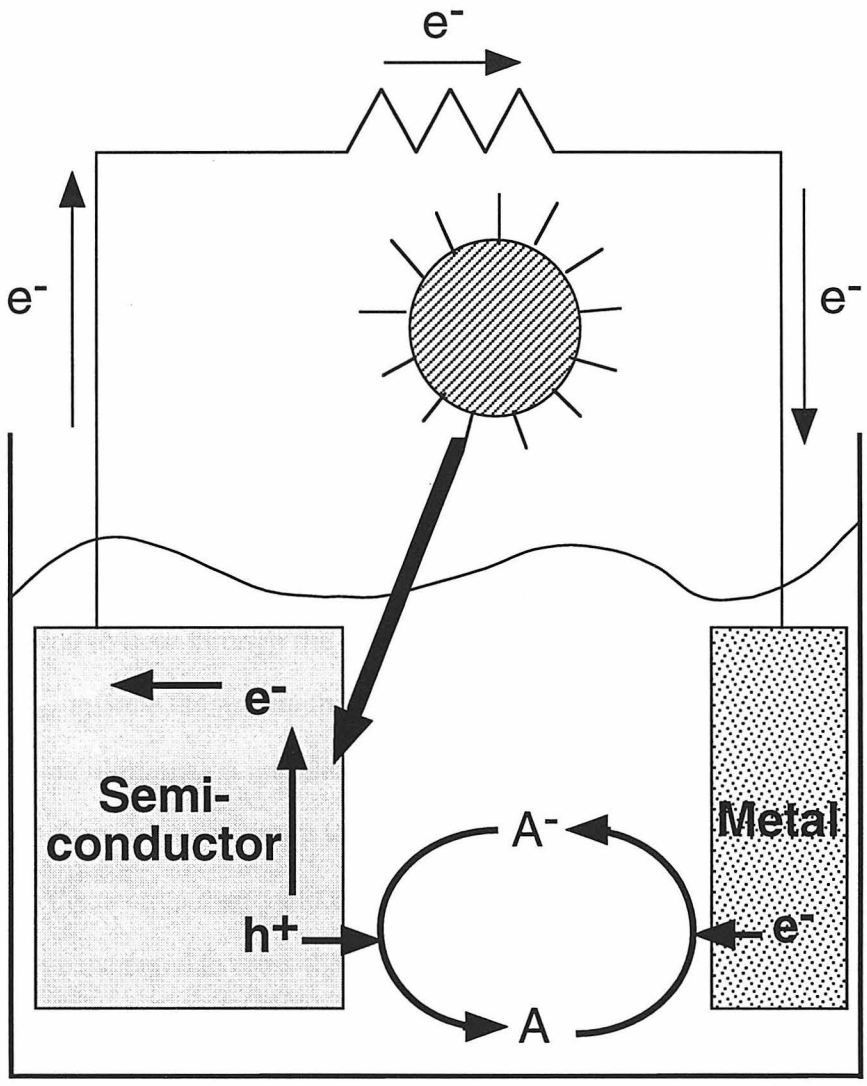
e-
e-
e-
e-
Semi-
conductor
h+
A-
A
Metal
e-

This process sets up an electric field at the interface, in the semiconductor, and is responsible for charge separation.

In a typical regenerative PEC cell shown in Figure 1, electron-hole pairs created in the semiconductor near the interface, are separated by the electric field at the interface. The minority carriers (holes for an n-type semiconductor) move towards the front of the semiconductor and transfer across the surface to oxidize A^- to A. The electrons move to the back of the semiconductor, traverse through external load, and come out of the Pt counter electrode, reducing A back to A^-. No net chemical reaction takes place in this process and the solar energy is converted only into electrical current flowing through the external circuit. When the current flowing through the external circuit is plotted as a function of the voltage developed between the two electrodes, a current-voltage (I-V) plot is obtained.

The three quantities on this I-V plot (Figure 2) that define the characteristics of the junction are the open circuit voltage (V_{oc}), the short circuit current (J_{sc}) and the fill factor (ff). The open circuit potential (V_{oc}) is the potential developed by the junction when no current is allowed to flow through the external circuit , i.e. when the system is at open circuit. The V_{oc} reflects the maximum Gibbs free energy developed by the photogenerated carriers at a given illumination intensity. J_{sc} is the short circuit current density that is observed when there is no resistance to the flow of electrons in the external circuit . J_{sc} is proportional to the net quantum yield for charge separation and is representative of minority carriers that have managed to cross the semiconductor/liquid interface without recombining. For systems with non significant series resistance, the J_{sc} is equal to the photogenerated current density (J_{ph}). Any point along the curve between V_{oc} and J_{sc}, represents the power output of the illuminated junction, given by the product of V times J. A point on that curve, that corresponds to maximum power generated by the junction, is called P_{max}. The fill factor of the I-V curve is then defined as $ff = P_{max}/(V_{oc}.J_{sc})$. The fill factor indicates the power that can be extracted from that photoelectrochemical cell as compared to power obtainable from an unattainable ideal cell having no kinetic limitations on charge transport

Figure 2. Current-voltage plot of an ideal and a non-ideal diode. The three important attributes of this curve are the open circuit voltage (V_{oc}), the short circuit current (J_{sc}) and the fill factor (ff). Sigmoid curves show lower fill factor and hence lower efficiency.

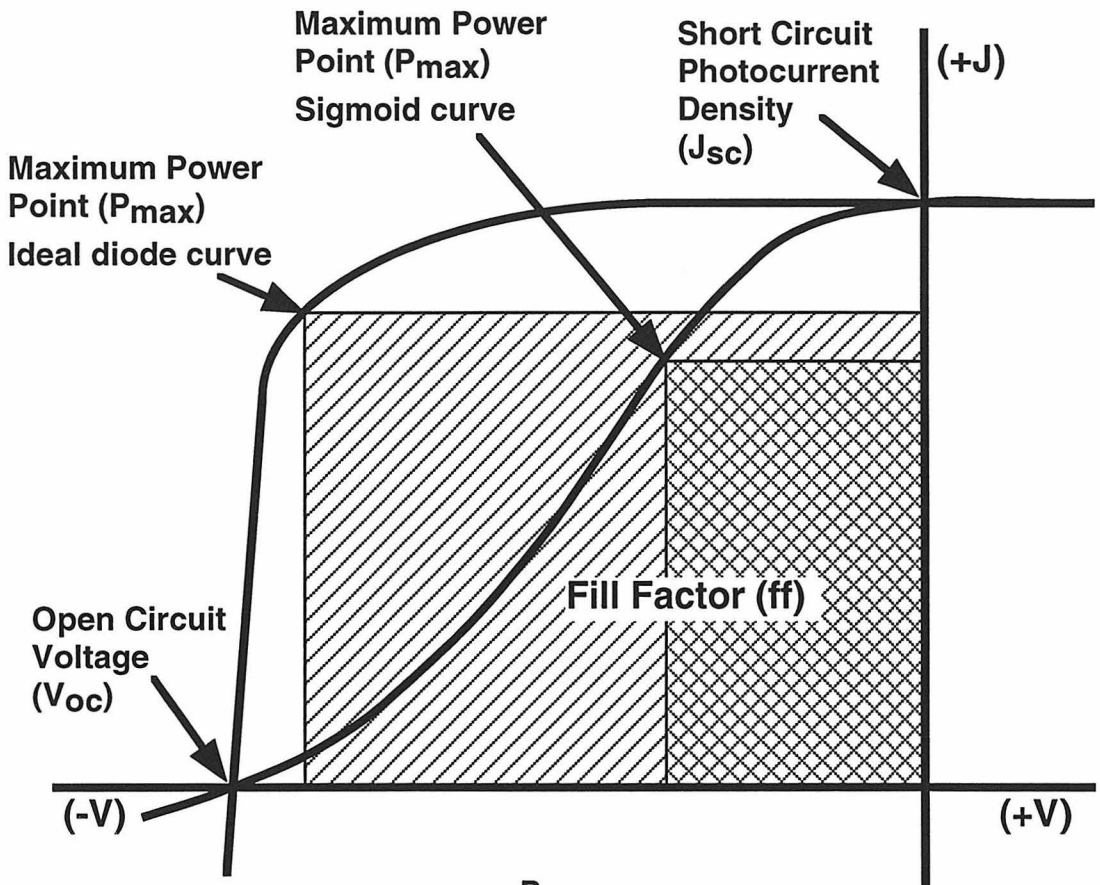

$$ff = \frac{P_{max}}{V_{oc} \cdot J_{sc}}$$

through the semiconductor, liquid or the junction. For a junction exhibiting diode behavior, V_{oc} is related to J_{sc} (=J_{ph}) by the equation

$$V_{oc} = \frac{AkT}{q} \ln\left(\frac{J_{ph}}{J_0}\right) \qquad (1)$$

where A is the diode quality factor, k is the Boltzmann constant, T is the temperature of the junction, q is the unit charge, J_{ph} is the photocurrent density, and J_o is the equilibrium exchange current density in the dark. The theoretical maximum for the fill factor given by the above equation is 0.85. For junctions where significant recombination of charge carriers exists or where there is a significant resistance to charge flow across the junction, lower fill factor are observed.[2,3] For increasing the efficiency of the PEC cell, the challenge is to simultaneously optimize all the three quantities. A significant research effort has therefore focused on finding combinations of semiconductor and redox couples that can maximise the absorption of solar energy and its conversion to electrical energy.

Besides optimizing the efficiency of the cell, significant effort has also been directed towards increasing the chemical/photoelectrochemical stability of the semiconductor electrodes in liquid environments. The thrust behind research in this direction comes from the early efforts to make stable and efficient water based semiconductor/liquid junction PEC cells[4-11] and from the classical paradox that efficient small bandgap semiconductors are unstable in aqueous environments and semiconductor electrodes stable in aqueous environments are not efficient harvesters of solar energy. Despite almost forty years of intense research and significant advances in the understanding of the semiconductor/liquid junction,[12-18] the goal of a stable and efficient semiconductor/liquid junction PEC cell still remains elusive and a challenge to one and all in this field.

To create stable efficient PEC cells, several different strategies are being employed. One approach to increasing the light harvesting efficiency of large bandgap semiconductors, eg. TiO_2, has involved the use of surface adsorbed dyes to sensitize the semiconductor.[19] The role of the dye is to extend the wavelength response of the

semiconductor into the visible region and create a better overlap with the solar spectrum. In this system, the surface adsorbed dye is the light absorbing component and the semiconductor is the charge separating component. PEC cells based on this approach are claimed to be reasonably stable and efficient and compared to other approaches mentioned below, are closest to commercialization.[19] Other strategies to create stable and efficient PEC cells have focused on small bandgap semiconductors where stability rather than light absorption is the key issue. One strategy is to employ redox couples that can kinetically compete with the photocorrosion reaction at the semiconductor surface.[1,12,20-27] Large concentrations of such redox couples should be able to compete with the undesirable reactions at the semiconductor surface and minimize surface corrosion. A second strategy involves the use of non aqueous solvents to completely remove the "offending" aqueous electrolyte. This strategy has been quite successful in creating stable semiconductor liquid junctions, albeit *sans* water.[28-35] PEC cells based on non aqueous electrolytes have been very useful in furthering the fundamental understanding of the process of charge transfer at semiconductor/liquid junctions.

A yet another strategy for creating stable and efficient PEC cells, and one that is the central theme of this thesis, is chemical modification of the semiconductor surfaces.[36-46] The main goal of this strategy is to increase the stability of the semiconductor by either increasing the rate of charge transfer across the semiconductor/liquid interface,[3,36-39,47] by decreasing the rate of recombination of the photogenerated carriers at the surface[13,43,48,49] or by decreasing photocorrosion and photooxidation at the semiconductor surface.[50-53] Increasing this rate of charge transfer across the semiconductor/liquid interface decreases the number of photogenerated carriers being lost to recombination and therefore increases the efficiency of the cell. A similar argument applies to the passivation of surface recombination. Any decrease in the rate of recombination of photogenerated charge carriers due to a decrease in the number of recombination centers at the surface will increase the efficiency of the junction.

The issue of oxidation and corrosion of the semiconductor surface can be interpreted as a special case of the general charge transfer and recombination argument mentioned above. Oxidation of a semiconductor surface can often introduce oxide layers on the surface that are resistive (e.g., SiO_2). As this oxide layer grows on the surface, it impedes further charge transfer. This results in a decrease in the efficiency and the effective lifetime of the cell. Any surface modification that prevents oxide formation can thus maintain the initial efficiency of the junction and increase the operating lifetime of the cell. Corrosion reactions, on the other hand, can create chemical species on the surface which can act as recombination centers and decrease the efficiency of the cell. Any surface modification that can decrease the number of recombination centers or make them less effective towards recombination can result in increasing the lifetime of the cell.

Chemical modification of semiconductor surfaces, as a means of gaining control over the physical, chemical and electrical properties of these surface and of the interfaces formed from these surfaces, forms the central theme of this thesis. Chapter 2 describes the modification of GaAs surface with transition metal ions. These metal-ion-treatments are known to increase the efficiency of the n-GaAs/$Se^{-/2-}$ junction by electrocatalyzing charge transfer from the semiconductor to the selenide redox couple. The work described in this chapter focuses on cause of the observed improvement in efficiency, distinguishing between the formation of a buried semiconductor/metal Schottky junction in which the liquid does not play a role, and the formation of a hybrid semiconductor/metal/liquid junction in which the liquid is an integral part of the junction.

Chapter 3 describes the modification of Si(111) surface by a two-step halogenation/alkylation reaction that results in a monolayer of alkyl groups that are covalently attached to the alkane surface without an anchoring layer of oxide. The chemical and physical properties of the alkyl modified surfaces were extensively characterized using a number of surface science techniques such as XPS, HREELS, IRS, AES, TPD, ellipsometry, contact angle goniometry etc. Results indicate that the silicon surface is

covered with a half monolayer of alkyl groups that are covalently bound to the surface. These surfaces are found to be more resistant to oxidation than the H-terminated surfaces, in air or in contact with wet chemical environments.

Chapter 4 describes the electrical properties of these alkyl terminated silicon surfaces, which indicate that the modified silicon surfaces are as good as the H-terminated surface. Additionally, the alkyl surfaces are found to be more resistant to oxidation in aqueous environments than the H-terminated surface. The results described in this chapter clearly indicate that with more work in the right direction, formation of a stable and efficient PEC cell from a small bandgap semiconductor and an aqueous electrolyte is an achievable goal.

II. REFERENCES

(1) Tan, M. X.; Laibinis, P. E.; Nguyen, S. T.; Kesselman, J. M.; Stanton, C. E.; Lewis, N. S. *Prog. Inorg. Chem.* **1994**, *41*, 21.

(2) Tufts, B. J.; Casagrande, L. G.; Lewis, N. S.; Grunthaner, F. J. *Appl. Phys. Lett.* **1990**, *57*, 2262.

(3) Tufts, B. J.; Abrahams, I. L.; Casagrande, L. G.; Lewis, N. S. *J. Phys. Chem.* **1989**, *93*, 3260.

(4) Boddy, P. J. *J. Electrochem. Soc.* **1968**, *115*, 199.

(5) Brattain, W. H.; Garret, C. G. B. *Phys. Rev.* **1954**, *94*, 750.

(6) Gerischer, H. *Z. Phys. Chem.* **1960**, *26*, 223.

(7) Gerischer, H.; Mindt, W. *Electrochim. Acta* **1968**, *13*, 1329.

(8) Memming, R. In *Electroanalytical Chemistry* ; A. J. Bard, Ed.; Marcel Dekker, Inc.: New York, 1979; Vol. 11; pp 1.

(9) Memming, R. *J. Electrochem. Soc.* **1969**, *116*, 785.

(10) Morrison, S. R. *Electrochemistry at Semiconductor and Oxidized Metal Electrodes*; Plenum: New York, 1980.

(11) Beckmann, K. H.; Memming, R. *J. Electrochem. Soc.* **1969**, *116*, 368.

(12) Miller, B.; Heller, A. *Nature* **1976**, *262*, 680.

(13) Heller, A. *Acc. Chem. Res.* **1981**, *14*, 154.

(14) Wrighton, M. S. *Acc. Chem. Res.* **1979**, *12*, 303.

(15) Gerischer, H. *J. Electroanal. Chem.* **1983**, *150*, 553.

(16) Tributsch, H. *Structure and Bonding* **1982**, *49*, 127.

(17) Lewis, N. S. *Acc. Chem. Res.* **1990**, *23*, 176.

(18) Lewis, N. S. *Ann. Rev. Phys. Chem.* **1991**, *42*, 543.

(19) O'Regan, B.; Grätzel, M. *Nature* **1991**, *353*, 737.

(20) Ellis, A. B.; Kaiser, S. W.; Wrighton, M. S. *J. Am. Chem. Soc.* **1976**, *98*, 1635.

(21) Ellis, A. B.; Kaiser, S. W.; Wrighton, M. S. *J. Am. Chem. Soc.* **1976**, *98*, 6855.

(22) Ellis, A. B.; Kaiser, S. W.; Wrighton, M. S. *J. Am. Chem. Soc.* **1976**, *98*, 6418.

(23) Hodes, G.; Manassen, J.; Cahen, D. *Nature* **1976**, *261*, 403.

(24) Ellis, A. B.; Bolts, J. M.; Wrighton, M. S. *J. Electrochem. Soc.* **1977**, *124*, 1603.

(25) Ellis, A. B.; Kaiser, S. W.; M., B. J.; Wrighton, M. S. *J. Am. Chem. Soc.* **1977**, *99*, 2839.

(26) Ellis, A. B.; Bolts, J. M.; Kaiser, S. W.; Wrighton, M. S. *J. Am. Chem. Soc.* **1977**, *99*, 2848.

(27) Chang, K. C.; Heller, A.; Schwartz, B.; Menezes, S.; Miller, B. *Science* **1977**, *196*, 1097.

(28) Lewis, N. S.; Rosenbluth, M. L.; Casagrande, L. G.; Tufts, B. J. In *Homogeneous and Heterogeneous Photocatalysis* ; E. Pelizzetti and N. Serpone, Ed.; Reidel: Dordrecht, 1986; Vol. 174; pp 343.

(29) Legg, K. D.; Ellis, A. B.; Bolts, J. M.; Wrighton, M. S. *Proc. Natl. Acad. Sci.* **1977**, *74*, 4116.

(30) Kautek, W.; Gerischer, H. *Ber. Bunsenges. Phys. Chem.* **1980**, *84*, 645.

(31) Jorné, J.; Pai, P. G. *J. Electrochem. Soc.* **1985**, *132*, 1612.

(32) Gibbons, J. F.; Cogan, G. W.; Gronet, C. M.; Lewis, N. S. *Appl. Phys. Lett.* **1984**, *45*, 1095.

(33) Fornarini, L.; Stirpe, F.; Scrosati, B. *J. Electrochem. Soc.* **1982**, 1155.

(34) Aruchamy, A.; Bruce, J. A.; Tanaka, S.; Wrighton, M. S. *J. Electrochem. Soc.* **1983**, *130*, 359.

(35) Rosenbluth, M. L.; Lieber, C. M.; Lewis, N. S. *Appl. Phys. Lett.* **1984**, *45*, 423.

(36) Bolts, J. M.; Wrighton, M. S. *J. Am. Chem. Soc.* **1978**, *100*, 5257.

(37) Bolts, J. M.; Wrighton, M. S. *J. Am. Chem. Soc.* **1979**, *101*, 6179.

(38) Bolts, J. M.; Bocarsly, A. B.; Palazzotto, M. C.; Walton, E. G.; Lewis, N. S.; Wrighton, M. S. *J. Am. Chem. Soc.* **1979**, *101*, 1378.

(39) Bocarsly, A. B.; Walton, E. G.; Wrighton, M. S. *J. Am. Chem. Soc.* **1980**, *102*, 3390.

(40) Fox, M. A. *DOE Contractor's Meeting* **1990**, 49.

(41) Koyama, H.; Koshida, N. *J. Electrochem. Soc.* **1991**, *138*, 254.

(42) Murray, R. W. In *Electroanalytical Chemistry* ; A. J. Bard, Ed.; Marcel Dekker, Inc.: New York, 1983; Vol. 13; pp 191.

(43) Parkinson, B. A.; Heller, A.; Miller, B. *Appl. Phys. Lett.* **1978**, *33*, 521.

(44) Sato, S. *Langmuir* **1988**, *4*, 1156.

(45) Tan, M. X.; Newcomb, C.; Kumar, A.; Lunt, S. R.; Sailor, M. J.; Tufts, B. J.; Lewis, N. S. *J. Phys. Chem.* **1991**, *95*, 10133.

(46) Tufts, B. J.; Abrahams, I. L.; Santangelo, P. G.; Ryba, G. N.; Casagrande, L. G.; Lewis, N. S. *Nature* **1987**, *326*, 861.

(47) Allongue, P.; Cachet, H. *J. Electrochem. Soc.* **1984**, *131*, 2861.

(48) Parkinson, B. A.; Heller, A.; Miller, B. *J. Electrochem. Soc.* **1979**, *126*, 954.

(49) Heller, A. In *Photoeffects at Semiconductor-Electrolyte Interfaces* ; A. J. Nozik, Ed.; The Society: Washington, D.C., 1981; Vol. 146; pp 57.

(50) Noufi, R.; Frank, A. J.; Nozik, A. J. *J. Am. Chem. Soc.* **1981**, *103*, 1849.

(51) Fan, F.-R. F.; Wheeler, B. L.; Bard, A. J.; Noufi, R. N. *J. Electrochem. Soc.* **1981**, *128*, 2042.

(52) Skotheim, T.; Lundstrom, I.; Prejza, J. *J. Electrochem. Soc.* **1981**, *128*, 1625.

(53) Skotheim, T.; Petersson, L. G.; Inganaes, O.; Lundstrom, I. *J. Electrochem. Soc.* **1982**, *129*, 1737.

Chapter 2

Distinguishing Between Buried Semiconductor/ Metal Contacts and Hybrid Semiconductor/Metal/ Liquid Contacts at n-GaAs/KOH-$Se^{-/2-}$(aq) Junctions

Abstract

The Current-voltage properties of n-GaAs photoanodes were evaluated in KOH-$Se^{-/2-}$(aq), CH_3CN-ferrocene $(Fc)^{+/0}$, and CH_3CN-methyl viologen $(MV)^{2+/+}$ solutions. Chemisorption of transition-metal ions (Rh^{III}, Rh^{III}, Co^{III}, Os^{III}) onto GaAs has been shown previously to effect improved photoanode behavior for n-GaAs/KOH-$Se^{-/2-}$(aq) contacts, but it is not clear whether the chemisorbed metal forms a buried semiconductor/metal (Schottky) junction or results in a "hybrid" semiconductor/metal/liquid contact. After chemisorption of transition-metal ions, n-GaAs photoanodes displayed different open circuit voltages in contact with each electrolyte solution investigated. The role of the chemisorbed metal in the n-GaAs/KOH-$Se^{-/2-}$(aq) system is, therefore, best described as catalyzing interfacial charge transfer at the semiconductor/liquid interface, as opposed to forming a semiconductor/metal or semiconductor/insulator/metal contact that is exposed to, but not influenced by, the electrolyte solution.

I. INTRODUCTION

One of the important goals of semiconductor surface modifications is to increase the efficiency of photoelectrochemical cells by improving the current-voltage characteristics of the semiconductor-liquid junction. This strategy has now been successfully applied to many technologically important semiconductors, including Si,[1-4] GaAs,[5-7] InP,[8,9] and TiO_2.[10-12] As the first (and still one of the few) small bandgap semiconductor electrode (photoanode) to be found stable in aqueous electrolyte,[5] the n-GaAs/KOH-$Se^{-/2-}$(aq) junction has been of special significance as a model for understanding kinetic stability against photocorrosion.[13-17] Further impetus towards understanding the charge transfer characteristics at this junction came from a serendipitous discovery by Parkinson, Heller and Miller in 1978,[18-20] which showed that modification of GaAs photoanodes with certain metal ions resulted in an increase in the efficiency of the GaAs/KOH-$Se^{-/2-}$(aq) junction. They showed that chemisorption of transition metal ions such as Rh^{III}, Co^{III}, Ru^{III} and Os^{III}, among others, led to improved current-voltage (I-V) behavior of n-GaAs photoanodes. In fact, chemisorption of Os^{III} has resulted in one of the most efficient photoelectrochemical energy conversion devices reported to date.[6] Numerous attempts have since been made to understand the role of the metal ions in determining charge transfer processes at this interface.[5-7,13,17-32]

However, despite the intense study of the n-GaAs/KOH-$Se^{-/2-}$(aq) system, the mechanism of I-V improvement is still controversial. For minority carriers (holes in n-type GaAs), passivation of GaAs surface recombination[18,19,28,33,34] and electrocatalysis of hole transfer[7,17,24,31,32] have both been proposed to explain the beneficial effects of metal ion chemisorption. Most of the recent evidence, however, strongly suggests that, in contact with the KOH-$Se^{-/2-}$(aq) solution, the dominant effect of metal ion chemisorption can be ascribed to electrocatalysis of minority carrier processes.[7,17,31,32] Support for this hypothesis has been obtained from differential capacitance studies,[24] from steady-state I-V experiments,[7,31] from real-time luminescence decay studies,[32] and from suppression of

GaAs photocorrosion, in contact with KOH-$Se^{-/2-}$(aq).[17] However, the available data do not unambiguously address the effects of metal ion chemisorption on the majority carrier processes. One possibility is that the chemisorbed metal ions form a "buried" semiconductor/metal (Schottky) junction which is simply in electrical contact with the KOH-$Se^{-/2-}$(aq) electrolyte. In this case, the majority carrier kinetics would be dominated by recombination within a metal overlayer on the n-GaAs surface. The other possibility is that the entire GaAs/metal/liquid interface is a crucial component of the junction and the chemisorption step acts to enhance charge transfer interactions at the GaAs/liquid junction.

Distinguishing between these possibilities is significant because metal ion chemisorption is a widespread strategy for improving the I-V properties of semiconductor/liquid contacts.[5-7,13,17-32,35-45] However, if metal ion treatment of a semiconductor merely formed a "buried" Schottky barrier, then the I-V properties of the system would be determined by the semiconductor/metal junction. Under such conditions, the electrical contact to the solution would not be necessary for photovoltaic action, and the presence of the liquid phase would not influence the maximum attainable energy conversion efficiency of the device. Instead, the liquid would only complicate the system by adding possible corrosion pathways and increased ohmic losses to the cell.

In contrast, it is possible that metal ion chemisorption can selectively catalyze the charge transfer processes at semiconductor/liquid interfaces. This approach is desirable theoretically, because it could enhance the performance of semiconductor/liquid junctions. Such a junction would also not be restricted by the efficiency limitations that are inherent to semiconductor/metal Schottky barriers.[46] The key distinction between the "buried" Schottky junction and the "hybrid" semiconductor/metal/liquid contact[36] involves the recombination kinetics of the majority carriers. In the "buried" Schottky junction, recombination of majority carriers is dominated by charge injection into the metal overlayer.[46] In this situation, the presence of the electrolyte has no effect on the rate-determining recombination step (Figure 1a). In the hybrid semiconductor/metal/liquid

Figure 1. A comparison of the interfacial energetic behavior expected for "buried " semiconductor/metal contacts and for hybrid semiconductor/metal/liquid contacts. (a) For a "buried" semiconductor/metal junction in contact with a liquid, the initial electric potential in the semiconductor is dependent on the characteristics of the semiconductor/metal contact and is independent of the electrochemical potential of the liquid phase. Under these conditions, changes in the electrochemical potential of the solution will induce changes in the voltage drop at the metal/liquid interface, but will not effect the energetics of the semiconductor/metal contact. Under illumination of such contacts, the rate determining recombination step is dominated by capture of minority and majority carriers by the metal, with the liquid merely serving as a convenient monitor of the interfacial kinetics. (b) For a hybrid semiconductor/metal/liquid interface, the equilibrium electric potential drop in the semiconductor, and the carrier recombination kinetics of the contact, are influenced both by the nature of the semiconductor/metal contact and by the composition of the liquid phase. In both panels, the electrochemical potentials of the solutions are as follows: $\mathbf{E}(A/A^-) < \mathbf{E}(B/B^-)$, with $\mathbf{E}_v$ denoting the local vacuum level energy, $\mathbf{E}_{cb}$ denoting the energy of the bottom of the conduction band, $\mathbf{E}_{vb}$ denoting the energy of the top of the valence band, and $\mathbf{E}_f$ indicating the position of the Fermi level.

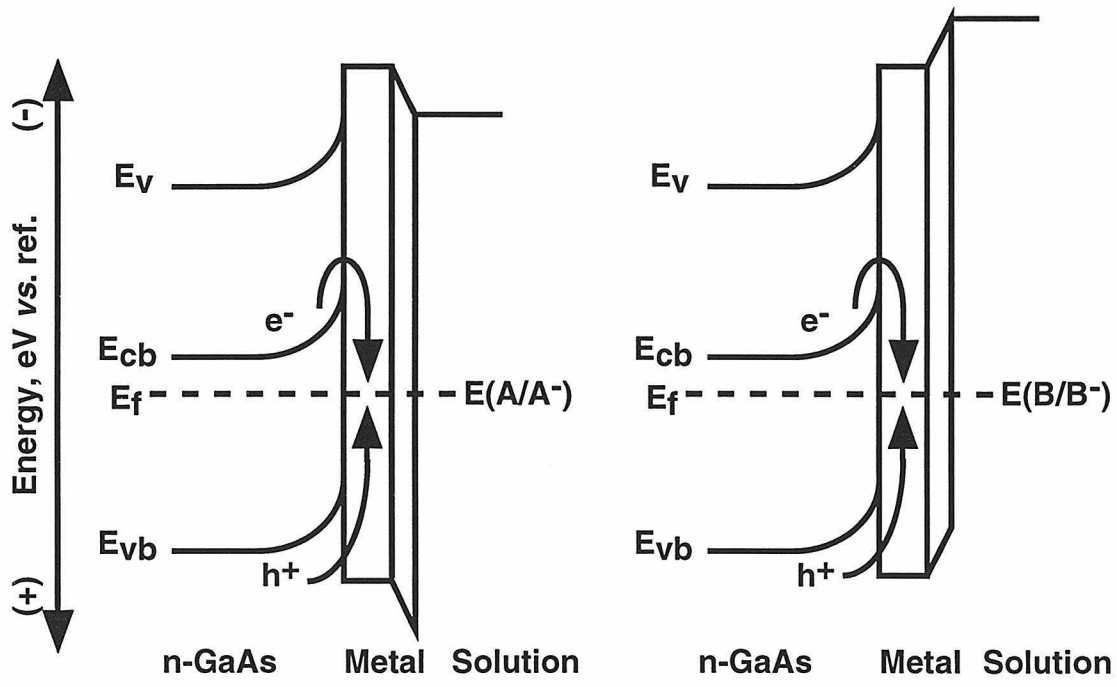
Energy, eV vs. ref.
(-)
(+)
E_v
e^-
E_{cb}
E_f
$E(A/A^-)$
E_{vb}
h^+
n-GaAs
Metal
Solution
E_v
e^-
E_{cb}
E_f
$E(B/B^-)$
E_{vb}
h^+
n-GaAs
Metal
Solution

(a)

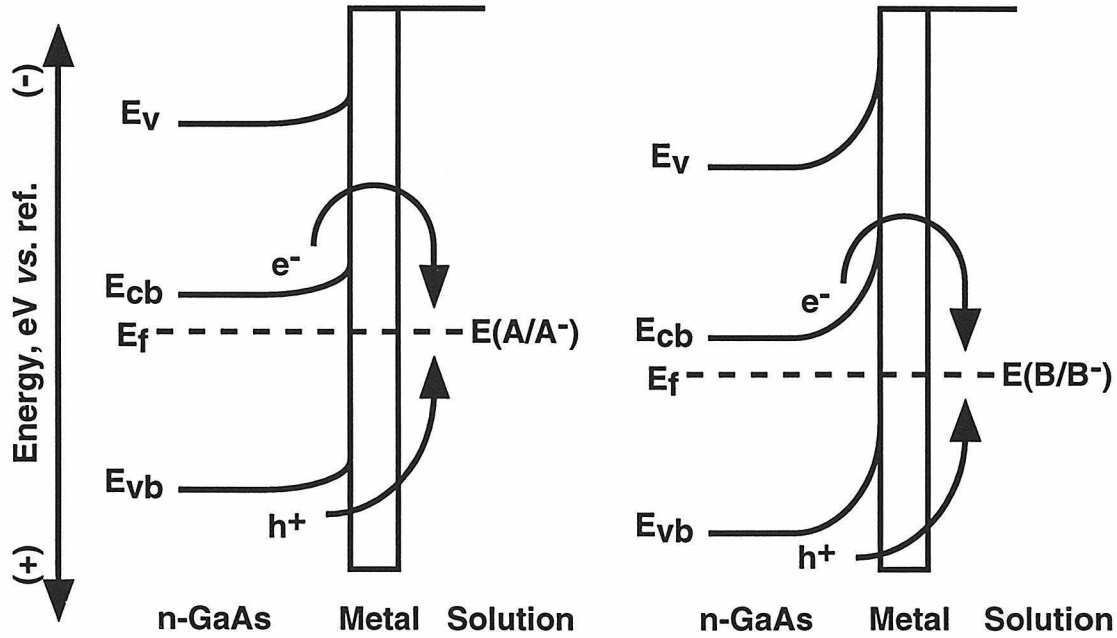
Energy, eV vs. ref.
(-)
(+)
E_v
e^-
E_{cb}
E_f
$E(A/A^-)$
E_{vb}
h^+
n-GaAs
Metal
Solution
E_v
e^-
E_{cb}
E_f
$E(B/B^-)$
E_{vb}
h^+
n-GaAs
Metal
Solution

(b)

system, the rate-determining recombination step, and therefore the cell performance, is critically influenced by the identity of the redox pair and electrolyte solution (Figure 1b). The n-GaAs/KOH-$Se^{-/2-}$(aq) junction comprises an ideal system on which to evaluate these alternatives, and on which to develop mechanistic probes of these types of semiconductor/metal/liquid contacts.[7]

The available data allows one immediately to rule out some limiting possibilities for the n-GaAs/metal/KOH-$Se^{-/2-}$(aq) system. Direct n-GaAs/metal contacts prepared in ultra high vacuum (UHV) have been extensively studied in the solid-state physics literature, and their I-V properties are well-known.[47-50] Deposition of metal overlayers onto GaAs surfaces generally leads to Fermi level pinning, with typical barrier heights of 0.7-0.9 V on n-type GaAs samples.[46,49,50] For such junctions, thermionic emission of majority carriers results in substantial recombination currents, and produces open circuit voltages (V_{oc}) of only 0.3-0.4 V under 1 Sun illumination.[51,52] Chemisorption of metal ions onto GaAs photoelectrodes clearly does not produce these types of Schottky barriers, because at similar short circuit photocurrent densities (J_{sc}), V_{oc} values in excess of 0.80 V have been observed for n-GaAs/metal/liquid contacts.[31,53] Assuming that the metal ions were indeed forming a conventional 0.90 V barrier height Schottky junction, a straightforward calculation shows that the area of such a Schottky barrier could not have covered more than 0.0002% of the GaAs surface area; otherwise, the V_{oc} would be lower than that measured experimentally. Thus, even though Fermi level pinning is known to occur for metal coverage as low as 0.1 monolayer in UHV experiments,[49] these types of contacts are not present in the n-GaAs/metal/KOH-$Se^{-/2-}$(aq) system.

This observation, however, does not rule out the possibility that the chemisorbed metal ions have created an improved Schottky barrier with a new, more favorable surface Fermi level position. In fact, electrodeposition of metal ions can produce Schottky barriers that display higher barrier heights and higher open circuit voltages than those prepared in UHV.[54,55] Although the V_{oc} values of n-GaAs/KOH-$Se^{-/2-}$(aq) interfaces are higher than

those for any known n-GaAs Schottky barrier, these values are still compatible with the presence of a Schottky barrier with a very high (≈1.3 V) barrier height.

Yet another alternative is that the chemisorption process produces a "buried" metal-insulator-semiconductor (MIS) device on the semiconductor photoelectrode. For n-GaAs, the V_{oc} values for MIS systems are typically higher than those of direct n-GaAs/metal contacts.[56,57] In fact, some n-GaAs MIS devices exhibit V_{oc} values which are comparable to those of n-GaAs/KOH-$Se^{-/2-}$(aq) contacts.[56,57] Although it would be advantageous to prepare such improved Schottky or MIS contacts using wet chemical methods, neither of these contacts would require, nor benefit from, the presence of the additional electrical contact to the liquid electrolyte. Distinguishing between the presence of a hybrid semiconductor/metal/liquid interface and the presence of a "buried" junction is therefore important in advancing our understanding of n-GaAs/liquid contacts.

In this work,[7] the I-V properties of GaAs/metal/liquid junctions were investigated in a variety of different electrolytes. If the metal chemisorption process has created a "buried" interfacial device, then the composition of the liquid phase, and the value of the solution redox potential, should not affect the I-V properties of the system. This conclusion should hold regardless of whether the contact is a "buried" semiconductor/metal or semiconductor/insulator/metal device. Alternatively, if changes in the liquid phase affect the I-V properties of the system, then the liquid must be considered as an integral part of the "hybrid" semiconductor/metal/liquid contact. In this case, the recombination kinetics of majority carriers will depend not only on the nature of the metal contact but also on composition of the electrolyte. As described below, a suitable test for such behavior is a comparison of the I-V properties of n-GaAs/metal/liquid contacts using KOH-$Se^{-/2-}$(aq), CH_3CN-ferrocene $(Fc)^{+/0}$, and CH_3CN-methyl viologen $(MV)^{2+/+}$ solutions.

II. EXPERIMENTAL

1. Materials

The n-GaAs samples were purchased from Laser Diode Co. They were 400-500 μm thick, (100) oriented, Si doped (donor density = 0.9-1.9x10^{17} cm^{-3}), single crystal wafers. For ohmic contact formation, 1000 Å of Au:Ge (88:12) was deposited, by thermal evaporation at 10^{-5} torr, onto the unpolished side these wafers, and the samples were then heated under forming gas (5% H_2: 95% N_2) at 480°C for 5 min. The crystals were then cut into small pieces (≈ 0.1 cm^2) and were attached to a wire using electrically conductive silver print (G C Electronics). The back side and edges of the electrode were then covered with epoxy, leaving only the polished surface of the crystal exposed. The exposed electrode areas were determined from enlarged photographs of the samples.

n-GaAs electrodes were etched by immersion into in 0.05%(v/v) Br_2-CH_3OH, followed by immersion into 1.0 **M** KOH(aq). The etching cycle was repeated three times for each electrode. This procedure has been shown to give an oxide free, stoichiometric surface with a mirror finish.[51,58,59]

2. Solvents and Electrolytes

KOH(s) and HCl(aq) were obtained from E M Science, and were of reagent grade. CH_3CN was either anhydrous quality (<0.005% water, Aldrich) or was reagent grade (GR, E M Science). The anhydrous quality CH_3CN was stored until use in an N_2 ambient, while the reagent grade solvent was dried over CaH_2 and P_2O_5 under N_2(g) and stored over activated sieves (Linde 3 Å) in an N_2 ambient. $LiClO_4$ (Aldrich) was dried at ≈300° C for 2-3 h under an active vacuum (10^{-5} torr). Tetrabutylammonium hexafluorophosphate ($TBAPF_6$) was prepared by the metathesis of TBABr (Aldrich) and HPF_6 (Aldrich) in water. The $TBAPF_6$ precipitate was filtered and purified by two different methods. In one method, the precipitate was extracted into CH_3CN, and the solvent was evaporated under vacuum. The compound was then dried overnight at 100°C

under active vacuum. The second method involved extraction of $TBAPF_6$ into CH_2Cl_2. The solution was washed with H_2O until the rinsing solution exhibited a neutral pH. The CH_2Cl_2 layer was then dried over sodium sulfate and filtered. The solvent was removed by rotary evaporation, yielding a white powder that was dried under active vacuum at 60°C for 18 h.

3. Redox Couples and Metal Ion Treatments

Ferrocene (Fc) (Aldrich) and cobaltocene ($CoCp_2$) (Strem) were purified by vacuum sublimation. $[CoCp_2]^+[PF_6]^-$ was obtained from Aldrich. The cobaltocene derivatives $CoCp(CpCOOCH_3)$ and $Co(CH_3Cp)_2$ were prepared by the method of Sheats and Rausch.[60,61] $Fc^+PF_6^-$ was prepared by oxidizing ferrocene with benzoquinone in HPF_6(aq). Methyl viologen hexafluorophosphate ($MV^{2+}(PF_6^-)_2$) was prepared by reacting $(MV^{2+})(Cl^-)_2$ hydrate (Aldrich) with a 1.2 molar excess of HPF_6. The precipitate was washed with cold water, recrystallised from a 1:1:1 mixture of water, ethanol and ether, and then dried at 100-120°C under active vacuum (10^{-5} torr) for 24 h.

$OsCl_3$ (Strem), $RuCl_3$ (Alfa), $RhCl_3$, and $Co(NH_3)_6Cl_3$ (Strem) were used as received. For metal ion chemisorption, 0.010 **M** (pH 2.0) solutions of $OsCl_3$, $RuCl_3$ and $RhCl_3$ were made from dilute HCl(aq), while a 0.010 **M** solution of $Co(NH_3)_6Cl_3$ was made in 0.010 **M** KOH(aq) (pH 12.0). n-GaAs electrodes were immersed in the metal ion solutions for 60 s, rinsed with 18 MΩ-cm resistivity deionized water, and blown dry under a stream of nitrogen.

To prepare basic aqueous solutions of $Se^{-/2-}$, H_2Se(g) was generated in situ from Al_2Se_3 and HCl(aq), and was then bubbled through 3.0 **M** KOH(aq).[30] The oxidized form of the $Se^{-/2-}$ couple was obtained by exposing the KOH-Se^{2-}(aq) solution to air until the solution acquired a red-brown color. To determine the total selenium concentration, an aliquot of the sample was oxidized to Se metal. The Se^0 precipitate was filtered, washed with water, dried and weighed. The total selenium concentration in the five samples used in this work was 0.81 **M,** 0.84 **M,** 0.93 **M,** 1.0 **M** and 1.15 **M,** and the concentration of

oxidized species was ≈0.01 **M** in each case. The ferrocene solution contained 0.70 **M** $LiClO_4$-0.10 **M** Fc- ≈0.5 mM $Fc^+PF_6^-$ in acetonitrile. The cobaltocene solution contained 0.70 **M** $LiClO_4$-0.050 **M** $CoCp_2$- ≈0.5 mM $CoCp_2^+PF_6^-$ in acetonitrile. The methyl viologen solution was prepared by bulk electrolysis of a 17 ml solution of 0.30 **M** $TBAPF_6$-0.020 **M** $(MV^{2+})(PF_6^-)_2$. Passage of approximately 16 C of cathodic charge generated enough MV^+ (≈50% conversion) to achieve a good compromise between undesirable photocurrent limitations due to mass transport limit (at low MV^+ concentrations) and extensive solution absorbance (at high MV^+ concentrations).

4. Electrochemical Cells and Methods

The samples were illuminated with ELH or ENH type tungsten-halogen bulbs[30] that had been modified by lining the inside of the dichroic reflector with aluminum foil. This modification (suggested by Dr. Gary Shreve) increased the projected red/IR component of the illumination, and effected a three-fold increase in the net power incident on the GaAs electrode surface. For the highly colored CH_3CN-$MV^{2+/+}$ solution, a biconvex lens was used in conjunction with the light source to further increase the light intensity incident at the electrode. Cool air was continuously blown over the methyl viologen cell to minimize changes in V_{oc} arising from an increase in the cell temperature. The unmodified ELH or ENH bulbs were used for experiments with CH_3CN-$CoCp_2^{+/0}$ solutions.

The I-V characteristics were plotted on a Houston Instruments Model 2000 X-Y recorder at a scan rate of 50 mV/s. Potential control was accomplished with a Princeton Applied Research Model 173 potentiostat and Model 175 universal programmer. The limiting photocurrent density, J_{ph} was measured at +0.050 V *vs.* the Nernstian potential of the cell. All cell potentials were recorded *vs.* a Pt wire that was poised at the Nernstian cell potential of each redox couple.

For n-GaAs/M/KOH-$Se^{-/2-}$(aq) junctions, V_{oc} increased significantly during the first few scans between short circuit and open circuit. Generally thereafter, the I-V curves exhibited only small changes between scans, and all data reported in this work were obtained after the electrode behavior had stabilized. A slight increase in V_{oc} was also observed during the initial electrochemical cycles of the n-GaAs/CH_3CN-$Fc^{+/0}$ junction, and the reported data refer to the I-V properties after V_{oc} had stabilized. For n-GaAs/CH_3CN-$MV^{2+/+}$ contacts, J_{ph} increased during the first few I-V scans, presumably due to a slight increase in cell temperature that affected the equilibrium constant for the highly colored MV^+ and dimeric $(MV^+)_2$ species. To compensate for this change in J_{ph}, the light intensity was adjusted to obtain the desired J_{ph} value, and the I-V properties were then recorded.

For pulsed laser experiments (performed by Dr. Ming Tan), the n-GaAs electrodes were etched as described above, and were then immersed in 1.0 M $Na_2S•9H_2O$(aq) for 30 s. The electrodes were then dried under a stream of flowing N_2(g) for 30 min, and were rinsed briefly (1-2 s) with H_2O before drying under a stream of N_2(g) in air. The electrodes were then immersed into a CH_3CN-0.70 **M** $LiClO_4$-0.050 **M** $CoCp_2$- ≈0.5 mM $CoCp_2^+PF_6^-$ solution and were exposed to 532 nm illumination from a Coherent Antares Nd:Yag laser. The laser beam was 1 mm in radius, had a pulse duration of 70 ps with a repetition frequency of 76 MHz, and contained 2 W of power. This produced an energy density of 1 $\mu J/cm^2$ onto the illuminated portion of the sample. The sample was exposed to the laser beam for 150 s, during which time the specimen was translated manually in order to expose the entire 0.10 cm^2 sample area to the illumination source.

Since less than micromolar concentrations of the metal ions can cause significant changes in the I-V curves of n-GaAs/KOH-$Se^{-/2-}$(aq) junctions,[31] strict precautions were taken to avoid any such contamination. In all experiments, a separate set of working, reference and counter electrodes were used for each metal ion. Additionally, fresh solutions were used whenever the I-V curves of the etched n-GaAs electrode deviated

significantly from those measured in a fresh aliquot of the KOH-$Se^{-/2-}$(aq) solution. Uncontaminated solutions consistently yielded I-V characteristics in accord with those reported previously for n-GaAs/KOH-$Se^{-/2-}$(aq) contacts.[6,17,19,28,30,31]

III. RESULTS AND DISCUSSION

1. Current-Voltage Behavior of n-GaAs in Contact with KOH-$Se^{-/2-}$(aq) Solutions

Figure 2 displays the J-V data for etched n-GaAs photoanodes in contact with the KOH-$Se^{-/2-}$(aq) electrolyte. These data provided a reproducible reference point for evaluating the effects of metal ion chemisorption. In this electrolyte, the J-V curves exhibited a characteristic sigmoidal shape and a low fill factor (Figure 2a-d, dashed curves). This behavior is in accord with previous photoelectrochemical studies of the n-GaAs/KOH-$Se^{-/2-}$(aq) interface.[6,17,19,28,30,31]

After chemisorption of metal ions onto the n-GaAs surface, the J-V behavior of the n-GaAs/KOH-$Se^{-/2-}$(aq) contact improved substantially.[6,7,17-19,23,24,27,28,30-32] For example, the solid curve in Figure 2a displays the data after chemisorption of Ru^{III} onto the GaAs surface. If such electrodes were not etched after exposure to the KOH-$Se^{-/2-}$(aq) solution, they could be removed from the solution, rinsed with water and re-immersed into the KOH-$Se^{-/2-}$(aq) electrolyte without producing significant changes in the improved J-V behavior. The effects of metal ion chemisorption could, however, be completely eliminated by thorough etching of the electrode surface. As displayed in Table I and Figure 2, the most significant changes effected by the metal ion treatment were the increased fill factors and the improved V_{oc} values.

Figure 2. Current density-voltage characteristics of (100)-oriented n-GaAs electrodes in contact with KOH-$Se^{-/2-}$(aq). In each measurement, the illumination intensity was adjusted to obtain a current density of 5.0 mA/cm^2 at +0.05 V *vs.* the Nernstian potential of the cell. The dashed sigmoidal curve represents the J-V behavior of an etched n-GaAs electrode in each separate experiment. The solid lines represent the J-V data after exposure of the n-GaAs surface to the following metal ion solutions: (a) 0.010 **M** (pH 2.0) $RuCl_3$; (b) 0.010 **M** (pH 2.0) $RhCl_3$; (c) 0.010 **M** (pH 12.0) $Co(NH_3)_6Cl_3$; (d) 0.010 **M** (pH 2.0) $OsCl_3$. The electrode was cycled (scan rate: 50 mV/s) between -0.85 V and +0.05 V *vs.* the cell potential for each J-V measurement.

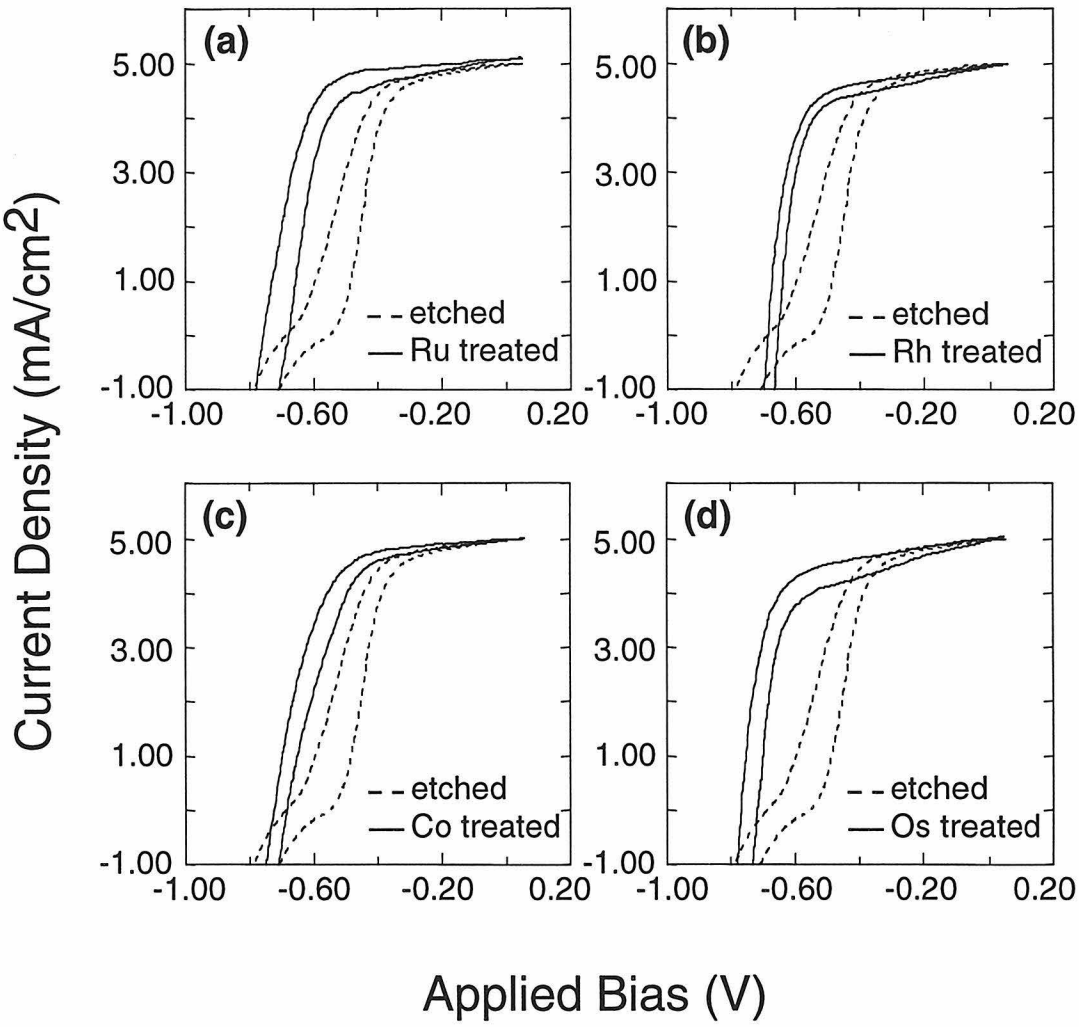
(a)
(b)
(c)
(d)
5.00
3.00
1.00
-1.00
-1.00
-0.60
-0.20
0.20
- - etched
— Ru treated
— Rh treated
— Co treated
— Os treated
Current Density (mA/cm2)
Applied Bias (V)

Table I. Open circuit voltages in mV (at J_{ph} = 5.0 mA/cm^2) of (100)-oriented n-GaAs electrodes in contact with KOH-$Se^{-/2-}$(aq) and CH_3CN-$Fc^{+/0}$ electrolytes. Etched n-GaAs surfaces were exposed to aqueous solutions of the indicated metal, as described in the experimental section.

	V_{oc} (KOH-$Se^{-/2-}$(aq))	V_{oc} (CH_3CN-$Fc^{+/0}$)
Etched	661 ± 21	688 ± 20
Rh^{III}	662 ± 21	671 ± 24
Co^{III}	717 ± 19	678 ± 21
Ru^{III}	746 ± 22	672 ± 21
Os^{III}	757 ± 17	677 ± 14

2. Current-Voltage Behavior of n-GaAs in Contact with CH_3CN-$Fc^{+/0}$ Solutions

One test for the presence or absence of a "buried" semiconductor/metal interface is provided by the I-V behavior of GaAs/CH_3CN-$Fc^{+/0}$ contacts. Figure 3 (dashed curve) displays the J-V curves obtained for etched n-GaAs electrodes in contact with this electrolyte. In accord with previous studies, etched n-GaAs surfaces exhibited high fill factors and relatively large V_{oc} values in contact with the CH_3CN-$Fc^{+/0}$ system.[51,62,63]

Figure 3 also displays representative J-V data for GaAs electrodes that had been either exposed to metal ions or had been exposed to metal ions and electrochemically cycled in KOH-$Se^{-/2-}$(aq) before exposure to CH_3CN-$Fc^{+/0}$ (solid curves). Regardless of the history of the electrode, the photoanode behavior in CH_3CN-$Fc^{+/0}$ was not significantly different from that of etched GaAs photoanodes. The V_{oc} data for these systems are also summarized in Table I.

Several controls were performed to ensure that exposure to the CH_3CN-$Fc^{+/0}$ electrolyte did not induce a beneficial chemisorption process at the GaAs surface. Etched n-GaAs electrodes that had been cycled in KOH-$Se^{-/2-}$(aq), exposed to CH_3CN-$Fc^{+/0}$, and then re-immersed in KOH-$Se^{-/2-}$(aq) did not exhibit significant improvements in the fill factor or V_{oc} relative to their initial behavior in the KOH-$Se^{-/2-}$(aq) system. Furthermore, the beneficial effects of chemisorbed Rh^{III}, Co^{III}, Ru^{III} and Os^{III} in contact with KOH-$Se^{-/2-}$(aq) were retained even after exposure of treated electrodes to the CH_3CN-$Fc^{+/0}$ electrolyte system. Thus, the different V_{oc} values for the various n-GaAs/KOH-$Se^{-/2-}$(aq), n-GaAs/CH_3CN-$Fc^{+/0}$, and n-GaAs/M/KOH-$Se^{-/2-}$(aq) contacts imply that the excellent I-V behavior of the n-GaAs/CH_3CN-$Fc^{+/0}$ interface was not due to an irreversible, beneficial metal ion chemisorption process.

For M=Os and Ru, the V_{oc} values for n-GaAs/M/KOH-$Se^{-/2-}$(aq) contacts were significantly different from those of n-GaAs/M/CH_3CN-$Fc^{+/0}$ contacts (Table I). This clearly indicated that chemisorption of these two metals did not produce "buried" contacts

Figure 3. Current density-voltage characteristics of (100)-oriented n-GaAs electrodes in contact with CH_3CN-0.70 **M** $LiClO_4$-0.10 **M** $FeCp_2$- ≈0.5 mM $FeCp_2^+PF_6^-$. In each measurement, the illumination intensity was adjusted to obtain a current density of 5.0 mA/cm^2 at +0.05 V *vs.* the Nernstian potential of the cell. The dashed curve represents the J-V behavior of an etched n-GaAs electrode in each separate experiment. The solid lines represent the J-V data after exposure of the n-GaAs surface to the following metal ion solutions: (a) 0.010 **M** (pH 2.0) $RuCl_3$; (b) 0.010 **M** (pH 2.0) $RhCl_3$; (c) 0.010 **M** (pH 12.0) $Co(NH_3)_6Cl_3$; (d) 0.010 **M** (pH 2.0) $OsCl_3$. The electrode was cycled (scan rate: 50 mV/s) between -0.85 V and +0.05 V *vs.* the cell potential for each J-V measurement.

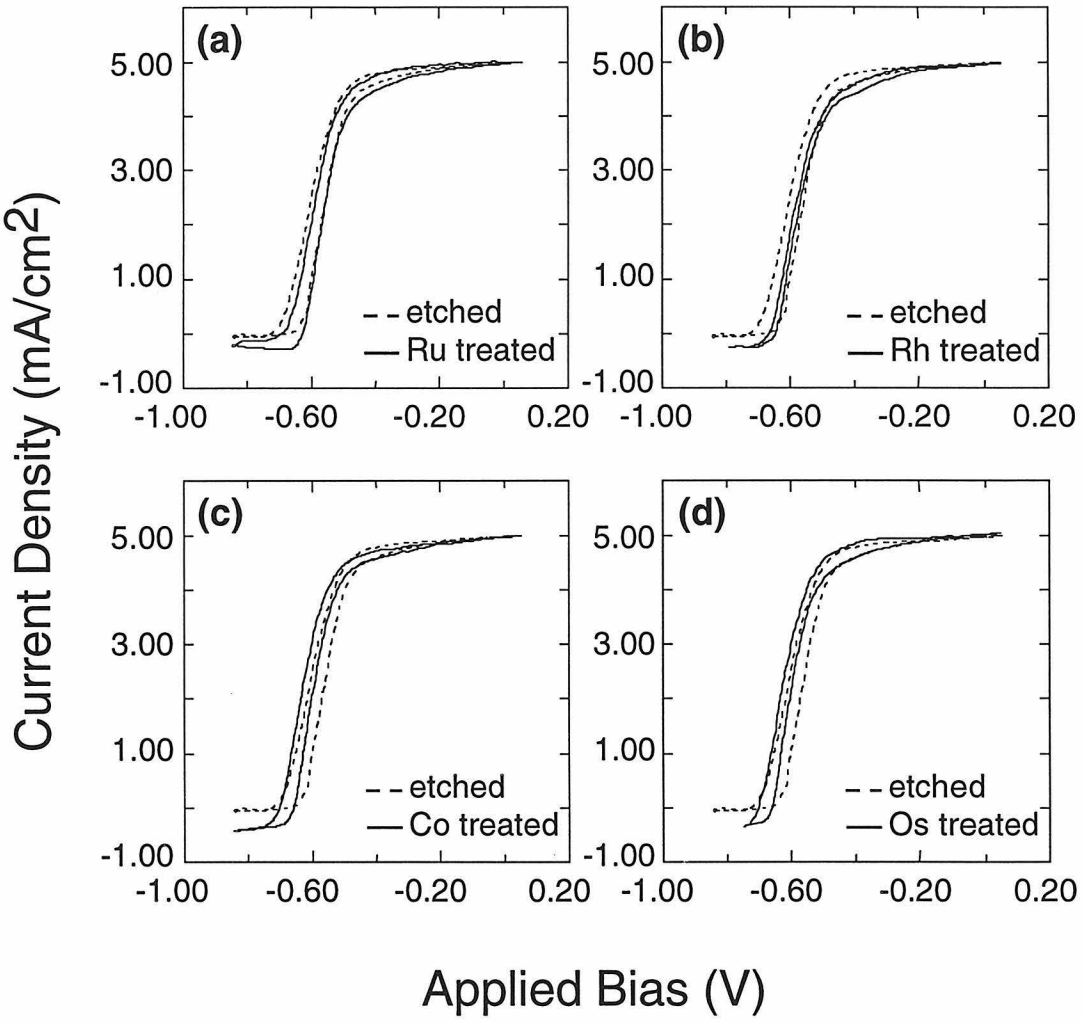
(a)
(b)
(c)
(d)
5.00
3.00
1.00
-1.00
-1.00
-0.60
-0.20
0.20
- - etched
— Ru treated
— Rh treated
— Co treated
— Os treated
Current Density (mA/cm2)
Applied Bias (V)

which were insensitive to the composition of the contacting liquid phase. For M=Co and Rh, however, the V_{oc} values of n-GaAs/M/CH_3CN-$Fc^{+/0}$ contacts were very close to those of n-GaAs/M/KOH-$Se^{-/2-}$(aq) contacts. Conclusive evaluation of these two contacts therefore required the use of a different redox solution, as detailed in the next section.

3. Current-Voltage Behavior of n-GaAs in Contact with CH_3CN-$MV^{2+/+}$ Solutions

CH_3CN-$MV^{2+/+}$ was identified as a suitable redox couple and electrolyte for evaluation of the n-GaAs/Rh/liquid and n-GaAs/Co/liquid contacts. For etched n-GaAs photoanodes, the negative redox potential of the CH_3CN-$MV^{2+/+}$ solution resulted in lower V_{oc} values than those of n-GaAs/CH_3CN-$Fc^{+/0}$ contacts.[64] The $MV^{2+/+}$ redox couple was also desirable because it contains no transition metals, and because it is a well-behaved, one-electron redox couple that exhibits rapid charge transfer kinetics at most electrode surfaces.[64-68] Figure 4 shows the J-V curves of n-GaAs surfaces in contact with this electrolyte. As expected, the fill factor was high, but the open circuit voltage was relatively small, with V_{oc} =(0.463 ± 0.017) V at J_{ph}=1 mA/cm^2 (Table II).

Chemisorption of Rh^{III}, Co^{III}, Ru^{III} or Os^{III} onto n-GaAs resulted in no change in the shape of the J-V curve in the CH_3CN-$MV^{2+/+}$ electrolyte (Figure 4). The V_{oc} for n-GaAs/M/CH_3CN-$MV^{2+/+}$ contacts was 0.44-0.47 V, which was the same as the value for the etched n-GaAs electrode in contact with CH_3CN-$MV^{2+/+}$ electrolyte (Figure 4, Table II). Notably, this value was significantly lower than any of the V_{oc} values for n-GaAs/M/KOH-$Se^{-/2-}$(aq) contacts. These data, in conjunction with the experiments in CH_3CN-$Fc^{+/0}$ electrolytes (*vide supra*), therefore imply that none of the metal ions studied in this work formed "buried" junctions on the GaAs surface.

Several additional control experiments were performed to strengthen this conclusion. Immersion and electrochemical cycling of GaAs electrodes in CH_3CN-$MV^{2+/+}$ solutions had no effect on the I-V behavior of n-GaAs/KOH-$Se^{-/2-}$(aq), n-GaAs/M/KOH-$Se^{-/2-}$(aq), or n-GaAs/CH_3CN-$Fc^{+/0}$ contacts. For example, in one

Figure 4. Current density-voltage characteristics of (100)-oriented n-GaAs electrodes in contact with CH_3CN-0.30 **M** $TBAPF_6$-≈0.010 **M** MV^+-≈0.010 **M** MV^{+2}. In each measurement, the illumination intensity was adjusted to obtain a current density of 1.0 mA/cm^2 at +0.05 V *vs.* the Nernstian potential of the cell. The dashed curve represents the J-V behavior of an etched n-GaAs electrode in each separate experiment. The solid lines represent the J-V data after exposure of the n-GaAs surface to the following metal ion solutions: (a) 0.010 **M** (pH 2.0) $RuCl_3$; (b) 0.010 **M** (pH 2.0) $RhCl_3$; (c) 0.010 **M** (pH 12.0) $Co(NH_3)_6Cl_3$; (d) 0.010 **M** (pH 2.0) $OsCl_3$. The electrode was cycled (scan rate: 50 mV/s) between -0.60 V and +0.05 V *vs.* the cell potential for each J-V measurement.

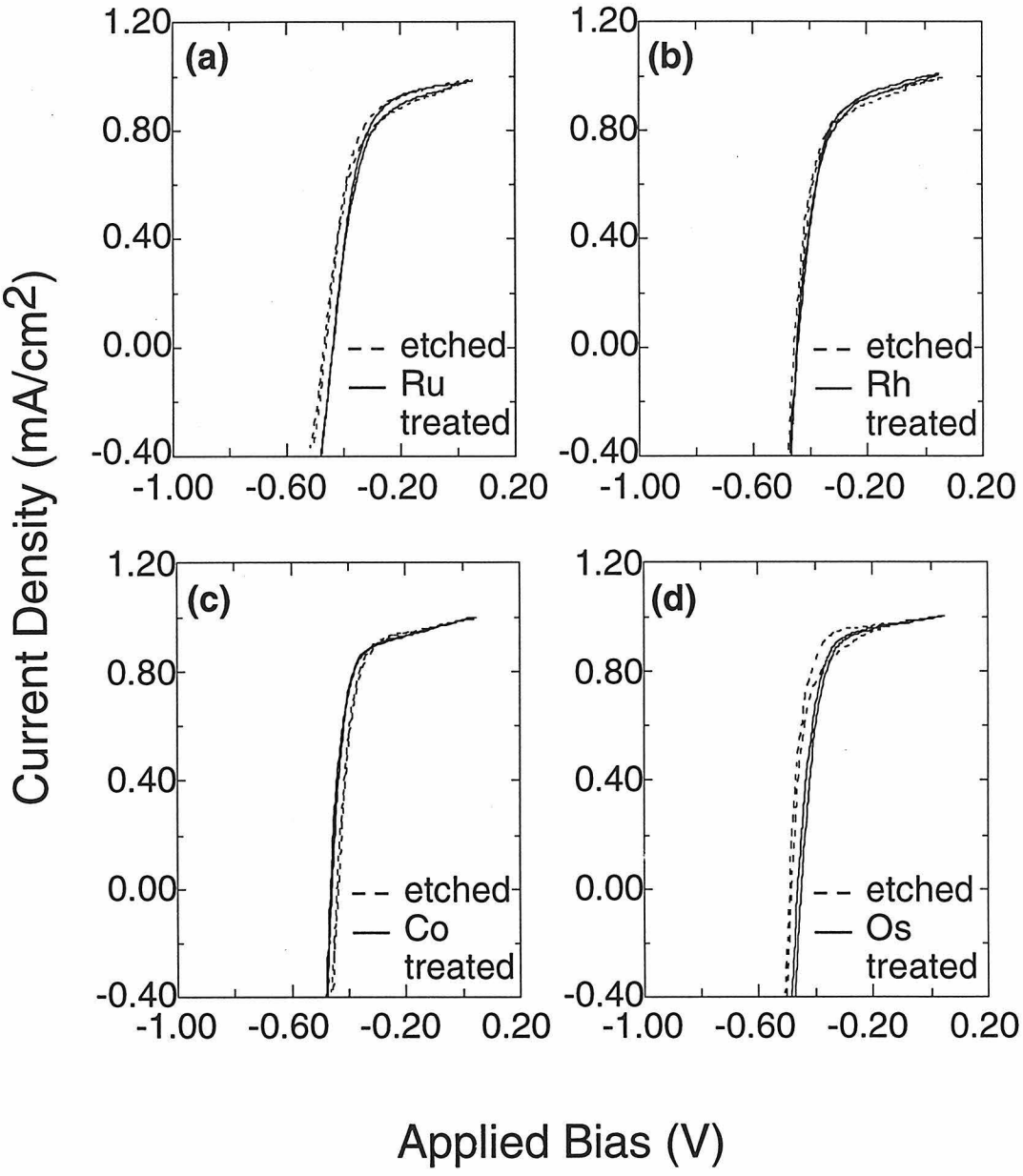
(a)
(b)
(c)
(d)
1.20
0.80
0.40
0.00
-0.40
-1.00
-0.60
-0.20
0.20
-- etched
— Ru
treated
-- etched
— Rh
treated
-- etched
— Co
treated
-- etched
— Os
treated
Current Density (mA/cm2)
Applied Bias (V)

Table II. Open circuit voltages in mV (at J_{ph} = 1.0 mA/cm^2) of (100)-oriented n-GaAs electrodes in contact with KOH-$Se^{-/2-}$(aq), CH_3CN-$MV^{2+/+}$ and CH_3CN-$Fc^{+/0}$ electrolytes. A light-limited photocurrent density of 1.0 mA/cm^2 was used in these experiments because mass transport limitations precluded reliable measurements at higher photocurrent densities at the CH_3CN-$MV^{2+/+}$ electrolyte. Etched n-GaAs surfaces were exposed to aqueous solutions of the indicated metal, as described in the experimental section.

	V_{oc} (KOH-$Se^{-/2-}$(aq))	V_{oc} (CH_3CN-$MV^{2+/+}$)	V_{oc} (CH_3CN-$Fc^{+/0}$)
Etched	602 ± 18	463 ± 17	643 ± 17
Rh^{III}	630 ± 19	440 ± 19	580 ± 21
Co^{III}	658 ± 13	470 ± 13	616 ± 19
Ru^{III}	662 ± 16	451 ± 11	623 ± 19
Os^{III}	657 ± 16	470 ± 13	600 ± 18

representative experiment, a freshly etched electrode was first immersed in CH_3CN-$Fc^{+/0}$, and J-V data similar to that in Figure 5a (dashed curve) were observed. This electrode was then immersed in KOH-$Se^{-/2-}$(aq), and the J-V data were then consistent with that of a freshly etched GaAs surface (Figure 5b, dashed curve). Upon immersion in CH_3CN-$MV^{2+/+}$, this electrode then displayed a high fill factor and a low V_{oc}, as shown in Figure 5c (dashed curve). The electrode was then immersed for 60 seconds in a 0.010 **M** solution of $RuCl_3$ (pH 2.0), rinsed with water, dried and immersed in CH_3CN-$Fc^{+/0}$. As expected, this contact displayed J-V behavior in accord with Figure 5a (solid curve). Next this electrode was immersed in KOH-$Se^{-/2-}$(aq) solution, and the J-V behavior was as expected for a typical n-GaAs/Ru/KOH-$Se^{-/2-}$(aq) contact (Figure 5b, solid curve). This electrode was then transferred to a CH_3CN-$MV^{2+/+}$ solution, and the expected J-V curve for a n-GaAs/CH_3CN-$MV^{2+/+}$ contact (Figure 5c, solid curve) was obtained. This same electrode was further electrochemically cycled in the three solutions in the order: CH_3CN-$Fc^{+/0}$, CH_3CN-$MV^{2+/+}$, CH_3CN-$Fc^{+/0}$, CH_3CN-$MV^{2+/+}$, KOH-$Se^{-/2-}$(aq), CH_3CN-$MV^{2+/+}$, KOH-$Se^{-/2-}$(aq). In each solution the I-V curve observed was characteristic, in shape and V_{oc} value, of the solution in which the n-GaAs/Ru^{III} electrode was immersed. Finally this electrode was etched and re-immersed into the KOH-$Se^{-/2-}$(aq) solution. The sigmoidal curve and low V_{oc} value observed at this point discounted the possibility that the high fill factor and V_{oc} observed for the metal-ion treated surface in KOH-$Se^{-/2-}$(aq) was due to contamination of the solution by the previous electrochemical treatments. Results from similar experiments performed with Rh^{III}, Co^{III} and Os^{III} are shown in Figures 6, 7 and 8 respectively. This extensive set of controls clearly demonstrated that the composition of the liquid phase was critical in determining the electrical behavior of the semiconductor/liquid junction.

Figure 5. Current density-voltage characteristics (scan rate: 50 mV/s) for freshly etched (dashed curves) and Ru^{III}-exposed (solid curves) n-GaAs electrodes in (a) CH_3CN-$Fc^{+/0}$, (b) KOH-$Se^{-/2-}$(aq) and (c) CH_3CN-$MV^{2+/+}$ solutions. In each measurement, illumination intensity was adjusted to obtain a current density of 1.0 mA/cm^2 at +0.05 V*vs.* the Nernstian potential of the cell. The text contains a detailed protocol for this sequence of experiments. The key point is that the J-V properties of each contact were distinguishable from, and not affected by, the other contacts in the sequence.

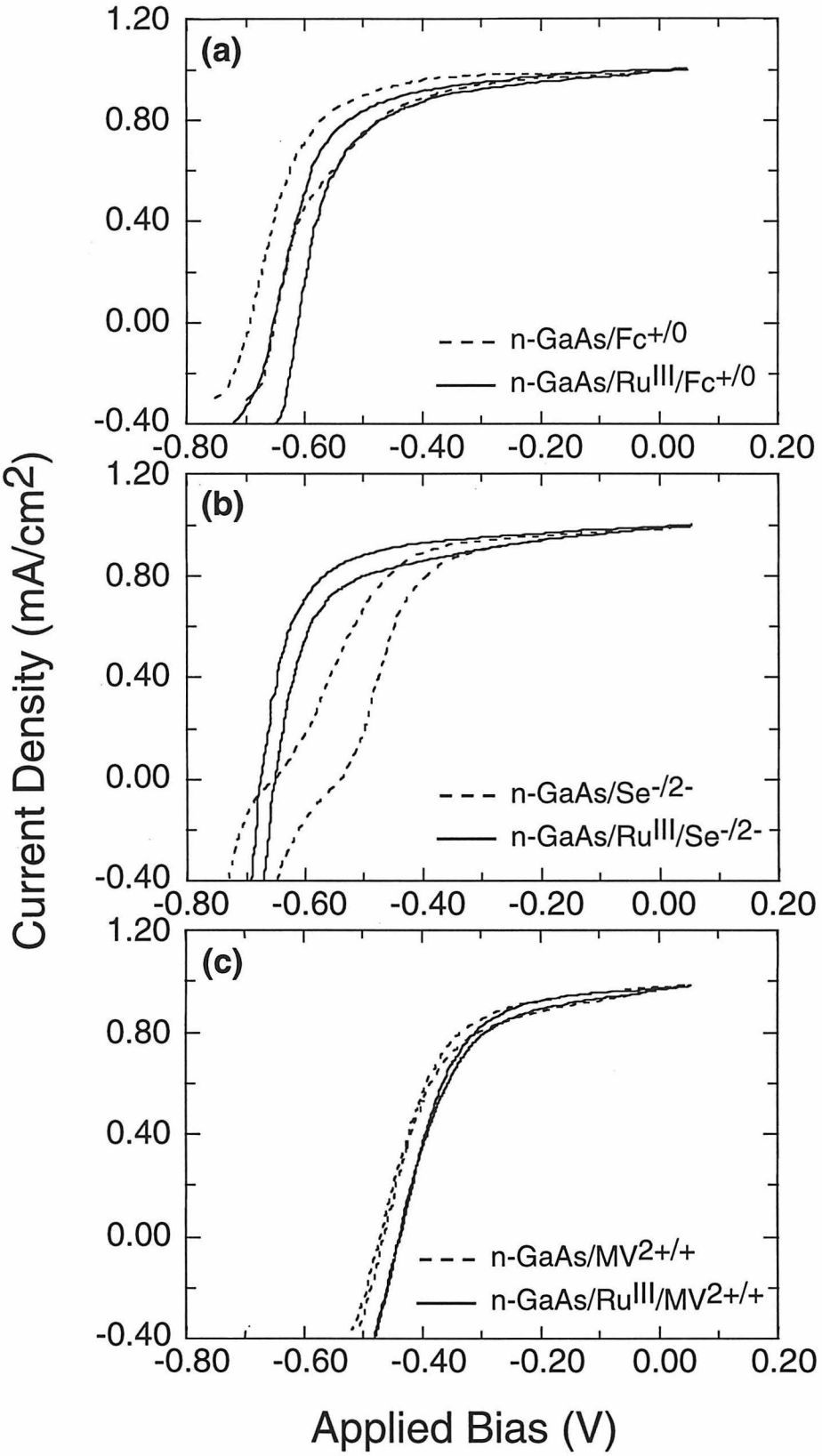
(a)
(b)
(c)
n-GaAs/Fc+/0
n-GaAs/RuIII/Fc+/0
n-GaAs/Se-/2-
n-GaAs/RuIII/Se-/2-
n-GaAs/MV2+/+
n-GaAs/RuIII/MV2+/+
1.20
0.80
0.40
0.00
-0.40
-0.80
-0.60
-0.40
-0.20
0.00
0.20
Current Density (mA/cm2)
Applied Bias (V)

Figure 6. Current density-voltage characteristics (scan rate: 50 mV/s) for freshly etched (dashed curves) and Rh^{III}-exposed (solid curves) n-GaAs electrodes in (a) $CH_3CN\text{-}Fc^{+/0}$, (b) $KOH\text{-}Se^{-/2-}(aq)$ and (c) $CH_3CN\text{-}MV^{2+/+}$ solutions. In each measurement, illumination intensity was adjusted to obtain a current density of 1.0 mA/cm^2 at +0.05 V*vs.* the Nernstian potential of the cell. The J-V properties of each contact were distinguishable from, and not affected by, the other contacts in the sequence.

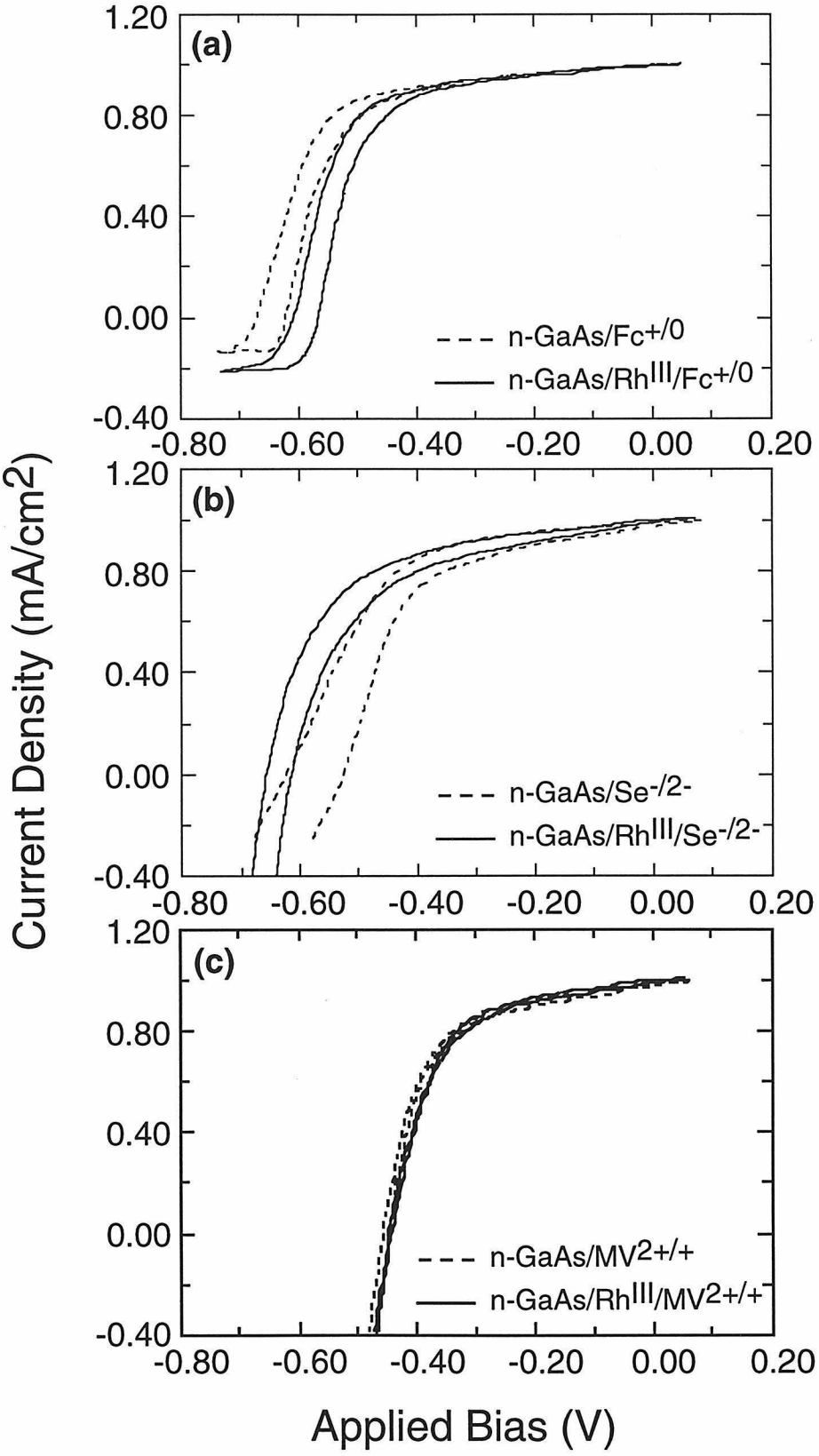
(a)
n-GaAs/Fc+/0
n-GaAs/RhIII/Fc+/0
(b)
n-GaAs/Se-/2-
n-GaAs/RhIII/Se-/2-
(c)
n-GaAs/MV2+/+
n-GaAs/RhIII/MV2+/+
1.20
0.80
0.40
0.00
-0.40
-0.80
-0.60
-0.40
-0.20
0.00
0.20
Current Density (mA/cm2)
Applied Bias (V)

Figure 7. Current density-voltage characteristics (scan rate: 50 mV/s) for freshly etched (dashed curves) and Co^{III}-exposed (solid curves) n-GaAs electrodes in (a) $CH_3CN\text{-}Fc^{+/0}$, (b) $KOH\text{-}Se^{-/2-}(aq)$ and (c) $CH_3CN\text{-}MV^{2+/+}$ solutions. In each measurement, illumination intensity was adjusted to obtain a current density of 1.0 mA/cm^2 at +0.05 V*vs.* the Nernstian potential of the cell. The J-V properties of each contact were distinguishable from, and not affected by, the other contacts in the sequence.

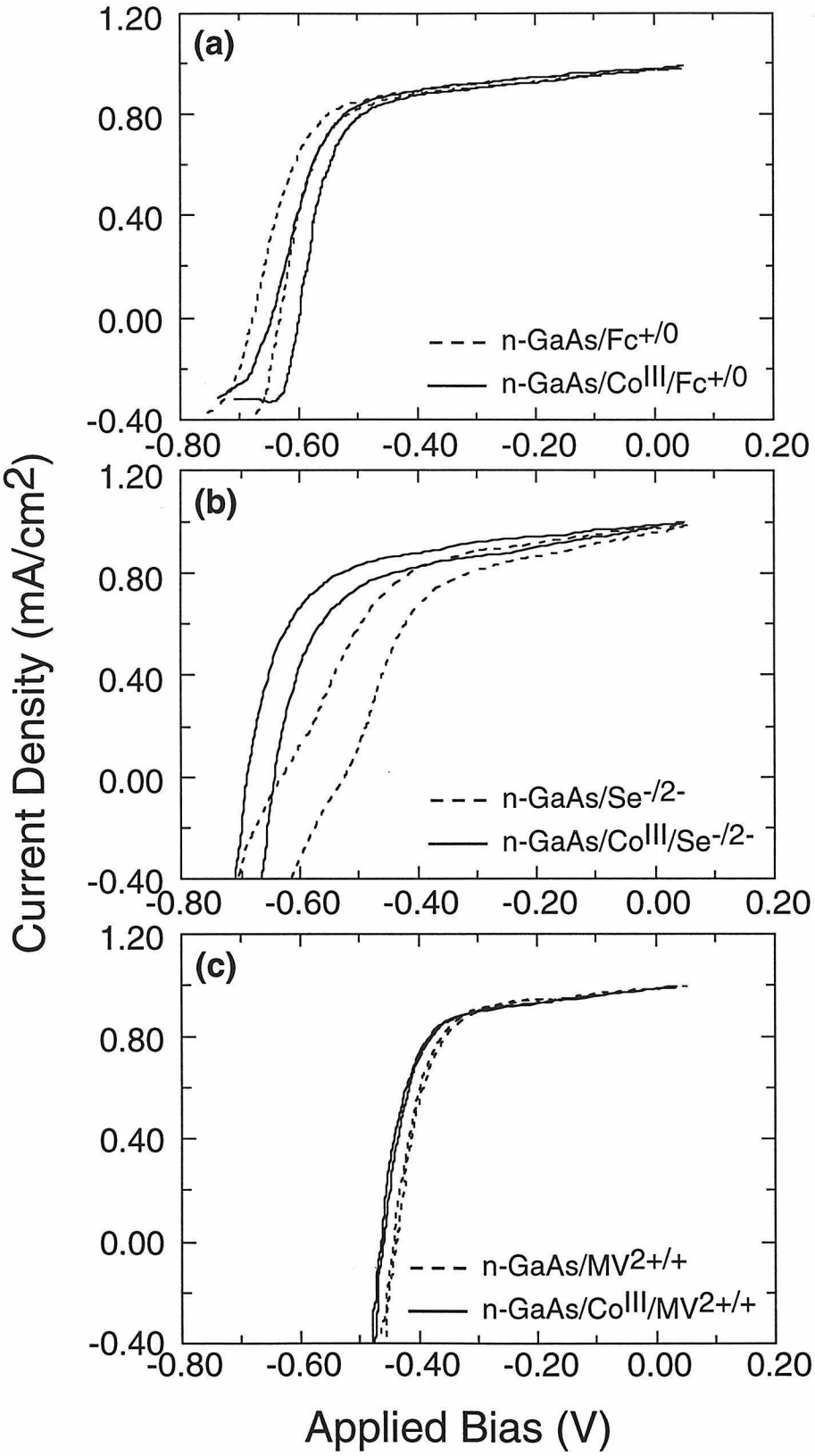
(a)
n-GaAs/Fc+/0
n-GaAs/CoIII/Fc+/0
(b)
n-GaAs/Se-/2-
n-GaAs/CoIII/Se-/2-
(c)
n-GaAs/MV2+/+
n-GaAs/CoIII/MV2+/+
Current Density (mA/cm2)
Applied Bias (V)
1.20
0.80
0.40
0.00
-0.40
-0.80
-0.60
-0.40
-0.20
0.00
0.20

Figure 8. Current density-voltage characteristics (scan rate: 50 mV/s) for freshly etched (dashed curves) and Os^{III}-exposed (solid curves) n-GaAs electrodes in (a) CH_3CN-$Fc^{+/0}$, (b) KOH-$Se^{-/2-}$(aq) and (c) CH_3CN-$MV^{2+/+}$ solutions. In each measurement, illumination intensity was adjusted to obtain a current density of 1.0 mA/cm^2 at +0.05 V*vs.* the Nernstian potential of the cell. The J-V properties of each contact were distinguishable from, and not affected by, the other contacts in the sequence.

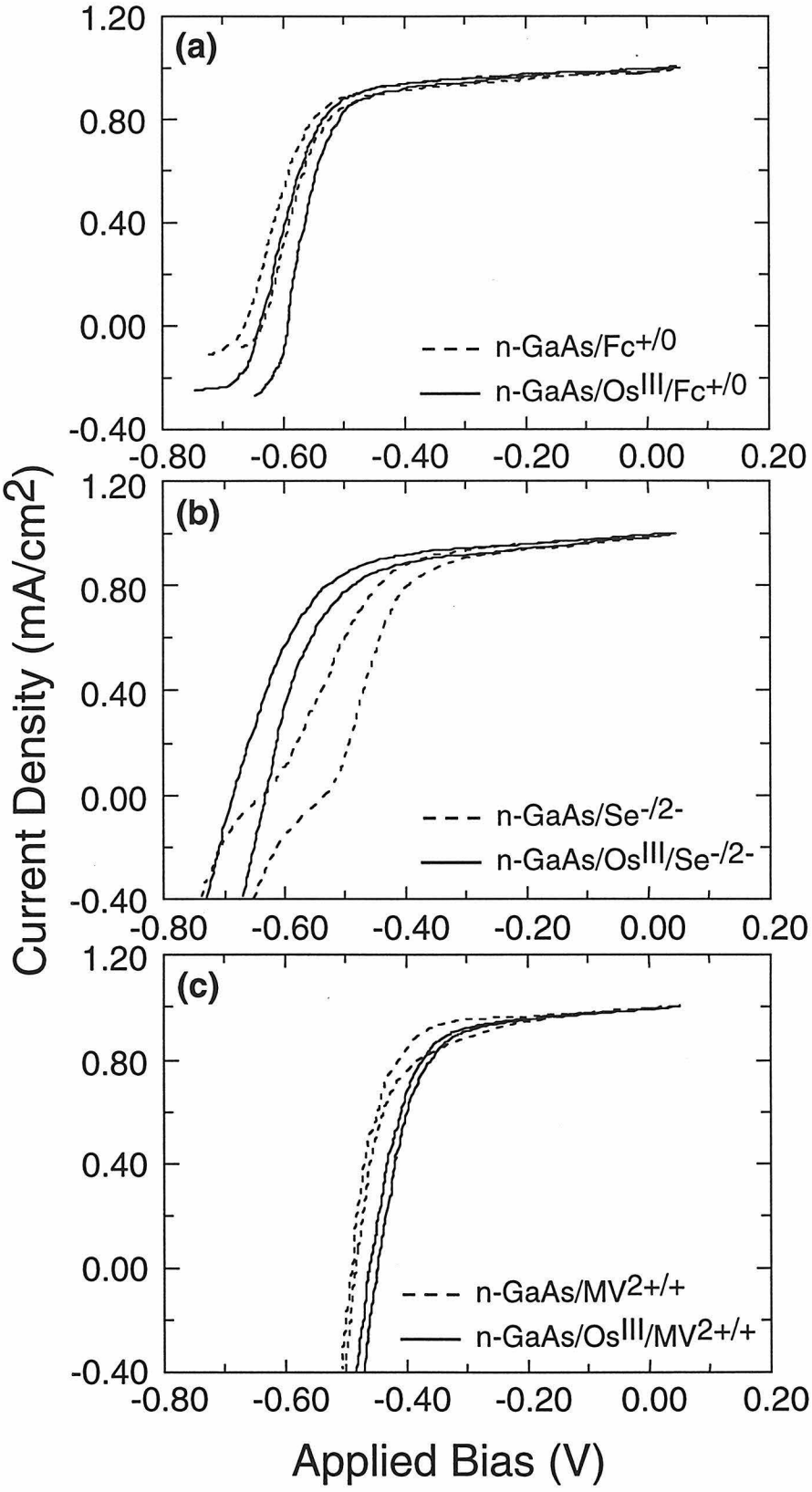
(a)
(b)
(c)
n-GaAs/Fc+/0
n-GaAs/OsIII/Fc+/0
n-GaAs/Se-/2-
n-GaAs/OsIII/Se-/2-
n-GaAs/MV2+/+
n-GaAs/OsIII/MV2+/+
1.20
0.80
0.40
0.00
-0.40
-0.80
-0.60
-0.40
-0.20
0.00
0.20
Current Density (mA/cm2)
Applied Bias (V)

4. General Comments on the n-GaAs/M/Liquid Contact

The I-V behavior of n-GaAs/M/liquid interfaces described above indicated that these types of junctions are best viewed as "hybrid" semiconductor/metal/liquid contacts. In such systems, all three components of the junction had a significant influence on the rate-determining process for majority carrier recombination. The role of the chemisorbed metal in the n-GaAs/M/KOH-$Se^{-/2-}$(aq) system was thus best described as catalyzing interfacial charge transfer at a semiconductor/liquid interface, as opposed to establishing a semiconductor/metal or semiconductor/insulator/metal contact that was exposed to, but not influenced by, the electrolyte solution.

The absence of Schottky barrier formation in the n-GaAs/M/KOH-$Se^{-/2-}$(aq) system was also in agreement with the analysis of data obtained from the short wavelength spectral response experiments for n-GaAs/metal/liquid interfaces.[69] This data indicated that the majority carrier collection velocity for n-GaAs/M/KOH-$Se^{-/2-}$(aq) contacts was $\leq 10^6$ cm/sec, whereas collection velocities $\approx 10^7$ cm/sec were observed for n-GaAs/metal Schottky barriers. The spectral response data did not, however, rule out "buried" MIS behavior for this system, nor did it establish a quantitative upper limit on the fractional coverage of Schottky barrier formation. The I-V data reported above not only complement these prior conclusions but also extended them quantitatively.

This difference between the electrical behavior of chemisorbed metal species and metallic deposits formed in UHV has important ramifications for photoelectrochemistry. It is required to account for the high V_{oc} values, and high energy conversion efficiencies, of n-GaAs/metal/poly-(3-methylthiophene)/liquid interfaces[70,71] and must also be considered when comparing the I-V properties of semiconductor/metal junctions made in UHV to those of semiconductor particles that are partially coated with chemically-deposited metal species.[72-75] Vacuum deposition methods should thus not generally be expected to produce contacts that are similar to those obtained from aqueous chemisorption techniques.

5. Current-Voltage Behavior of n-GaAs in Contact with CH_3CN-$CoCp_2^{+/0}$ Solutions

During the course of this study,[7] the I-V behavior of n-GaAs in contact with CH_3CN-$CoCp_2^{+/0}$ solutions was also investigated. This semiconductor/liquid contact displayed numerous complications, and it was eventually judged to be inappropriate for the purposes of this study. However, the results are briefly described below, because they are relevant to recent reports that have used GaAs/CH_3CN-$CoCp_2^{+/0}$ contacts in picosecond studies of interfacial charge transfer events.[76]

Figure 9a displays the J-V data for n-GaAs/CH_3CN-$CoCp_2^{+/0}$ contacts. Curiously, the open circuit voltage of etched n-GaAs anodes in CH_3CN-$CoCp_2^{+/0}$ was larger than that for n-GaAs/CH_3CN-$MV^{2+/+}$ contacts, despite the more negative redox potential of the CH_3CN-$CoCp_2^{+/0}$ solution. This observation was, however, consistent with prior investigations of n-GaAs/CH_3CN-$CoCp_2^{+/0}$ contacts.[61,64,66,77] An additional complication was observed when evaluating the chemical reactivity of n-GaAs/CH_3CN-$CoCp_2^{+/0}$ interfaces. Although immersion and electrochemical cycling in CH_3CN-$MV^{2+/+}$ or CH_3CN-$Fc^{+/0}$ electrolytes did not noticeably affect the J-V properties of n-GaAs photoanodes in contact with KOH-$Se^{-/2-}$(aq) electrolytes (*vide supra*), n-GaAs electrodes that had been electrochemically cycled in contact with CH_3CN-$CoCp_2^{+/0}$ solutions exhibited markedly improved J-V curves and significant changes in V_{oc} in contact with KOH-$Se^{-/2-}$(aq) solutions (Figure 9b). This behavior clearly indicated that chemical changes, producing an electrocatalyst for Se^{2-}(aq) oxidation, had occurred at the n-GaAs/CH_3CN-$CoCp_2^{+/0}$ interface. Similar changes in J-V behavior were observed for etched GaAs surfaces that had been exposed to 1.0 M $Na_2S{\bullet}9H_2O$(aq), rinsed with H_2O, and then briefly illuminated with 70 ps, 530 nm laser pulses in CH_3CN-$CoCp_2^{+/0}$ solutions prior to immersion in the KOH-$Se^{-/2-}$(aq) electrolyte.

For GaAs surfaces that had been exposed to CH_3CN-$CoCp_2^{+/0}$ solutions under our conditions, the reactivity of the 19-electron $CoCp_2$ complexes, coupled with the fact that

Figure 9. (a) Current density-voltage characteristics (scan rate: 50 mV/s) of n-GaAs/CH_3CN-0.70 **M** $LiClO_4$-0.050 **M** $CoCp_2$-≈0.50 mM $CoCp_2^+PF_6^-$ contacts. The dashed curve is the data from a freshly etched electrode, while the solid curve depicts the data after deliberate exposure of the n-GaAs surface to a solution of 0.010 **M** (pH 12.0) $Co(NH_3)_6Cl_3$. (b) Current density-voltage characteristics of n-GaAs/KOH-$Se^{-/2-}$(aq) contacts. The dashed curve is the data from a freshly etched electrode, while the solid curve represents the data for the same electrode after it had been electrochemically cycled in the CH_3CN-$CoCp_2^{+/0}$ solution. In each experiment of this figure, the illumination intensity was adjusted to obtain a current density of 5.0 mA/cm^2 at +0.05 V *vs.* the Nernstian potential of the cell.

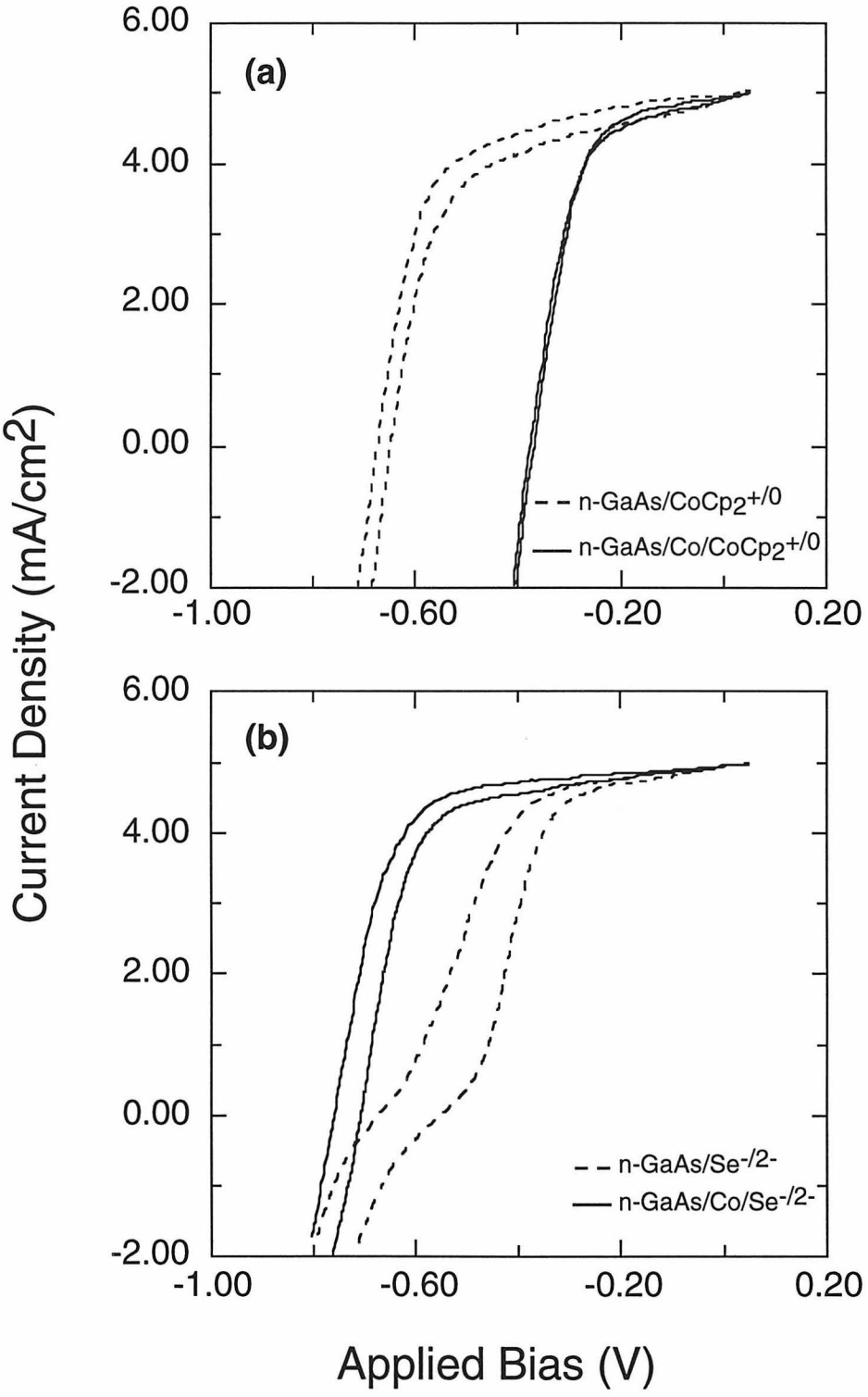
(a)
(b)
6.00
4.00
2.00
0.00
-2.00
-1.00
-0.60
-0.20
0.20
n-GaAs/CoCp2+/0
n-GaAs/Co/CoCp2+/0
n-GaAs/Se-/2-
n-GaAs/Co/Se-/2-
Current Density (mA/cm2)
Applied Bias (V)

the V_{oc} and fill factor of the resulting n-GaAs/KOH-$Se^{-/2-}$(aq) contacts were similar to those of n-GaAs/Co/KOH-$Se^{-/2-}$(aq) contacts,[31] suggested that cobalt had deposited onto the GaAs surface. In fact, similar changes were observed when n-GaAs electrodes were electrochemically cycled in CH_3CN solutions containing the derivatized cobaltocenes $CoCp(CpCOOCH_3)$ and $Co(CH_3Cp)_2$ and then evaluated in contact with the KOH-$Se^{-/2-}$(aq) electrolyte. However, the surface chemistry must be more complicated than this simple picture, because deliberate chemisorption of Co (from $[Co(NH_3)_6^{3+}(aq)]$) onto n-GaAs photoanodes only produced V_{oc} values of 0.37 V in contact with CH_3CN-$CoCp_2^{+/0}$ solutions.(Figure 9a, solid curve)

It is evident from the data presented above that, under our experimental conditions, CH_3CN-$CoCp_2^{+/0}$ solutions induced significant changes in the electrical properties of GaAs surfaces. These observations are relevant to the interpretation of a recent real-time kinetics study,[76] which concluded that electron transfer processes at GaAs/CH_3CN-$CoCp_2^{+/0}$ contacts were five orders of magnitude more rapid than predicted by theory. A rigorous comparison between such experiments and existing theory[78-80] requires that the dissolved acceptors act as purely outer sphere electron transfer reagents, that the acceptor concentration at the semiconductor/liquid interface equals the acceptor concentration in the bulk of the solution, that the acceptors are randomly distributed in distance relative to the solid/liquid interface, and that exposure to the electrolyte solution and light source does not induce changes in the surface chemistry or in the surface state density of the semiconductor.[80] The J-V experiments presented above clearly indicate that these criteria are not met for GaAs/CH_3CN-$CoCp_2^{+/0}$ contacts under the experimental conditions described in this work. The protocol established herein, of ensuring a chemically inert surface through electrical I-V measurements in various electrolytes, thus provided a convenient means for identifying semiconductor/liquid contacts that are suitable for unambiguous real-time kinetic analyses.

IV. CONCLUSIONS

The chemisorption of metal ions onto n-GaAs surfaces has been shown to yield improved I-V characteristics in contact with KOH-$Se^{-/2-}$(aq) electrolytes, but such chemisorption does not affect the electrical behavior of n-GaAs/CH_3CN-$Fc^{+/0}$ or n-GaAs/CH_3CN-$MV^{2+/+}$ contacts. n-GaAs/metal/liquid contacts (with M=Rh^{III}, Co^{III}, Ru^{III}, Os^{III}) responded to changes in the chemical composition of the liquid phase, and the electrical properties of such contacts were sensitive to the redox potential of the contacting solution. These observations demonstrated that such contacts were best represented as "hybrid" semiconductor/metal/liquid contacts, as opposed to "buried" semiconductor/metal or semiconductor/insulator/metal junctions in electrical contact with the electrolyte solution. n-GaAs/CH_3CN-$CoCp_2^{+/0}$ contacts were found to be chemically reactive under photoelectrochemical conditions, and did not provide useful systems for evaluating outer sphere charge transfer theories for semiconductor/liquid interfaces. These studies underscore one of the useful features of semiconductor/liquid contacts, which is the ability to evaluate sequentially the electrical properties of semiconductor surfaces in various contacting media without inducing irreversible chemical changes during the process of contact formation. "Hybrid" semiconductor/metal/liquid contacts offer potential efficiency advantages over "buried" semiconductor/metal Schottky barrier devices, and the identification of such behavior opens an interesting avenue for future research in the photoelectrochemistry of III-V materials.

V. REFERENCES

(1) Bolts, J. M.; Bocarsly, A. B.; Palazzotto, M. C.; Walton, E. G.; Lewis, N. S.; Wrighton, M. S. *J. Am. Chem. Soc.* **1979**, *101*, 1378.

(2) Bansal, A.; Li, X.; Lauermann, I.; Lewis, N. S.; Yi, S. I.; Weinberg, W. H. *J. Am. Chem. Soc.* **1996**, *118*, 7225.

(3) Linford, M. R.; Chidsey, C. E. D. *J. Am. Chem. Soc.* **1993**, *115*, 12631.

(4) Linford, M. R.; Fenter, P.; Eisenberger, P. M.; Chidsey, C. E. D. *J. Am. Chem. Soc.* **1995**, *117*, 3145.

(5) Chang, K. C.; Heller, A.; Schwartz, B.; Menezes, S.; Miller, B. *Science* **1977**, *196*, 1097.

(6) Tufts, B. J.; Abrahams, I. L.; Santangelo, P. G.; Ryba, G. N.; Casagrande, L. G.; Lewis, N. S. *Nature* **1987**, *326*, 861.

(7) Bansal, A.; Tan, M. X.; Tufts, B. J.; Lewis, N. S. *J. Phys. Chem.* **1993**, *97*, 7309.

(8) Gu, Y.; Lin, Z.; Butera, R. A.; Smentkowski, V. S.; Waldeck, D. H. *Langmuir* **1995**, *11*, 1849.

(9) Sturzenegger, M.; Lewis, N. S. *J. Am. Chem. Soc.* **1996**, *118*, 3045.

(10) Smestad, G.; Bignozzi, C.; Argazzi, R. *Solar Energy Mater. Solar Cells* **1994**, *32*, 259.

(11) Nazeeruddin, M. K.; Kay, A.; Rodicio, I.; Humphrybaker, R.; Muller, E.; Liska, P.; Vlachopoulos, N.; Grätzel, M. *J. Am. Chem. Soc.* **1993**, *115*, 6382.

(12) Parkinson, B. A.; Spitler, M. T. *Electrochim. Acta.* **1992**, *37*, 943.

(13) Ellis, A. B.; Bolts, J. M.; Kaiser, S. W.; Wrighton, M. S. *J. Am. Chem. Soc.* **1977**, *99*, 2848.

(14) Vanmaekelbergh, D.; Cardon, F. *Electrochim. Acta* **1992**, *37*, 837.

(15) Lunt, S. R.; Ryba, G. N.; Santangelo, P. G.; Lewis, N. S. *J. Appl. Phys.* **1991**, *70*, 7449.

(16) Lunt, S. R.; Casagrande, L. G.; Tufts, B. J.; Lewis, N. S. *J. Phys. Chem.* **1988**, *92*, 5766.

(17) Tan, M. X.; Newcomb, C.; Kumar, A.; Lunt, S. R.; Sailor, M. J.; Tufts, B. J.; Lewis, N. S. *J. Phys. Chem.* **1991**, *95*, 10133.

(18) Parkinson, B. A.; Heller, A.; Miller, B. *Appl. Phys. Lett.* **1978**, *33*, 521.

(19) Parkinson, B. A.; Heller, A.; Miller, B. *J. Electrochem. Soc.* **1979**, *126*, 954.

(20) Heller, A. *Acc. Chem. Res.* **1981**, *14*, 154.

(21) Allongue, P.; Cachet, H.; Horowitz, G. *J. Electrochem. Soc.* **1983**, *130*, 2352.

(22) Allongue, P.; Cachet, H. *J. Electrochem. Soc.* **1985**, *132*, 45.

(23) Allongue, P.; Cachet, H. *Sol. St. Commun.* **1985**, *55*, 49.

(24) Allongue, P.; Cachet, H. *J. Electrochem. Soc.* **1984**, *131*, 2861.

(25) Noufi, R.; Tench, D. *J. Electrochem. Soc.* **1980**, *127*, 188.

(26) Burk, J., A. A.; Johnson, P. B.; Hobson, W. S.; Ellis, A. B. *J. Appl. Phys.* **1986**, *59*, 1621.

(27) Heller, A.; Lewerenz, H. J.; Miller, B. *Ber. Bunsenges. Phys. Chem.* **1980**, *84*, 592.

(28) Heller, A. In *Photoeffects at Semiconductor-Electrolyte Interfaces* ; A. J. Nozik, Ed.; The Society: Washington, D.C., 1981; Vol. 146; pp 57.

(29) Gomez-Jahn, L. A.; Kasinski, J. J.; Miller, R. J. D. In *SPIE Int. Soc. Opt. Eng.*; 1990; pp 97.

(30) Gronet, C. M.; Lewis, N. S. *J. Phys. Chem.* **1984**, *88*, 1310.

(31) Tufts, B. J.; Abrahams, I. L.; Casagrande, L. G.; Lewis, N. S. *J. Phys. Chem.* **1989**, *93*, 3260.

(32) Ryba, G. N.; Kenyon, C. N.; Lewis, N. S. *J. Phys. Chem.* **1993**, *97*, 13814.

(33) Ali, S. T.; Ghosh, S.; Bose, D. N. *Appl. Surf. Sci.* **1996**, *93*, 37.

(34) Nelson, R. J.; Williams, J. S.; Leamy, H. J.; Miller, B.; Casey, H. C., Jr.; Parkinson, B. A.; Heller, A. *Applied Physics Letters* **1980**, *36*, 76.

(35) Nakato, Y.; Ohnishi, T.; Tsubomura, H. *Chem. Lett.* **1975**, 883.

(36) Nakato, Y.; Abe, K.; Tsubomura, H. *Ber. Bunsenges. Phys. Chem.* **1976**, *80*, 1002.

(37) Nakato, Y.; Yano, H.; Tsubomura, H. *Chem. Lett.* **1986**, 987.

(38) Nakato, Y.; Tsubomura, H. *Ber. Bunsenges Phys. Chem.* **1987**, *91*, 405.

(39) Nakato, Y.; Ueda, K.; Yano, H.; Tsubomura, H. *J. Phys. Chem.* **1988**, *92*, 2316.

(40) Kobayashi, H.; Mizuno, F.; Nakato, Y.; Tsubomura, H. *J. Phys. Chem.* **1991**, *95*, 819.

(41) Heller, A. In *Energy Resour. Photochem. Catal.* ; M. Grätzel, Ed.; Academic: New York, 1983; pp 385.

(42) Rubin, H.-D.; Humphrey, B. D.; Bocarsly, A. B. *Nature* **1984**, *308*, 339.

(43) Mandel, K. C.; Basu, S.; Bose, D. N. *J. Phys. Chem.* **1987**, *91*, 4011.

(44) Lewerenz, H. J.; Goslowsky, H. *J. Appl. Phys.* **1988**, *63*, 2420.

(45) Dominey, R. N.; Lewis, N. S.; Wrighton, M. S. *J. Am. Chem. Soc.* **1981**, *103*, 1261.

(46) Rhoderick, E. H.; Williams, R. H. *Metal-Semiconductor Contacts;* 2nd ed.; Oxford University Press: New York, 1988.

(47) Sze, S. M. *The Physics of Semiconductor Devices;* 2nd ed.; Wiley: New York, 1981.

(48) Brillson, L. J. *Surf. Sci. Rep.* **1982**, *2*, 123.

(49) Spicer, W. E.; Lindau, I.; Skeath, P.; Su, C. Y. *J. Vac. Sci. Technol.* **1980**, *17*, 1019.

(50) Spicer, W. E.; Kendelewicz, T. J.; Newman, N.; Chin, K. K.; Lindau, I. *Surf. Sci.* **1986**, *168*, 240.

(51) Tufts, B. J.; Casagrande, L. G.; Lewis, N. S.; Grunthaner, F. J. *Appl. Phys. Lett.* **1990**, *57*, 2262.

(52) Stirn, R. J. *Appl. Phys. Commun.* **1981**, *1*, 43.

(53) Casagrande, L. G.; Lewis, N. S. *J. Am. Chem. Soc.* **1985**, *107*, 5793.

(54) Allongue, P.; Souteyrand, E. *J. Vac. Sci. Technol.* **1987**, *B 5*, 1644.

(55) Reineke, R.; Memming, R. *Surf. Sci.* **1987**, *192*, 66.

(56) Childs, R. B.; Ruths, J. M.; Sullivan, T. M.; Fonash, S. J. *J. Vac. Sci. Technol.* **1978**, *15*, 1397.

(57) Stirn, R. J.; Yeh, Y. C. M. *Appl. Phys. Lett.* **1975**, *27*, 95.

(58) Vasquez, R. P.; Lewis, B. F.; Grunthaner, F. J. *J. Vac. Sci. Technol.* **1983**, *B1*, 791.

(59) Stocker, H. J.; Aspnes, D. E. *Appl. Phys. Lett.* **1983**, *42*, 85.

(60) Sheats, J. E.; Rausch, M. D. *J. Org. Chem.* **1970**, *35*, 3245.

(61) Casagrande, L. G. Ph.D. Thesis, Stanford University, 1988.

(62) Gronet, C. M.; Lewis, N. S. *Appl. Phys. Lett.* **1983**, *43*, 115.

(63) Kohl, P. A.; Bard, A. J. *J. Electrochem. Soc.* **1979**, *126*, 603.

(64) Ba, B.; Fotouhi, B.; Gabouze, N.; Gorochov, O.; Cachet, H. *J. Electroanal. Chem.* **1992**, *334*, 263.

(65) Fan, F. R. F.; Reichman, B.; Bard, A. J. *J. Am. Chem. Soc.* **1980**, *102*, 1488.

(66) Gabouze, N.; Fotouhi, B.; Gorochov, O.; Cachet, H.; Yao, N. A. *J. Electroanal. Chem.* **1987**, *237*, 289.

(67) Rosenbluth, M. L.; Lewis, N. S. *J. Am. Chem. Soc.* **1986**, *108*, 4689.

(68) Bocarsly, A. B.; Bookbinder, D. C.; Dominey, R. N.; Lewis, N. S.; Wrighton, M. S. *J. Am. Chem. Soc.* **1980**, *102*, 3683.

(69) Kumar, A.; Lewis, N. S. *J. Phys. Chem.* **1990**, *94*, 6002.

(70) Horowitz, G.; Tourillon, G.; Garnier, F. *J. Electrochem. Soc.* **1984**, *131*, 151.

(71) Horowitz, G.; Garnier, F. *J. Electrochem. Soc.* **1985**, *132*, 634.

(72) Memming, R. In *Topics in Current Chemistry* ; E. Stickham, Ed.; Springer Verlag: 1978; Vol. 143; pp 79.

(73) Wang, C.-M.; Heller, A.; Gerischer, H. *J. Am. Chem. Soc.* **1992**, *114*, 5230.

(74) Yesodharan, E.; Grätzel, M. *Helv. Chim. Acta* **1983**, *66*, 2145.

(75) Vrachnou, E.; Grätzel, M.; McEvoy, A. J. *J. Electroanal. Chem.* **1989**, *258*, 193.

(76) Rosenwaks, Y.; Thacker, B. R.; Ahrenkiel, R. K.; Nozik, A. J. *J. Phys. Chem.* **1992**, *96*, 10096.

(77) Ba, B.; Cachet, H.; Fotouhi, B.; Gorochov, O. *Electrochim. Acta* **1992**, *37*, 309.

(78) Marcus, R. A. *J. Phys. Chem.* **1990**, *94*, 1050.

(79) Gerischer, H. *Electrochim. Acta* **1990**, *35*, 1677.

(80) Lewis, N. S. *Ann. Rev. Phys. Chem.* **1991**, *42*, 543.

Chapter 3

Modification of Si(111) Surfaces with Covalently Attached Alkane Chains

Abstract

The ability to modify Si surface without partial oxidation or formation of electrical defects is potentially important for fabrication of improved electronic devices and for fundamental charge transfer studies at semiconductor/liquid interfaces. However, little is known about the chemistry of Si surfaces under ambient temperature and pressure. A two-step halogenation/alkylation route to chemical functionalization of the Si(111) surface is described here that allows covalent attachment of alkyl functionalities without concomitant oxidation of the silicon surface. In the first step, a hydrogen-terminated silicon surface is treated with a chlorinating agent to obtain a chlorine-terminated silicon surface. In the second step, the chlorinated surface is reacted with alkyl lithium or alkyl Grignard to obtain an alkyl-terminated surface. The surface of silicon at each step of the preparation has been extensively analyzed using a number of surface science techniques, including x-ray photoelectron spectroscopy (XPS), high resolution electron energy loss spectroscopy (HREELS), infrared spectroscopy (IRS), Auger electron spectroscopy (AES), and Temperature programmed desorption (TPD). The alkyl monolayers are found to be chemically robust and, as compared to an H-terminated surface, the alkyl-terminated surfaces are more resistant to oxidation either in air or in contact with wet chemical environments.

I. INTRODUCTION

Despite the fact that the H-terminated silicon surface is the starting point for the construction of most contemporary electronic devices,[1] very little is known about the chemical reactions of this surface under ambient temperature and pressure.[2-9] The excellent physical and electrical properties of these H-terminated surfaces are short lived due to oxidation in the air.[10] Also, these surfaces are unstable in contact with aqueous media and photooxidize or photocorrode rapidly under illumination.[11-14] Functionalization of Si without partial oxidation and/or formation of electrical defects is potentially important in fabricating improved electronic devices[15,16] as well as in measurement of charge transfer rate constants at semiconductor/liquid contacts.[17] Carefully designed surface modifications can also provide a means to control the chemical, physical and electrical properties of semiconductor/liquid interfaces for other applications such as catalysis,[18-20] corrosion,[21,22] lubrication,[23,24] adhesion,[25] sensors,[26,27] lithography,[28-32] non-linear optics,[33] molecular electronics,[34,35] solar energy conversion,[2-4,36] toxic waste treatment,[37-42] and non-destructive materials' characterization.[43,44]

The formation of monomolecular assemblies at semiconductor surfaces provides a rational approach for fabricating interfaces with a well-defined composition, structure, thickness and properties.[26,27,32,45,46] Prior modifications of the silicon surface using this approach have included surface attachment of various electroactive moieties,[14,47-49] preparing surfaces with desired functional groups as sensors,[26,27,50] lithographic patterning of organosilane self-assembling monolayers[32,51-56] and Langmuir-Blodgett films.[45,46,57] The chemistry involved in this process is now well understood, and mostly consists of oxidation followed by conventional oxide functionalization through use of silanization agents. The non-optimal oxides introduced by this process can induce electrical defects at the Si/Si-oxide interface and can degrade the electrical properties of the interface. In this mode of surface functionalization, the electrical properties of the Si surface are sacrificed in order to obtain desirable chemical attributes.

Bansal et al.[2] and Linford et al.[3,4] recently showed that well-defined monolayers of reagents with desired functional groups can be prepared on the silicon surface by covalently linking the molecules directly to the unoxidized silicon surface without the formation of a intervening oxide layer. This chapter describes the two-step chlorination/alkylation procedure by which the silicon surface can be modified without concomitant oxidation of the surface.[2] Extensive characterization of this silicon surface using surface science techniques has provided the first clear proof that the alkyl chains can be bound covalently to the surface silicon atoms. As compared to the H-terminated surface, silicon surfaces modified by this two-step process are shown to be more resistant towards oxidation in air and in contact with various wet chemical environments.

II. EXPERIMENTAL

1. Silicon Samples

The silicon (111) samples used in these experiments were of three different types. The silicon samples used for x-ray photoelectron spectroscopy (XPS), high resolution electron energy loss spectroscopy (HREELS), temperature programmed desorption (TPD) and Auger electron spectroscopy (AES) were phosphorus doped n-type, single crystal Si(111) wafers of 100 mm diameter polished on one side, and were purchased from Wafernet Inc. They were either 500±50 μm thick and of 1.5-3.0 ohm cm resistivity or 575±20 μm thick and of 3-6 ohm cm resistivity. The wafers were cut into small pieces and derivatized as described below. The single crystal n-Si(111) samples used in glancing transmission IR (TIR) experiments were 525±25 μm thick, 100 mm diameter, double-polished wafers of 24-34 ohm cm resistivity. These double-polished wafers were generously provided by Mr. Daniel L. McDonald of Wacker Siltronic Corp. Samples of approximately 3 cm x 7 cm were cut and derivatized as described below. The silicon ATR "plates" used for attenuated total multiple internal reflection IR (ATR) experiments were

purchased from Harrick Scientific Corporation. They were 50 mm x 15 mm x 1 mm pieces of silicon in which the large parallel (50 mm x 15 mm) faces were (111) oriented and the two small ends (15 mm x 1 mm) had 45° bevels on each side through which infrared light entered and exited the sample (Figure 5b inset).

2. Chemicals

Anhydrous methanol (GR label) obtained from EM Science was further dried over powdered magnesium under nitrogen. Anhydrous tetrahydrofuran (THF) (GR label) was bought from EM Science and was dried over Na/benzophenone under nitrogen. The solvents were distilled under nitrogen, from their respective drying agents into 500 ml flasks and stored in a nitrogen purged glove box for further use. Anhydrous THF obtained from Aldrich (in 800 ml sureseal bottles) was taken into the glove box and used as received. Dichloromethane (Omnisolve grade) and 30% H_2O_2 were bought from EM Science. Concentrated H_2SO_4 was obtained from J.T. Baker

The following chemicals were purchased from Aldrich and were used as such: phosphorus pentachloride (PCl_5), chlorobenzene, benzoyl peroxide, CH_3MgBr (3.0 **M** in diethyl ether), C_2H_5MgBr (3.0 **M** in diethyl ether), C_4H_9Li (2.5 **M** in hexanes), C_4H_9MgCl (2.0 **M** in diethyl ether), $C_5H_{11}MgBr$ (3.0 **M** in diethyl ether), $C_6H_{13}Li$ (2.0 **M** in hexane), $C_6H_{13}MgBr$ (2.0 **M** in diethyl ether), $C_8H_{17}MgCl$ (2.0 **M** in THF), $C_{10}H_{21}MgBr$ (1.0 **M** in diethyl ether), $C_{12}H_{25}MgBr$ (1.0 **M** in diethyl ether), $C_{18}H_{37}MgCl$ (0.5 **M** in THF). $C_{10}H_{21}Li$ was prepared according to the method of Gilman et al.[58,59] and was used as such. $CF_3(CH_2)_3MgBr$ was prepared by reacting $CF_3(CH_2)_3Br$ (PCR Inc.) with Mg shavings.[60] CF_3CH_2OLi (0.77 **M**) was prepared by dissolving Li pieces in CF_3CH_2OH (Aldrich). Hydrofluoric acid buffered with ammonium fluoride (HF/NH_4F) solution and 40% ammonium fluoride (NH_4F) solution were obtained from Transene Co. (Rowland, MA).[61]

3. Surface Preparation

(a) Oxidation and Etching

Following literature procedure,[4] the silicon samples were oxidized in a "Pirhana" solution which consisted of conc H_2SO_4:H_2O_2 in the ratio 3:1 (v/v), heated to approx. 100°C. **Caution:** *The acidic "Pirhana" solution is extremely dangerous, particularly in contact with organic materials and should be handled extremely carefully.* Silicon samples were etched in HF/NH_4F solution for 1-2 min and were immersed in the Pirhana solution for 1 hour. The samples were then taken out, rinsed with copious amounts of water, dried at ~80°C and stored for further use. The silicon samples used in these experiments were always freshly etched just before use as this procedure was found to result in good quality surfaces. The samples were typically etched first in HF/NH_4F solution for 30-60 sec and then without rinsing were transferred to the ammonium fluoride solution (from Transene Co.) where they were kept for 10-15 min.[62] During this period, tiny bubbles appeared on the (111) face of the samples. The extent of surface uniformity, as measured by the intensity of silicon monohydride signal by IR spectroscopy, seemed to be insensitive to the exact immersion time in NH_4F. The samples were subsequently emmersed from NH_4F, rinsed briefly with flash photolysed water, dried under a stream of nitrogen and immediately characterized.

(b) Chlorination

The entire chlorination procedure was carried out in a custom-built nitrogen purged glove box that was connected via a gate valve to the UHV system housing the XPS spectrometer (Figure 1). The chlorinating solution was prepared by dissolving enough PCl_5 in chlorobenzene to form a near saturated solution (typically 0.6 **M**-0.7 **M**). PCl_5 did not dissolve in chlorobenzene right away and the solution had to be warmed to about 60 °C for a few hours to ensure that all PCl_5 had dissolved. Just before use, a small portion of the stock chlorinating solution was poured into a vial, a few grains of benzoyl peroxide

Figure 1. A Schematic of the UHV system used for XPS and LEED studies. Samples could be introduced either from air, through external load lock, or from a custom-built nitrogen purged glove box, through the internal load lock. All chlorination and alkylation reactions were performed in the glove box.

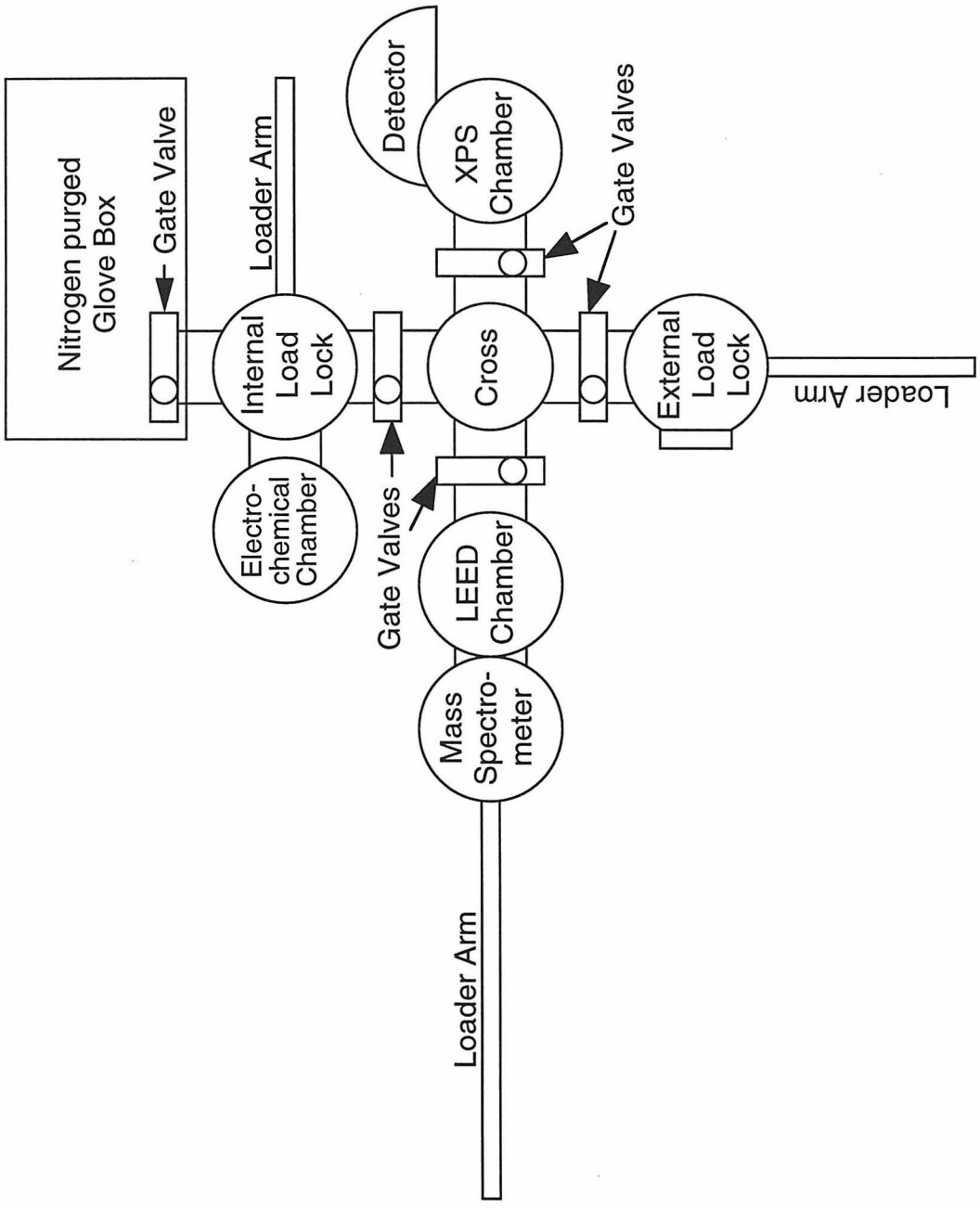
Nitrogen purged Glove Box
Gate Valve
Loader Arm
Internal Load Lock
Electro-chemical Chamber
Gate Valves
Cross
Detector
XPS Chamber
Gate Valves
External Load Lock
Loader Arm
LEED Chamber
Mass Spectro-meter
Loader Arm

were added (approximately 30-40 mg of benzoyl peroxide in 10 ml PCl_5/chloro-benzene solution) and the sample was immersed in this solution.[63,64] The solution containing the sample was then heated to 90-100 °C for 40-50 min. The sample was then taken out of the solution, rinsed with anhydrous THF followed by anhydrous methanol, and dried in a stream of nitrogen. The samples were then mounted on the XPS stub and taken into UHV for characterization.

(c) Alkylation

Alkylation of the chlorinated surfaces was also performed inside the nitrogen purged glove box. In the alkylation step, the chlorinated Si(111) surfaces were immersed in alkyl lithium (RLi: R = C_4H_9, C_6H_{13}, $C_{10}H_{21}$) or alkyl Grignard (RMgX: R = CH_3, C_2H_5, C_4H_9, $C_4H_6F_3$, C_5H_{11}, C_6H_{13}, C_8H_{17}, $C_{10}H_{21}$, $C_{12}H_{25}$, $C_{18}H_{37}$; X = Br, Cl) solutions at 65-80°C for duration ranging from 30 min to 8 days (depending on the chain length of the alkyl group).[58,65,66] The samples were subsequently emmersed, rinsed copiously with anhydrous THF and then rinsed with anhydrous methanol. The samples were then immersed in anhydrous methanol in a vial and taken out into air for sonication. The samples were sonicated in methanol and then in dichloromethane for 5 min each. Finally they were rinsed with methanol, dried in a stream of air for 2-4 seconds, and taken into UHV for characterization.[67]

4. Surface Characterization Techniques

(a) X-ray Photoelectron Spectroscopy (XPS)

(i) The Instrument

The X-ray photoelectron spectroscopic (XPS) experiments were done in an M-probe surface spectrometer (V.G. Instruments) that was pumped by a CTI Cryogenics-8 cryo pump. The spectrometer was attached via gate valves to other custom-built chambers that housed the LEED, quadrupole mass spectrometer etc. and were also pumped by CTI Cryogenics cryo-pumps (Figure 1). Samples could be introduced into these chambers

through two load locks that were also connected through gate valves and were pumped by turbomolecular pumps (Varian models V80 and V200) that were backed by Varian model SD-300 mechanical pumps. These two load locks were always backfilled with oxygen free nitrogen and could be taken from atmospheric pressure to approximately 10^{-7} torr pressure in about 10 minutes. The "external" load lock opened to atmosphere and samples could be introduced from air into the UHV system through this load lock. The "internal" load lock opened through a gate valve into a custom-built glove box that was continuously purged with oxygen free nitrogen. Samples prepared in inert atmosphere could be introduced directly into the UHV system through this load lock without ever exposing them to air. Samples could be transferred from one chamber to another via stainless steel loader arms.

The XPS chamber was maintained at a base pressure of less than $2x10^{-10}$ torr. However, during data collection, the pressure was typically less than $2x10^{-8}$ torr. Monochromatic Al K_α x-rays (1486.6 eV) incident at 55° from surface normal were used to excite electrons from the sample and the emitted electrons were collected by a hemispherical analyzer at a take off angle of 35° from the plane of the sample surface. The incident x-rays and the analyzer axis were in vertical planes that were at right angles to each other. The silicon samples were mounted on custom made stainless steel or aluminum sample stubs with the help of gold-plated molybdenum clips or gold-plated screws which also served to ground the samples. Since all samples were sufficiently conducting, all reported energy measurements were referenced to the spectrometer Fermi level.

(ii) Data Collection and Analysis

Data collection and analysis were performed using M-probe package software version 3.4. Two types of spectra were collected using this instrument. The "survey scan" was collected in the scanned mode with an elliptic spot of size 800 μm x 1500 μm. The "high resolution scans" were collected in an unscanned mode with the same spot size. The pass energies corresponding to the survey scan and the high resolution scan were 154.97 eV and 53.98 eV, respectively. Their corresponding energy window in which the electrons

were collected were 21.45 and 6.85 eV, respectively. This instrument had a resolution (FWHM for Au $4f_{7/2}$ peak) of 1.50±0.01 eV and 1.00±0.01 eV, respectively, for the survey and high resolution scans. A typical XPS measurement of a surface consisted of one survey scan from 0-700 eV binding energy and a high resolution scan of the Si 2p region (98.6-105.4 eV binding energy). Additionally high resolution scans of Cl 2p (197.4-204.2 eV), F 1s (685.9-692.7 eV) and/or C 1s (282.2-289.0 eV) regions were also collected as necessary.

Peak fitting routines provided by the M-Probe package software were routinely used to analyze the data. Peak areas in the survey scan were calculated by the software after a straight line background subtraction and were normalized for the number of scans and collection time per channel. The high resolution scans for Si 2p, C 1s, F 1s and Cl 2p regions were smoothed by a 3 point smoothing routine before measuring the area under the curve using a Shirley background subtraction. The Si 2p high resolution peak was also routinely deconvoluted into $2p_{1/2}$ and $2p_{3/2}$ components as well as a third component to determine the contribution from the surface silicon atoms in the chlorinated or the oxidized surface. In the deconvolution procedure, the starting values for the full width at half maximum (FWHM) for the component peaks were often adjusted so as to get final results which minimized the difference between the FWHM values for the two peaks. Typically this difference was less than 0.02 eV. The overall spectra were best fit by using 95% Gaussian/5% Lorentzian and 15% asymmetric lineshapes.

The surface coverage of chlorine, fluorine or alkyl overlayer on the silicon substrate was estimated using the substrate-overlayer model.[68] The model assumed that the chlorine, fluorine or alkane overlayer was closest to the silicon substrate and adventitious hydrocarbon layer made up the solid-vacuum interface. Peak areas in the survey scans, which were normalized by the M-Probe package software for number of scans and collection time per channel, were ratioed to the area of similarly normalized Si 2p peak for

comparison and for calculation of elemental surface coverage. The thickness of the overlayer was calculated using the equation[68]

$$\frac{I_{ov}}{I_{Si}} = \left(\frac{SF_{ov}}{SF_{Si}}\right)\left(\frac{\rho_{ov}}{\rho_{Si}}\right)\left[\frac{1-\exp\left(-\frac{d_{ov}}{\lambda_{ov}\,Sin\theta}\right)}{\exp\left(-\frac{d_{ov}}{\lambda_{Si}\,Sin\theta}\right)}\right] \qquad (1)$$

where I_{ov}/I_{Si} is the raw intensity ratio of the overlayer element peak area to the Si 2p peak area, SF_{ov} and SF_{Si} are modified sensitivity factors for overlayer and for substrate silicon, ρ_{ov} and ρ_{Si} are *atomic* densities of relevant atoms in the overlayer and of substrate silicon, d_{ov} is the overlayer thickness, λ_{ov} and λ_{sub} are the escape depths through the overlayer, for the relevant electrons originating from overlayer and substrate, respectively, and θ is the take off angle from the horizontal.

A number of factors used in the above equation were estimated or calculated as described below. The elemental sensitivity factors used for these calculations were modified Scofield factors (SF_{mod}) calculated according to the equation

$$SF_{mod} = SF_{Scof}\left[\frac{1486-BE}{1486-284}\right]^{S_{exp}} \qquad (2)$$

as provided in the M-probe package software version 3.4, where SF_{scof} were the unmodified Scofield factors[69] and S_{exp} was the sensitivity exponent, which was 0.65 for the survey scan and 0.6 for the high resolution scans. 1486 (eV) was the energy of the monochromatic K_α line from Al target and 284 (eV) was the binding energy of the C 1s peak. All sensitivity factors and peak positions were normalized to the C 1s peak, which was assumed to have values of 1.00 and 284.6 eV, respectively. The modified sensitivity factors calculated using the above equation are given in Table I.

Since the value for escape depth of Si 2p electrons through a Cl overlayer was not available in the literature, the value of this parameter was taken to be equal to the attenuation length for these electrons through elemental Cl. It was calculated using the approximate

Table I. XPS parameters used in the calculations of various coverages.

Peak	Binding Energy (eV)	Scofield Sensitivity Factors (SF_{scof})	Modified Scofield Factors	
			Survey Scan	High Resolution Scan
Sensitivity Exponent			0.65	0.60
F 1s	686	4.43	3.40	3.47
O 1s	532	2.93	2.52	2.55
C 1s	284.6	1.00	1.00	1.00
Cl 2s	270	1.69	1.70	1.70
Cl 2p	200	2.285	2.39	2.382
Si 2s	149	0.955	1.022	1.017
Si 2p	99	0.817	0.897	0.891

empirical relationship

$$\lambda = 0.41 a^{1.5} E^{0.5} \quad (3)$$

as described by Seah and Dench,[68] where E is the electron kinetic energy in electronvolts and λ and "a" are the attenuation length and thickness of a monolayer in nm, respectively. The thickness of a monolayer of chlorine was calculated using the equation[68]

$$A_{ov} = 1000\, D_{ov}\, N_{Av}\, a_{ov}^3 \quad (4)$$

where D_{ov} (not to be confused with ρ_{ov}) is the overlayer density in Kg m^{-3}, N_{Av} is the Avogadro's number, a_{ov} is the overlayer thickness and A_{ov} is the mean atomic weight of the overlayer atoms. For these calculations, the surface density of Cl atoms was taken to be equal to the density of liquid chlorine, 1.5 g.cm^{-3}.[70] Application of the above equation gave a_{Cl} = 3.4 Å. The escape depths (λ) through the Cl overlayer were calculated to be 29 Å for the Cl 2p photoelectrons, 28 Å for the Cl 2s photoelectrons, and 30 Å for the Si 2p photoelectrons.

For calculation of the coverage of chlorinated surface silicon atoms, Si_{Cl}, the high resolution Si 2p spectrum was deconvoluted as follows. For the $2p_{1/2}$ and $2p_{3/2}$ components, the difference in the peak positions (0.6 eV), the peak area ratios (0.51) and the FWHM (~0.77 eV) was fixed.[71,72] A third peak (Si_{Cl}) was then added to the spectrum and the positions of the three peaks, and the width of the third peak, were optimized to obtain the best fit to the overall spectrum. No attempt was made to deconvolve the Si_{Cl} peak into its $2p_{1/2}$ and $2p_{3/2}$ components, due to uncertainty in their area ratios and separation, and since initial efforts to use such process did not improve the fits. In keeping with published procedure,[73] the ratio of the Si_{Cl} peak to the sum of the $2p_{1/2}$ and $2p_{3/2}$ components, i.e. the ratio Si_{Cl}/(Si $2p_{1/2}$+Si $2p_{3/2}$)) was used to calculate the coverage of chlorinated silicon atoms, using equation (1) above. In this case, the ratio of silicon atomic densities and sensitivity factors became unity. λ = 16 Å was used for the substrate and overlayer.[74] Peak fitting for thin oxide covered samples was done similarly and was

relatively more accurate since the position of the third peak was well separated from that of the bulk silicon peaks.

For analyzing the areal density of the alkyl overlayers on surfaces prepared using the $CF_3(CH_2)_3MgBr$ and CF_3CH_2OLi reagents, the F 1s signal was ratioed to Si 2p signal and the overlayer-substrate model was applied to calculate the coverage of fluorine atoms on the surface. The overlayer thickness was calculated by assuming that the $-CF_3$ groups were at the solid-vacuum interface, being fixed there by the underlying methylene groups which were anchored rigidly to the silicon surface by covalent Si-C and Si-O bonds. This assumption was, however, not necessary to arrive at the same coverage of alkyl chains (see discussion). A value of λ_{ov} of 26.5 was used for the F 1s signal and $\lambda = 39$ Å was used for C 1s signal from the overlayer.[75] The escape depth of Si 2p electrons through the alkyl monolayer (λ_{sub}) was taken to be 35 Å.[74] The coverage of the F atoms for the two molecules was divided by 3 to calculate the density of alkyl chains on the silicon surface. The alkyl chain density was then divided by the number of surface atoms in the Si(111) plane to get the effective alkyl coverage on the surface in monolayers.

(b) Infrared Spectroscopy

Infrared spectra were obtained using a Mattson Galaxy series (4326 upgrade) Polaris FT-IR spectrometer and additional custom assembled external optics that consisted of mirrors (Janos), a KRS-5 polarizer (Graseby Specac), and sample stages and detectors (EG&G Judson). The apparatus was housed in a custom-built plexiglass chamber that was continuously purged with dry nitrogen. The detector consisted of a single dewar flask equipped with parallel concentric Indium Antimonide (InSb) and Mercury Cadmium Telluride (MCT) windows for probing the 4000-1800 cm^{-1} and 1800-800 cm^{-1} regions, respectively. The spectra were collected at 1 cm^{-1} resolution in two different modes - the glancing transmission (TIR) mode and attenuated total internal multiple reflection (ATR) mode. The transmission spectra were collected using large pieces of double-polished, single crystal Si(111) wafers, with the polarized IR light incident on the sample at

Brewster's angle. For the ATR measurements, special silicon ATR plates which had large (111) faces and contained 45° bevel edges at the two ends were purchased from Harrick Scientific Corporation (Figure 5b inset). During experiments the ATR plates were held in a custom-built holder with a polarizer in the path of the IR beam. Data collection and analysis were performed on a PC using the WinFirst software package provided by ATI Mattson with the spectrometer.

S- and p-polarized data were collected in TIR or ATR mode, for the "pirhana" oxidized, H-terminated, chlorine-terminated and alkyl-terminated silicon surfaces. The absorbance data for the H-terminated surface were obtained by ratioing its transmission spectrum to the transmission spectrum of the oxidized silicon sample. The absorption data for the chlorine or alkyl-terminated surfaces were obtained by ratioing their transmission spectra to the transmission spectra of either the oxidized silicon sample or the H-terminated sample. The molecular orientation (tilt and twist angles) of the alkane chains were determined from the s- and p-polarized data employing the method of Linford et al.[4] The IR dichroic ratio, defined as the ratio of s-polarized to p-polarized absorption intensities ($D = A_{s\text{-}pol}/A_{p\text{-}pol}$), was determined for $-C_{12}H_{25}$ and $-C_{18}H_{37}$ alkyl chains. The angle between the surface normal and the dipole moments of the methylene symmetric and asymmetric stretches (α_{sym} and α_{asym}, respectively) were determined from the calculations of Tillman et al.[76] The chain tilt angle (θ) and twist angle (γ) were then calculated using equations (5) and (6).[4]

$$\mathrm{Cos}^2\theta = 1 - \mathrm{Cos}^2\alpha_{sym} - \mathrm{Cos}^2\alpha_{asym} \qquad (5)$$

$$\mathrm{Cos}\gamma = \frac{\mathrm{Cos}\alpha_{sym}}{\mathrm{Sin}\theta} \qquad (6)$$

The error in all the calculated angles was less than ±4°.

(c) High Resolution Electron Energy Loss Spectroscopy (HREELS)

The high resolution electron energy loss spectroscopy (HREELS) experiments were done in collaboration with Dr. Henry Weinberg, Department of Chemical Engineering at University of California, Santa Barbara and were performed by a graduate student, Sang I. Yi. The HREELS measurements were carried out in a UHV chamber (base pressure 7 x 10^{-11} Torr), which was pumped by a 1000 l/s turbomolecular pump.[77] An external load lock and a UHV sample transfer system allowed fast loading of the samples in the chamber. The silicon specimens were mounted on a molybdenum sample holder using two molybdenum tabs that were held with screws. The sample holder slid into a manipulator that was used for loading the samples into vacuum. The HREELS measurements were performed on a model LK-2000-14-R spectrometer (L K Technologies). Data were collected at liquid nitrogen temperature (and sometimes at room temperature) in the direct mode at an angle of incidence of 60° with respect to the surface normal, with a primary beam energy of 7.5 eV and an energy resolution of 80 cm^{-1}. Off-specular measurements were made by moving the detector by a few degrees in a plane perpendicular to the sample.

(d) Temperature Programmed Desorption (TPD) and Auger Electron Spectroscopy (AES)

Temperature programmed desorption (TPD) or thermal desorption and Auger electron spectroscopy (AES) experiments were also performed by Sang I. Yi at UCSB on the same samples and in the same UHV chamber as HREELS.[77] For TPD, the samples were heated indirectly from the back side by four heated tungsten filaments. Since direct sample-thermocouple connection was difficult due to frequent sample changes, a chromel-alumel thermocouple was spot-welded close to the sample onto the central block holding the sample holder. Due to the temperature difference between the sample and the thermocouple, the measured temperature was calibrated using an optical pyrometer and using some known TPD peaks that were observed to occur at certain temperatures. All data were collected between 110 K and 1200 K at a constant heating rate of either 0.5 K s^{-1} or at

1 K s^{-1}. A differentially-pumped quadrupole mass spectrometer (UTI-100C) with a cryoshroud was used to analyze the desorption products from the surface. For calibration, hydrogen gas was dosed onto Ar^+ ion sputtered and thermally annealed Si(111) surfaces via a pinhole gas doser which had a heated tungsten filament attached to it in order to produce atomic hydrogen. The desorption temperature of the mass 2 (H_2) peak was used to calibrate the thermocouple, and the area under the peak was used to estimate the intensity of signal produced by a monolayer coverage of hydrogen. Auger data was collected using a single pass cylindrical mirror analyzer with a 3 KeV electron beam energy.

(e) Ellipsometry

Ellipsometric measurements were made on a Gaertner variable angle ellipsometer model L116C using a helium-neon laser (λ = 632.8 nm), a 45° polarizer, and an incident angle of 70°. The software package provided by Gaertner was used for calculating the film thickness. An index of refraction N_{Si} = 3.850, and an absorption coefficient K_{Si} = -0.020 was used for the silicon substrate as provided in the software package by Gaertner and since they were close to the values determined by the ASTM standard and were within the ASTM limits of uncertainty.[78] An index of refraction N_C = 1.460 and K_C = 0 was used for the alkane films as well as for silicon oxide. Thicknesses were measured at two or more spots per sample and data were obtained at more than three times per spot. Measured values for alkyl-terminated samples were ±1 Å for a given spot, and ±2 Å on each sample.

(f) Contact Angle Goniometry

Contact angles of water and hexadecane were measured on derivatized silicon surfaces at ambient temperature and humidity using a Rame-Hart Inc. model 100-06 goniometer with a tiltable base. 18 Megaohm cm resistivity water obtained from a Barnsted Nanopure system or flash photolyzed water was used as such. Anhydrous hexadecane (Aldrich) was passed through a column of activated basic alumina (Aldrich) prior to use to remove any acidic impurities. In a typical measurement, a small (2 µl) drop of liquid was

formed at the end of a flat tipped stainless steel needle using a 2 ml micrometer syringe (Gilmont Instruments). The tip was then brought closer to the surface until the drop touched the silicon surface. More liquid was added as the tip was withdrawn from the surface, keeping the surface contact area of the drop approximately equal to the initial contact area. When the liquid volume reached about 5 μl, the needle was slowly pulled away without adding any more liquid until the drop detached from the tip of the needle. In this process, the drop edge advanced on the silicon surface. Contact angle measurements were then made on both sides of this sessile drop. The results were within ±2° for each drop and for each surface (typically three drops).

III. RESULTS

1. Surface Preparation

(a) Hydrogen-Terminated Silicon Surfaces (Si-H)

Figure 2a shows a typical XP survey spectra and Figure 3a shows the corresponding high resolution spectra of the Si 2p region of a freshly etched, H-terminated, silicon surface. The survey spectra (Figure 2a) showed two main peaks, at 149 eV and 99 eV binding energies corresponding to Si 2s and Si 2p photoelectrons. The peaks appearing at successive intervals of 17.5 eV binding energy higher than the two main peaks (i.e. at ~116.5 eV, 134.0 eV, 167.5 eV and 185 eV) were plasmon loss peaks from Si 2s and 2p peaks, and were characteristic of silicon substrates.[79,80] Occasionally, small peaks at 532 eV and 284.6 eV from O 1s and C 1s orbitals of adventitious carbonaceous material were also observed on this surface.[74,81] The lack of a F 1s signal, which would have appeared at 686 eV binding energy, confirmed that consistent with prior literature, the HF-etched silicon surface is not terminated by Si-F species.[82,83]

The high resolution spectra of the Si 2p region (Figure 3a) could be deconvoluted into a doublet of $2p_{1/2}$ and $2p_{3/2}$ components. Analysis of the two components (see

Figure 2. X-ray photoelectron "survey" spectra of (a) hydrogen-terminated Si(111) surface, (b) chlorine-terminated silicon surface and (c) $-C_6H_{13}$ terminated silicon surface. The main peaks observed in the three spectra are O 1s (532 eV), C 1s (284.6 eV), Cl 2s (270 eV), Cl 2p (199 eV), Si 2s (151 eV), and Si 2p (100 eV). Smaller peaks appearing between 116 eV and 185 eV are plasmon loss peaks from the two primary silicon peaks.

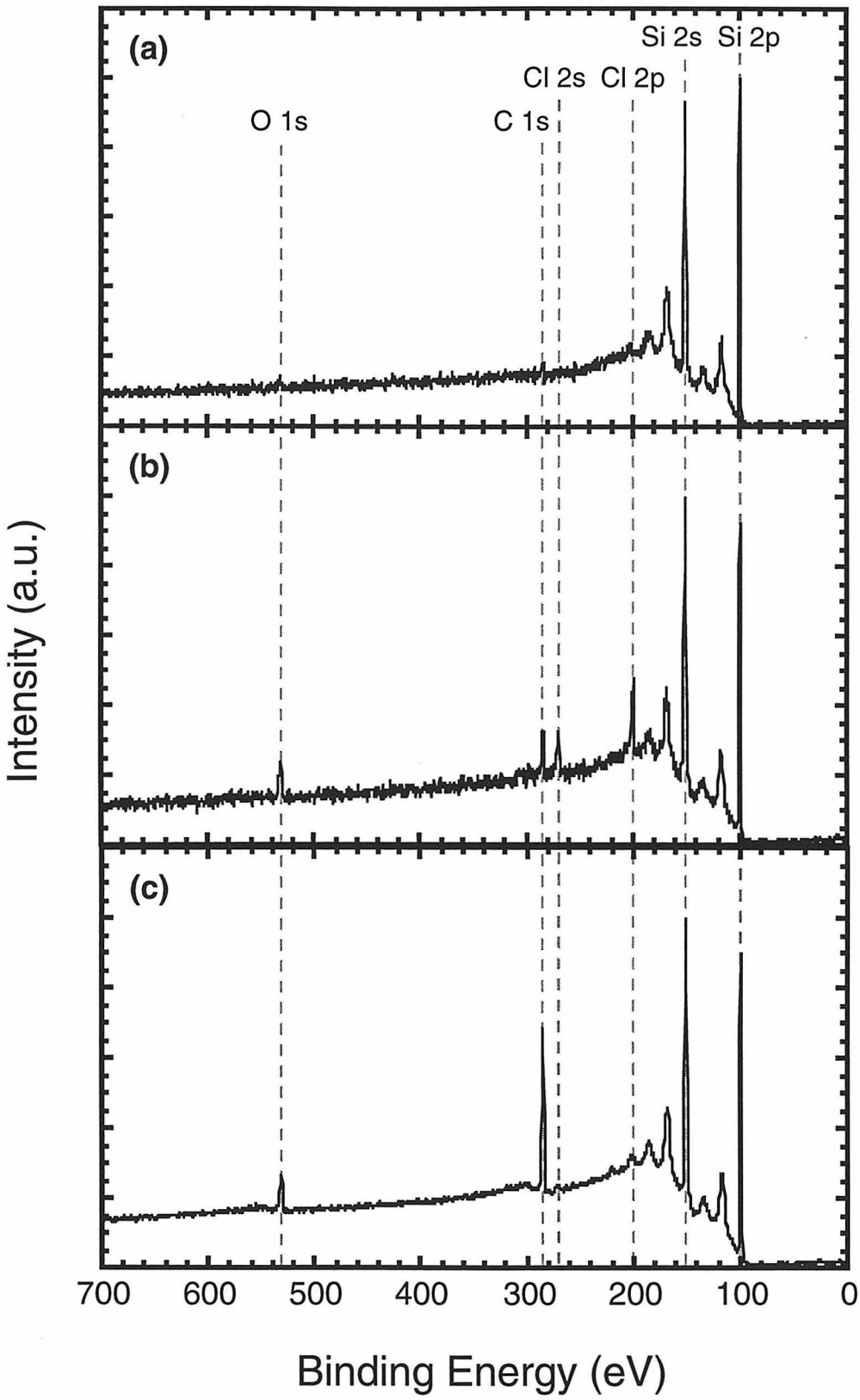
(a)
(b)
(c)
O 1s
C 1s
Cl 2s
Cl 2p
Si 2s
Si 2p
Intensity (a.u.)
700
600
500
400
300
200
100
0
Binding Energy (eV)

Figure 3. X-ray photoelectron "high resolution" spectra of the Si 2p region of (a) hydrogen-terminated Si(111) surface, (b) chlorine-terminated silicon surface and (c) $-C_6H_{13}$ terminated silicon surface. The H-terminated and alkyl-terminated surfaces could be deconvoluted only into a doublet of Si $2p_{1/2}$ (long dashed line) and Si $2p_{3/2}$ (short dashed line) components arising from the bulk silicon atoms. Contributions from the surface silicon atoms that were bound to hydrogen or carbon could not be resolved due to negligible chemical shift for the surface atoms relative to the bulk atoms.[87,88] The spectra observed from the chlorine-terminated surface could be resolved into a third peak (thick solid line) containing a contribution from the surface silicon atoms (see text). The thin solid line is the actual data and the open circles denote the overall fit of the component peaks with the data.

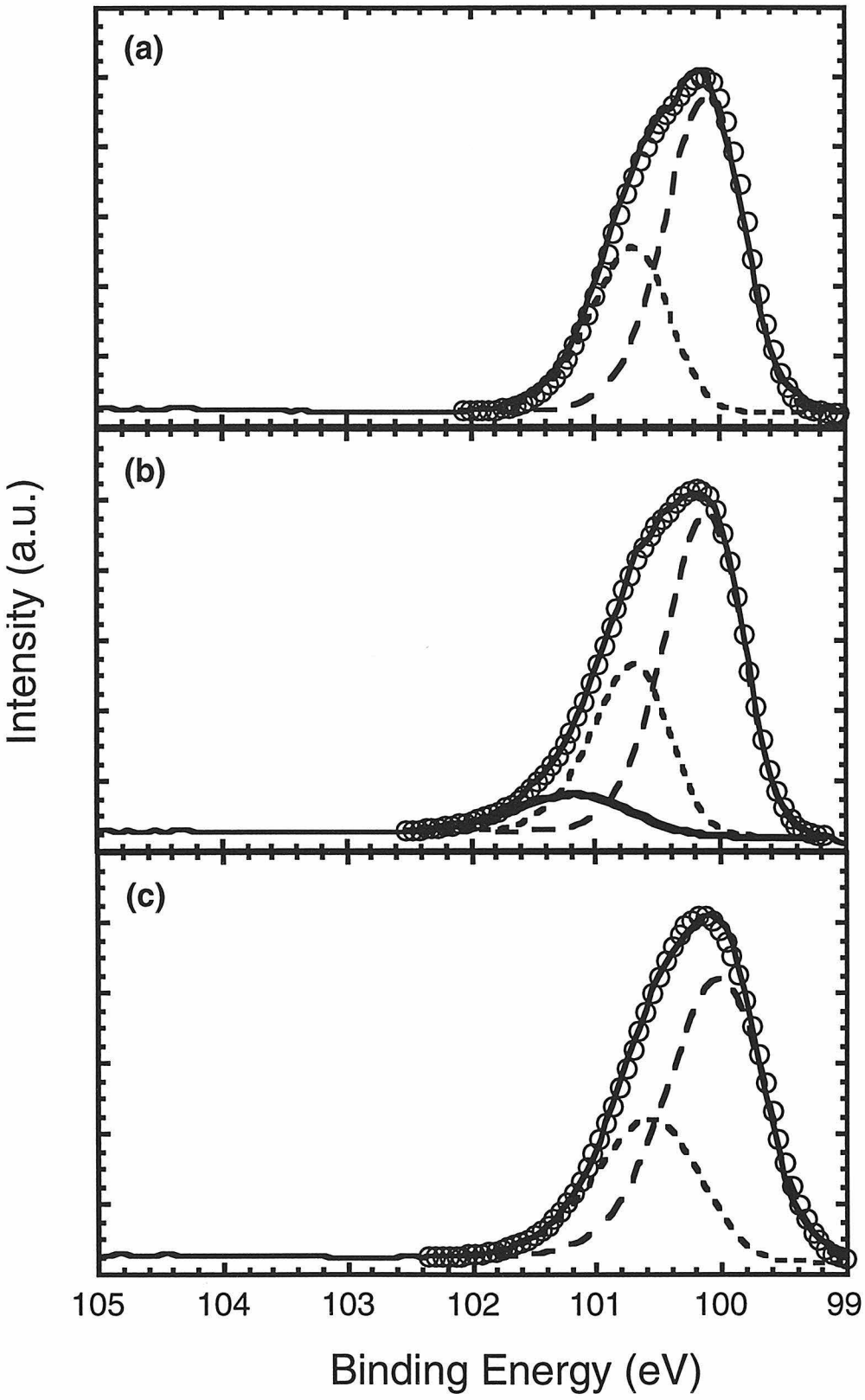
(a)
(b)
(c)
Intensity (a.u.)
105
104
103
102
101
100
99
Binding Energy (eV)

experimental section for details) exhibited an average peak separation ($E_{2p1/2}$-$E_{2p3/2}$) of 0.60±0.01 eV and area ratio ($2p_{1/2}/2p_{3/2}$) of 0.52±0.02, which are close to the theoretically expected values of 0.60 eV and 0.5, respectively.[74,84-86] A third peak, due to surface silicon atoms bonded to hydrogen, could not be resolved from the bulk peaks at our resolution.[87,88] Additionally, no oxidized Si could be detected in the Si 2p region, between 1 and 4 eV higher than the Si $2p_{3/2}$ component, indicating a lack of oxidation (< 0.2 monolayer) of surface silicon atoms.[74]

The Auger electron spectra of the HF-etched surfaces exhibited a large Si LMM peak at 92 eV due to bulk silicon and exhibited small KLL peaks from C and O at 272 eV and 503 eV, respectively, due to adventitious species on the surface (Figure 4a). Annealing the silicon surface up to 500 K lowered the carbon and oxygen signals but was not sufficient to eliminate them completely (Figure 4b). However, substrates that had been annealed to 1200 K and cooled to room temperature, exhibited only the bulk silicon peak and did not exhibit either C or O Auger signals (Figure 4c). Low energy electron diffraction (LEED) spectra of the hydrogen-terminated silicon surface exhibited a 1 x 1 pattern, consistent with prior literature reports.[89]

Infrared spectra of the H-terminated surface in the glancing transmission (TIR) or ATR mode (Figure 5) exhibited a sharp feature at 2083 cm^{-1} with p-polarized light, indicating the presence of silicon monohydride on the surface.[90-92] In the glancing transmission spectra (Figure 5a) taken on a large piece of a double-polished Si(111) single crystal wafer, no features could be resolved above noise in the region between 2100-2140 cm^{-1} (corresponding to SiH_2 and SiH_3 stretching vibrations) with either s- or p-polarized light, indicating that the silicon wafer surfaces were ideally monohydride-terminated.[90] However, some features in the 2100-2140 cm^{-1} range were seen in the ATR mode (Figure 5b) and are believed to be due to surface roughness of the ATR plates (as a result of undergoing several oxidation, etching and derivatization cycles). Small negative peaks seen in the C-H stretching (2750-3000 cm^{-1}) region indicated that the H-terminated surface

Figure 4. Auger spectra of an HF-etched sample. (a) Contributions from adventitious sources to the C (272 eV) and O (503 eV) signal could be seen routinely on the hydrogen-terminated surfaces. (b) The adventitious species remained on the surface even after annealing the surface to 500 K for several hours. (c) The adventitious material could be removed upon annealing the surface to 1200 K.

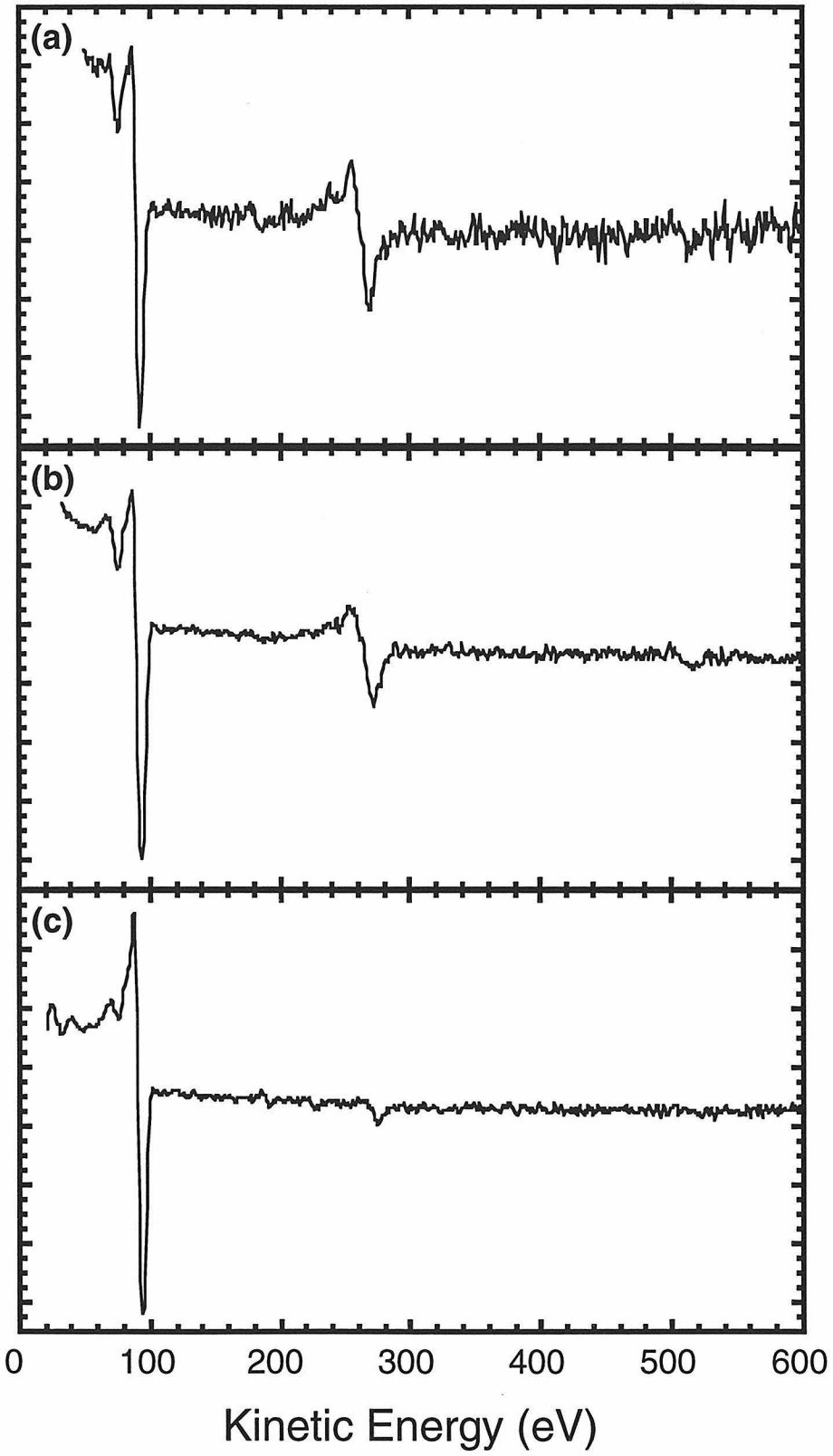
(a)
(b)
(c)
0
100
200
300
400
500
600
Kinetic Energy (eV)

Figure 5. S- and p-polarized infrared spectra for a H-terminated surface collected in (a) glancing transmission (TIR) mode and (b) in attenuated total multiple internal reflection (ATR) mode with an oxidized silicon surface as background. Both surfaces showed sharp peaks at 2083 cm^{-1} with p-polarized light, indicating the presence of silicon monohydride species.

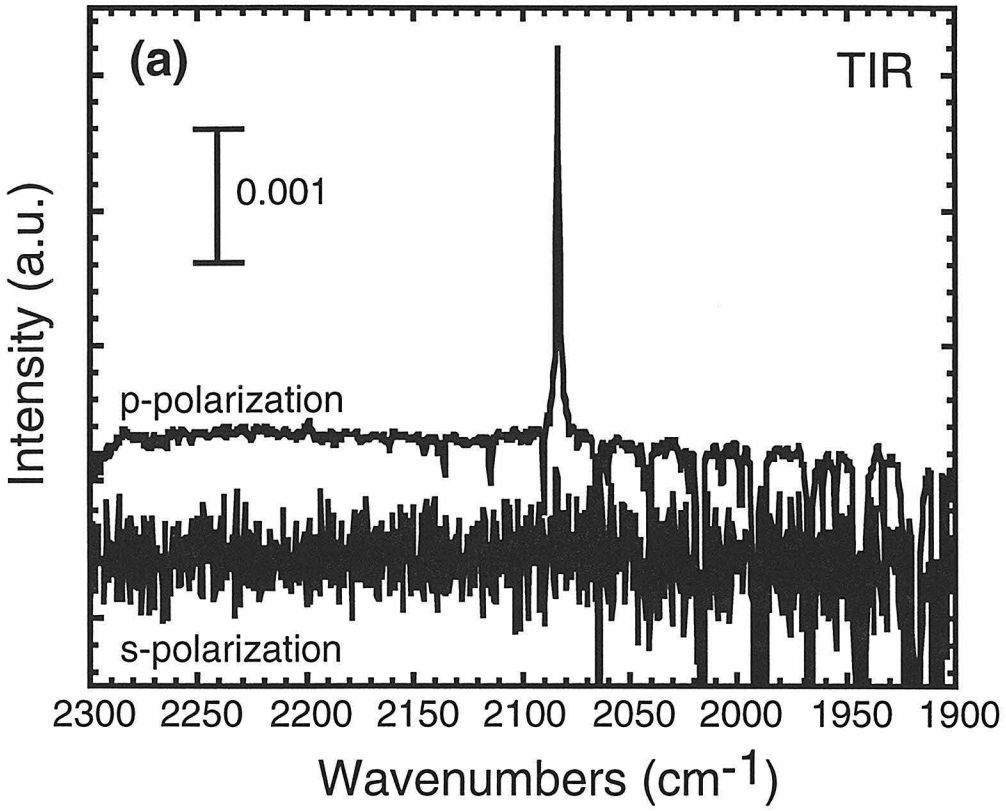
(a)
TIR
0.001
p-polarization
s-polarization
Intensity (a.u.)
2300 2250 2200 2150 2100 2050 2000 1950 1900
Wavenumbers (cm-1)

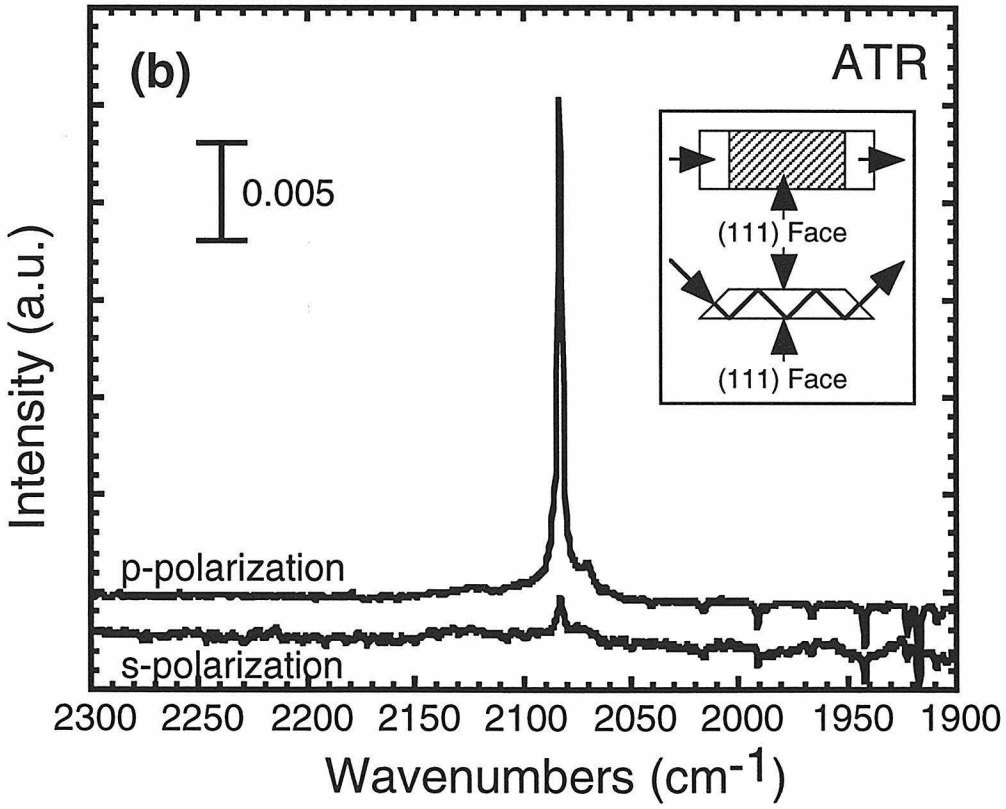
(b)
ATR
0.005
(111) Face
(111) Face
p-polarization
s-polarization
Intensity (a.u.)
2300 2250 2200 2150 2100 2050 2000 1950 1900
Wavenumbers (cm-1)

had a lower amount of adventitious coverage than the reference (oxidized silicon) sample.

HREEL spectra of the etched Si(111)-H surfaces (Figure 6) failed to show SiH stretching peaks at ~2100 cm^{-1} even when the samples were evacuated within 3 minutes of etching. It is suspected that even the small amount of adventitious carbonaceous material present on the surface (*vide supra*) was enough to prevent observation of the Si-H peaks in the spectra. These surfaces always exhibited peaks at 400 cm^{-1} (silicon bulk phonon modes), 900 cm^{-1} (CH_2 rocking mode), 1100 cm^{-1} (C-C stretching mode), 1400 cm^{-1} (CH_3 umbrella (wag) mode) and 2950 cm^{-1} (C-H stretching mode),[93] indicating the presence of adventitious hydrocarbons on the surface. This observation is thus consistent with the XPS and AES data. Annealing these surfaces to 600 K lowered the hydrocarbon coverage somewhat but was not sufficient to eliminate it completely. However, Si(111) samples that had been annealed in UHV to 1200 K and exposed to atomic hydrogen exhibited a distinct peak at ~2100 cm^{-1} (Figure 6). These spectra also showed peaks at 650 cm^{-1} and 850 cm^{-1} corresponding to Si-H bending modes and the subsurface Si-C stretching mode, respectively. For these samples, the 1100 cm^{-1}, 1400 cm^{-1} and 2950 cm^{-1} peaks were either not observed or their intensity was extremely small.

TPD spectra of the HF-etched surface did not show sharp peaks for mass 2 as expected for a hydrogen-terminated silicon surface.[94] Instead, large broad signals were observed at masses 28 (C_2H_4), 27 (C_2H_3) and 2 (H_2), consistent with the presence of adventitious material on the surface (Figure 7a). Peaks from mass 2 appeared at the same temperature as those of masses 28, 27 and others, suggesting that the mass 2 signal was most likely produced from the fragmentation product of adventitious hydrocarbons rather than from the surface SiH species. On the other hand, TPD spectra of Si(111) surfaces that had been annealed to 1200 K and subsequently dosed with atomic hydrogen gave a sharp peak for mass 2 at ~900 K (Figure 7b). The intensity of the mass 2 signal from atomic hydrogen dosed samples was also much less then the intensity of the signal produced by an HF-etched silicon surface, further suggesting that the mass 2 signal from the etched surface

Figure 6. High resolution electron energy loss spectra (HREELS) of H-terminated surface prepared (a) by etching Si(111) in HF/NH_4F solution and (b) by dosing a Si(111) surface, that had been previously sputtered with Ar^+ ions and annealed, with atomic hydrogen. Presence of even very small quantities of adventitious material prevented the observation of SiH stretching peak in the HF-etched surfaces.

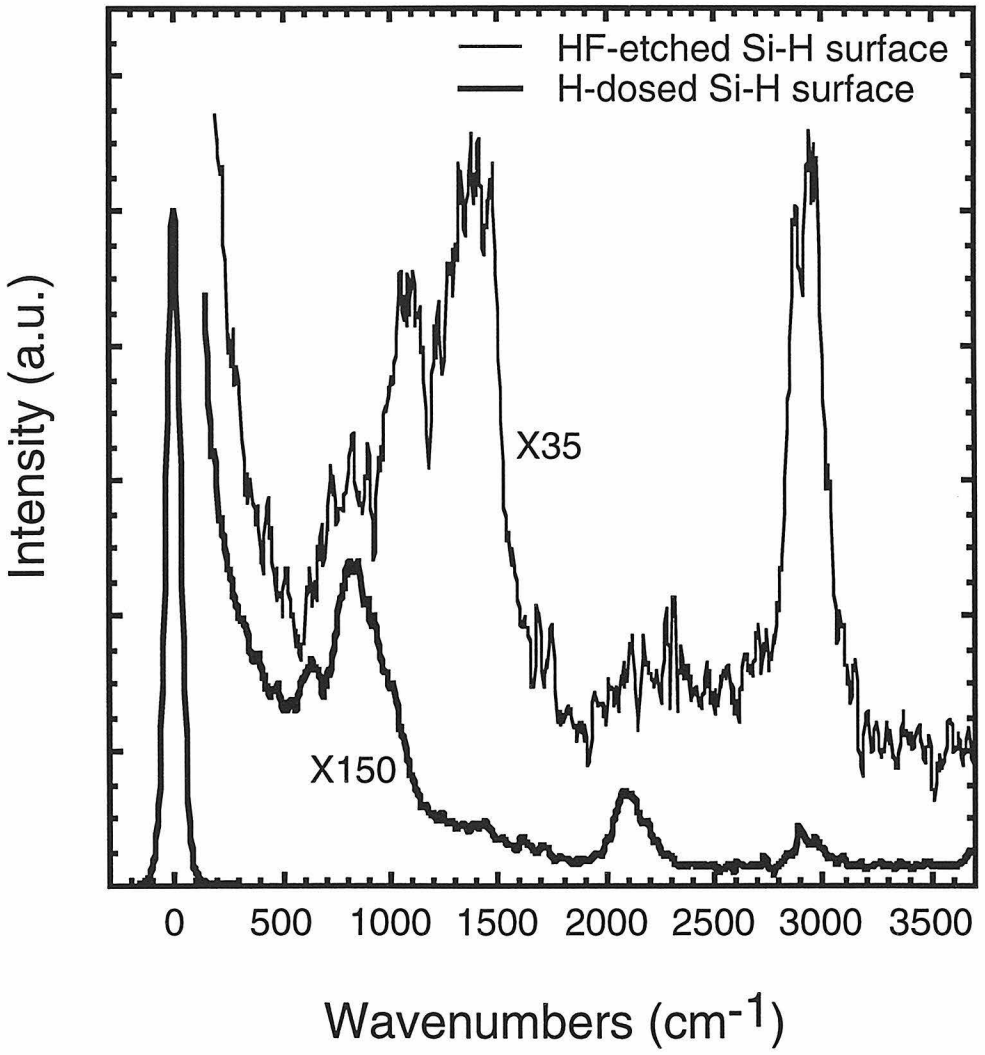
HF-etched Si-H surface
H-dosed Si-H surface
X35
X150
Intensity (a.u.)
0
500
1000
1500
2000
2500
3000
3500
Wavenumbers (cm-1)

Figure 7. Thermal desorption (TPD) of H-terminated surfaces prepared (a) by etching Si(111) in HF/NH_4F solution and (b) by dosing a Si(111) surface, that had been previously sputtered with Ar^+ ions and annealed, with atomic hydrogen. The HF-etched surfaces showed large broad peaks at mass 27 (thick solid line) and mass 28 (dashed line) corresponding to large amounts of adventitious species. The H_2 signal (mass 2) (thin solid line) was also large and broad and imitated the profile of masses 27 and 28, indicating that it was a fragmentation product of the adventitious material. In contrast, a sputtered silicon sample that had been dosed with atomic hydrogen exhibited a sharp peak for the desorbed hydrogen and very low intensity background for masses 27 and 28.

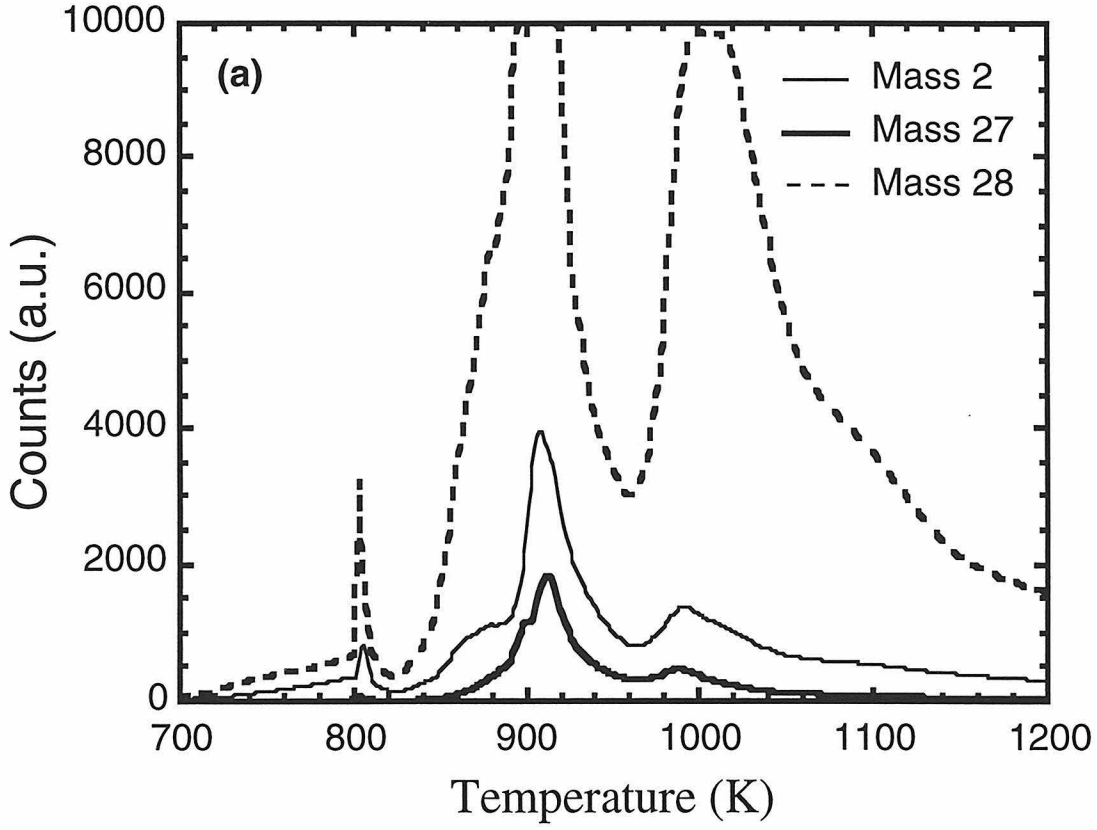
(a)
Mass 2
Mass 27
Mass 28
Counts (a.u.)
10000
8000
6000
4000
2000
0
700
800
900
1000
1100
1200
Temperature (K)

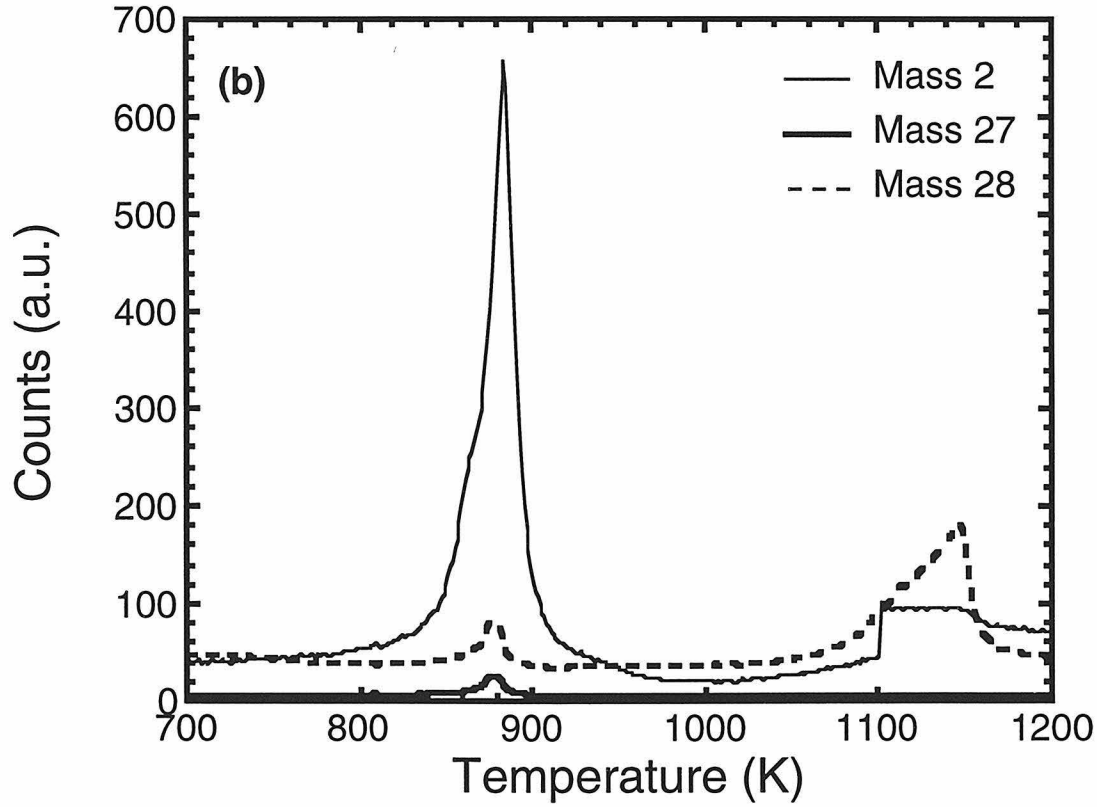
(b)
Mass 2
Mass 27
Mass 28
Counts (a.u.)
700
600
500
400
300
200
100
0
700
800
900
1000
1100
1200
Temperature (K)

was produced by fragmentation of hydrocarbon species.

(b) Chlorine-Terminated Silicon Surfaces (Si-Cl)

Hydrogen-terminated silicon surfaces were taken into a nitrogen purged glove box that was connected to the UHV system via a load lock. The samples were immersed in a solution of PCl_5 in chlorobenzene to which a few grains of benzoyl peroxide had been added just before sample immersion. The solution was then heated to 90-100 °C for 40-50 minutes, rinsed with anhydrous THF and then with anhydrous methanol, and taken into the XPS chamber for characterization. Figures 2b and 3b show the XP spectra of a representative chlorinated silicon surface. As compared to the H-terminated surface, the survey spectra for the chlorinated surface showed two extra peaks at 270 eV and 200 eV binding energy, respectively, corresponding to Cl 2s and Cl 2p photoelectrons.[95] This indicated the presence of chlorine atoms on the surface. The peak in the high resolution spectra of the Si 2p region was wider than that for the H-terminated surface. This high resolution spectrum could be deconvoluted into three peaks. Two of these corresponded to the $2p_{1/2}$ and $2p_{3/2}$ components of the bulk silicon, as seen for the H-terminated surface. The third peak was displaced towards higher binding energy than the bulk components. This peak is assigned to surface silicon atoms that were bound to the more electronegative chlorine atoms (Si_{Cl}). Optimization of the peak position and peak width of the Si_{Cl} peak to give the best fit to the overall spectrum, while holding the parameters of the $2p_{1/2}$ and $2p_{3/2}$ components constant, resulted in the Si_{Cl} peak being higher in binding energy than the Si $2p_{3/2}$ peak by 1.09±0.09 eV. This result was in accordance with XPS results observed earlier for Si(111) 7x7 surfaces that had been dosed with chlorine gas.[96] This observation suggested the formation of a surface silicon chlorine bond.

Auger spectra of the chlorine-terminated surface (Figure 8) exhibited a Cl LMM peak at 181 eV in addition to the bulk Si peak at 92 eV, and exhibited small signals due to adventitious O and C at 503 eV and 272 eV, respectively. Auger spectra taken after TPD did not show the Cl, C or O signals. LEED spectra of the chlorinated surface also showed

Figure 8. Auger spectra of a chlorine-terminated silicon sample, before and after thermal desorption. The chlorine signal at 181 eV was lost upon heating the surface to 1200 K.

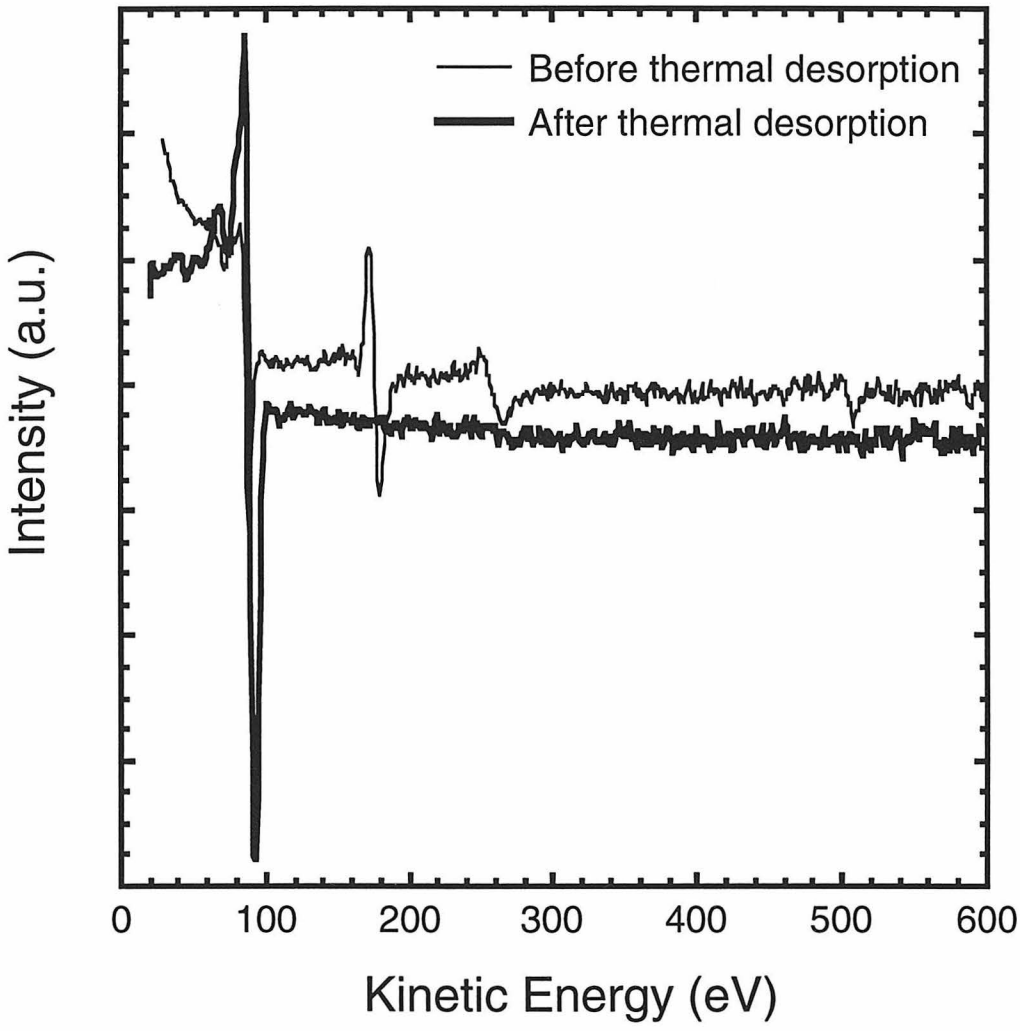
Before thermal desorption
After thermal desorption
Intensity (a.u.)
0
100
200
300
400
500
600
Kinetic Energy (eV)

a hexagonal 1 x 1 pattern, indicating that the silicon surface did not undergo reconstruction as a result of the chlorination procedure.[97] Qualitative Rutherford back scattering data collected on the chlorinated surface also showed chlorine present on the silicon surface.

Infrared spectra of the chlorinated surface exhibited a complete loss of the silicon hydride species. The Si-Cl bond, expected at about 550 cm^{-1}, could not be observed with our IR setup in either TIR or ATR mode, since both these configurations require that the IR beam penetrate completely through the silicon substrate, and silicon absorbs strongly below 1500 cm^{-1}. HREELS measurements were therefore performed to observe the formation of the Si-Cl bond. As expected according to the literature,[98] the HREELS spectra of the Si-Cl surface exhibited a peak at 550 cm^{-1} that was not present in the spectra for the Si-H surface, confirming the formation of Si-Cl bonds at the surface (Figure 9). After TPD, the 550 cm^{-1} peak due to surface Si-Cl was not observed in HREELS, in agreement with a lack of Cl signal in the Auger spectra.

TPD spectra of the chlorine-terminated silicon surfaces (Figure 10) exhibited signals due to SiCl (mass 63) and $SiCl_3$ (mass 133) that were consistent with the desorption of chlorinated species from the surface.[96,99] In addition, broad signals were observed at masses 28, 27 and 2. The presence of two peaks in the TPD signals for the chlorinated species suggested the formation of silicon di- and tri-chloride species in addition to silicon monochloride.[96,99] Uncertainty in the temperature scale of the TPD spectra precluded any further comparison of the desorption temperatures with data in the literature.

(c) Alkyl-Terminated Silicon Surfaces (Si-C_n)

The chlorinated silicon surfaces were immersed in alkyl Grignard (RMgX: R = CH_3, C_2H_5, C_4H_9, $C_4H_6F_3$, C_5H_{11}, C_6H_{13}, C_8H_{17}, $C_{10}H_{21}$, $C_{12}H_{25}$, $C_{18}H_{37}$; X = Br, Cl) or alkyl lithium (RLi: R = C_4H_9, C_6H_{13}, $C_{10}H_{21}$) solutions to produce alkyl-terminated surfaces. Figure 2c and 3c show the XPS spectra of a representative alkyl (-C_6H_{13}) terminated Si(111) surface. The survey scan of these alkylated surfaces showed

Figure 9. High resolution electron energy loss spectra (HREELS) of chlorine-terminated surface before and after thermal desorption. The peak at 550 cm^{-1}, present in the spectra before thermal desorption, corresponds to Si-Cl stretching mode.

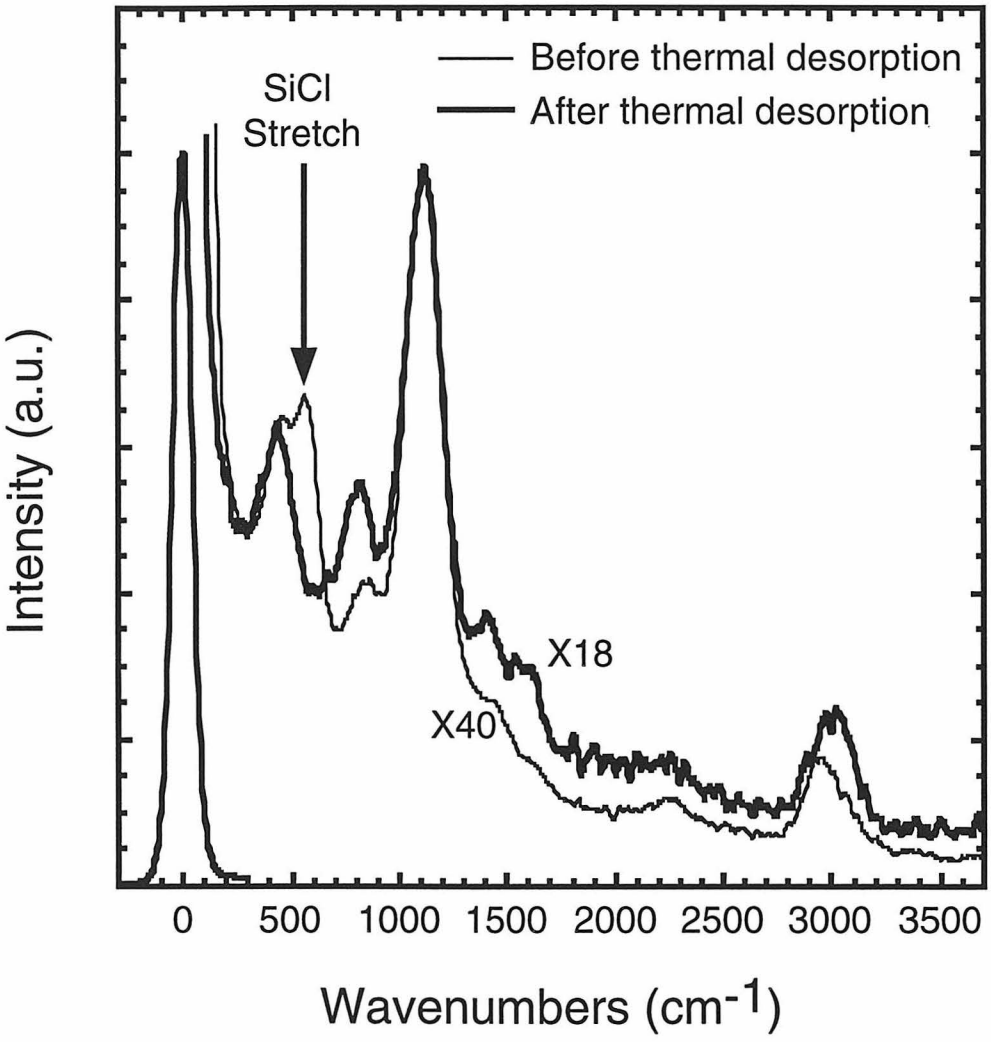
Before thermal desorption
After thermal desorption
SiCl
Stretch
X18
X40
Intensity (a.u.)
0
500
1000
1500
2000
2500
3000
3500
Wavenumbers (cm-1)

Figure 10. TPD spectra of the chlorine-terminated surface gave peaks at mass 63 (SiCl) and mass 133 ($SiCl_3$). Two peaks in the thermal desorption spectra suggested the formation of silicon di- and tri-chlorides in addition to silicon monochloride species on the surface.

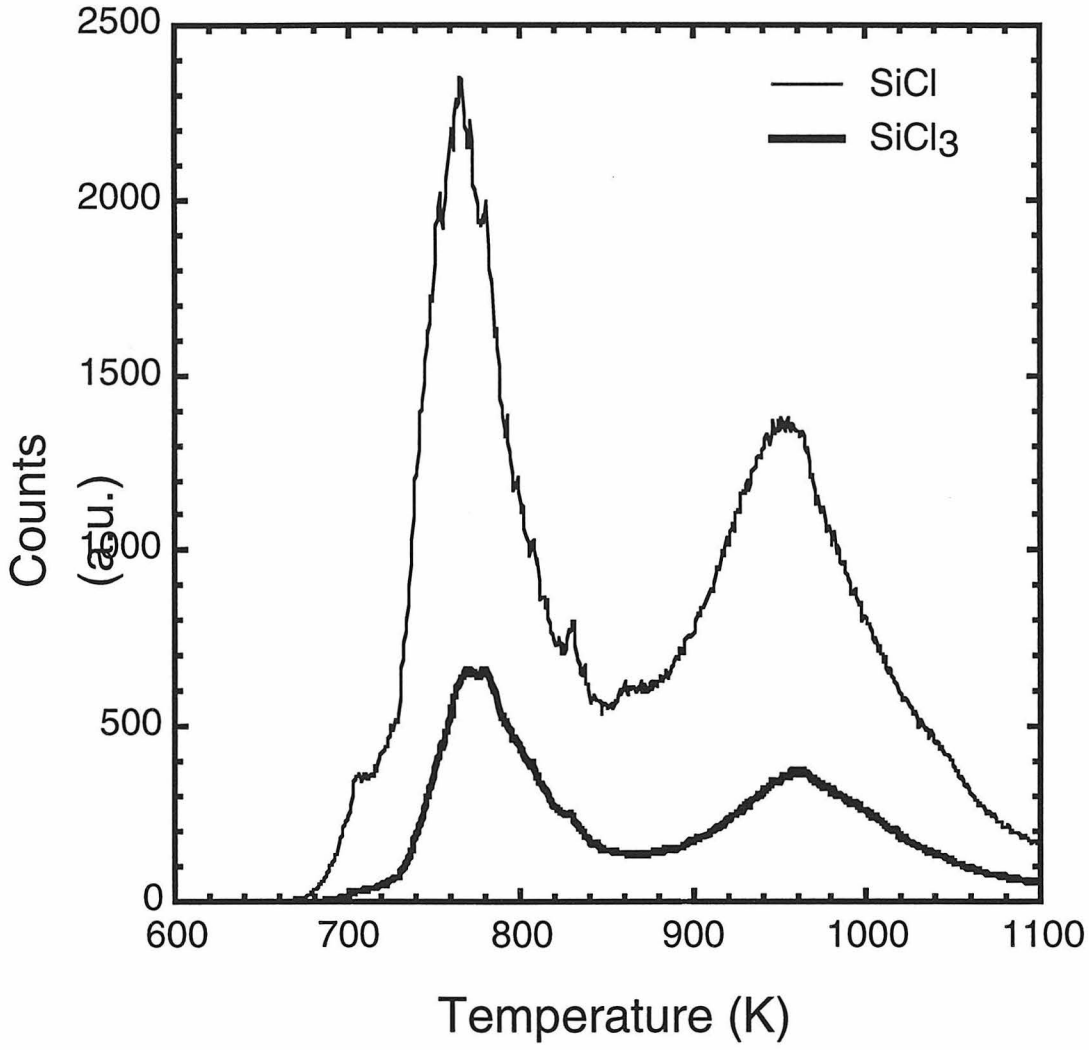
2500
2000
1500
1000
500
0
Counts
(a.u.)
600
700
800
900
1000
1100
Temperature (K)
SiCl
SiCl3

signals only due to Si, C and O. No Li, Mg or halide peaks could be detected from such surfaces. The high resolution spectra of the Si 2p region showed the disappearance of the high binding energy (Si_{Cl}) peak, and the spectra could once again be fit by two peaks, one from the $2p_{1/2}$ component and the other from the $2p_{3/2}$ component. As observed for the H-terminated surface, the chemical shift due to carbon bound surface silicon atoms was too small to be resolved relative to the bulk silicon atoms.[87] Consistent with the very small oxygen signal seen in the survey spectra, which is attributed to adventitious sources,[74] the high resolution scans for the alkylated surfaces did not show any oxidation of the silicon surface. Such signals would have appeared between 1 and 4 eV higher than the Si $2p_{3/2}$ peak.[74] AES spectra of the $-C_2H_5$ derivatized surfaces (Figure 11) showed signals due to C, O, Si and trace amounts of Cl.[100] The C, O and Cl signals disappeared after thermal desorption.

IR spectra of the alkyl-derivatized surfaces in either TIR (not shown) or ATR mode (Figure 12a) did not show any signal in the 2000-2200 cm^{-1} region, indicating that the surface silicon hydride species was not re-formed during the process of alkylation. As shown in Figure 12b, strong signals due to C-H stretching vibrations appeared at 2850 cm^{-1} ($\nu_s(CH_2)$), 2920 cm^{-1} ($\nu_a(CH_2)$), and 2965 cm^{-1} ($\nu_a(CH_3)$, ip). For the $-C_{18}H_{37}$ and $-C_{12}H_{25}$ terminated surfaces, the ATR spectra yielded asymmetric methylene C-H stretching peaks at 2923 and 2922 cm^{-1}, respectively, suggesting a semi-amorphous environment of the alkyl chains.[101,102] Si-C stretching frequencies which were expected near 650 cm^{-1}, could not be observed in either TIR or ATR modes due to strong absorption by silicon. No signal was seen in the 3200-3600 cm^{-1} range for the alkylated surface indicating absence of physisorbed or chemisorbed water or OH groups.[103]

The average orientation of the alkyl chains on the Si(111) surface was calculated from the IR dichroic ratio for the $-C_{12}H_{25}$ and $-C_{18}H_{37}$ alkyl chains. The ratio of IR stretching mode intensities obtained using s- and p-polarized IR light were determined for the symmetric and the asymmetric methylene stretches and the data were used to determine

Figure 11. Auger spectra of an ethyl-terminated sample before and after thermal desorption.

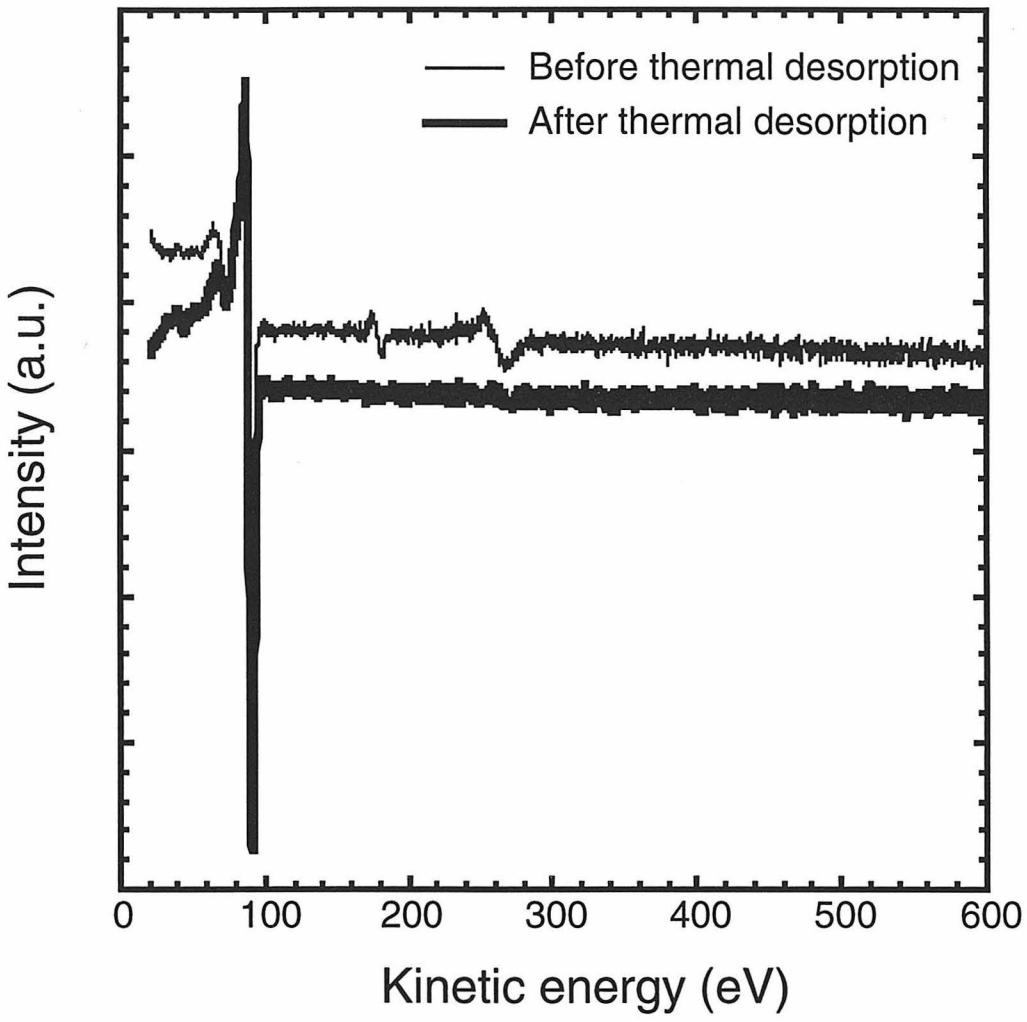
Before thermal desorption
After thermal desorption
Intensity (a.u.)
0
100
200
300
400
500
600
Kinetic energy (eV)

Figure 12. S- and p-polarized IR spectra of a representative alkyl ($-C_{12}H_{25}$) terminated surface. (a) A lack of signal in the Si-H stretching region indicates that no Si-H bonds are re-formed during the process of alkylation. A silicon oxide background was used for these spectra. (b) The C-H stretching region shows that alkylation results in a large increase in the C-H stretching peaks. Due to lower adventitious coverage, an H-terminated surface was used as a background for these spectra. The peak position for the C-H asymmetric stretching peak ($\nu_a(CH_2) = 2922\ cm^{-1}$) suggests a semi-amorphous environment for the alkyl chains.

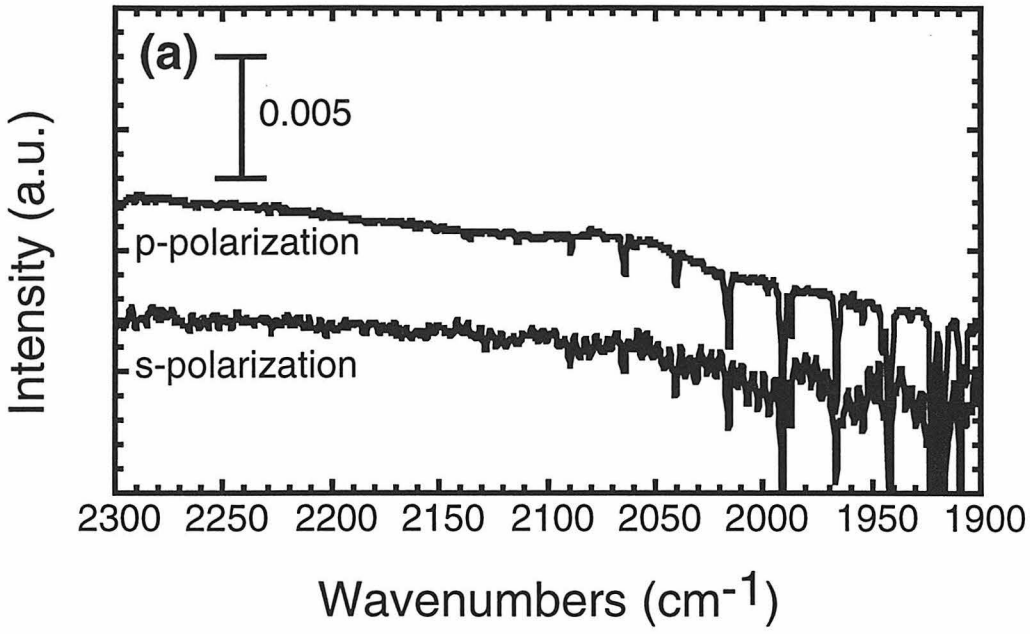
(a)
0.005
p-polarization
s-polarization
Intensity (a.u.)
2300 2250 2200 2150 2100 2050 2000 1950 1900
Wavenumbers (cm-1)

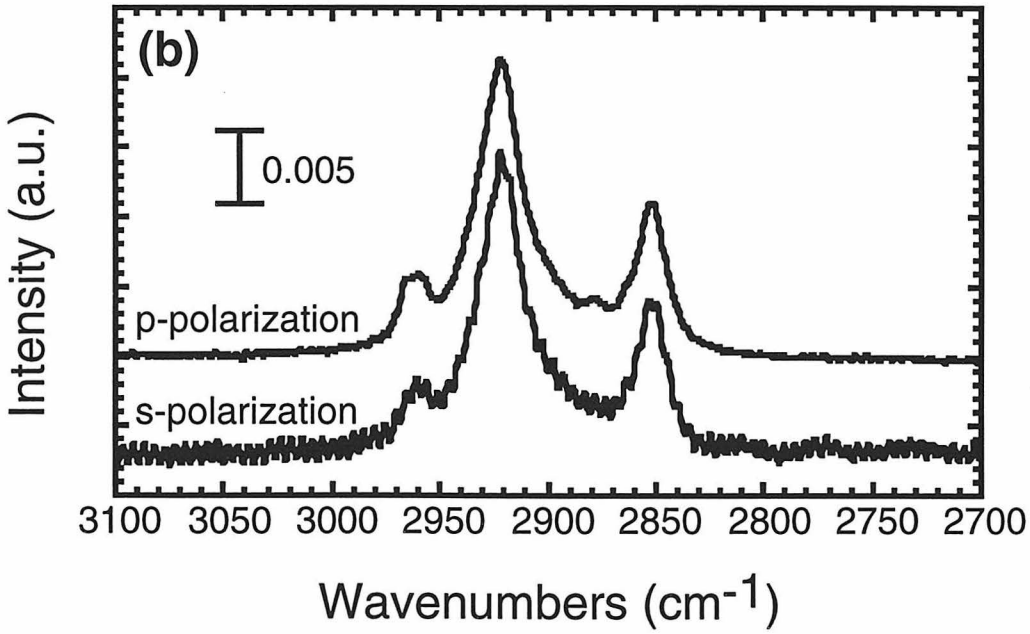
(b)
0.005
p-polarization
s-polarization
Intensity (a.u.)
3100 3050 3000 2950 2900 2850 2800 2750 2700
Wavenumbers (cm-1)

the angle between the methylene transition dipoles and the surface normal (α_{sym} and α_{asym}, respectively). α_{sym} and α_{asym} were determined to be 64° and 69° for the $-C_{12}H_{25}$ chain, and 62° and 55° for the $-C_{18}H_{37}$ chain, respectively. Using equation (5) and (6) (see experimental details), the tilt and twist angles determined were 35° and 34°, respectively, for the $-C_{12}H_{25}$ chain, and 48° and 51°, respectively, for the $-C_{18}H_{37}$ chain.

In order to confirm whether a surface Si-C bond had been formed as a result of the derivatization procedure, ethyl-terminated Si(111) surfaces were subject to HREELS. As shown in Figure 13, in addition to a peak for the C-H stretching mode at 2950 cm^{-1}, the CH_2 scissor mode and the CH_3 umbrella (wagging) mode of the terminal methyl group at 1450 cm^{-1}, the CH_2 twisting and wagging modes at 1200 cm^{-1}, and the C-C stretching mode and the CH_3 rocking mode at 1000 cm^{-1}, a strong signal was seen at 650 cm^{-1}. This peak was assigned to the Si-C stretching mode.[93,104,105] All of these vibrational peaks were either significantly reduced or disappeared completely after thermal desorption.

TPD spectra of the ethyl-terminated silicon surfaces exhibited broad peaks at masses 2, 26, 27, 28, 29 and 30. The intensities of these peaks were often significantly higher than what was expected from a monolayer of adsorbed alkyl species. The ratios of evolved masses were also not found to be constant for different samples or for a given sample over a significant temperature range. It was concluded therefore that the evolved masses were due to adventitious sources and did not arise predominantly from chemisorbed species.

2. Physical and Chemical Characterization

(a) Ellipsometry

The thickness and uniformity of the alkyl monolayers were determined from single wavelength ellipsometric measurements. An accurate evaluation of the film thickness using this method is dependent upon the use of correct refractive index and requires making the assumption that the film is isotropic and homogeneous. Although this assumption was not

Figure 13. High resolution electron energy loss spectra (HREELS) of ethyl-terminated surface before and after thermal desorption. The peak at 650 cm^{-1}, present in the spectra before thermal desorption, corresponds to Si-C stretching mode.

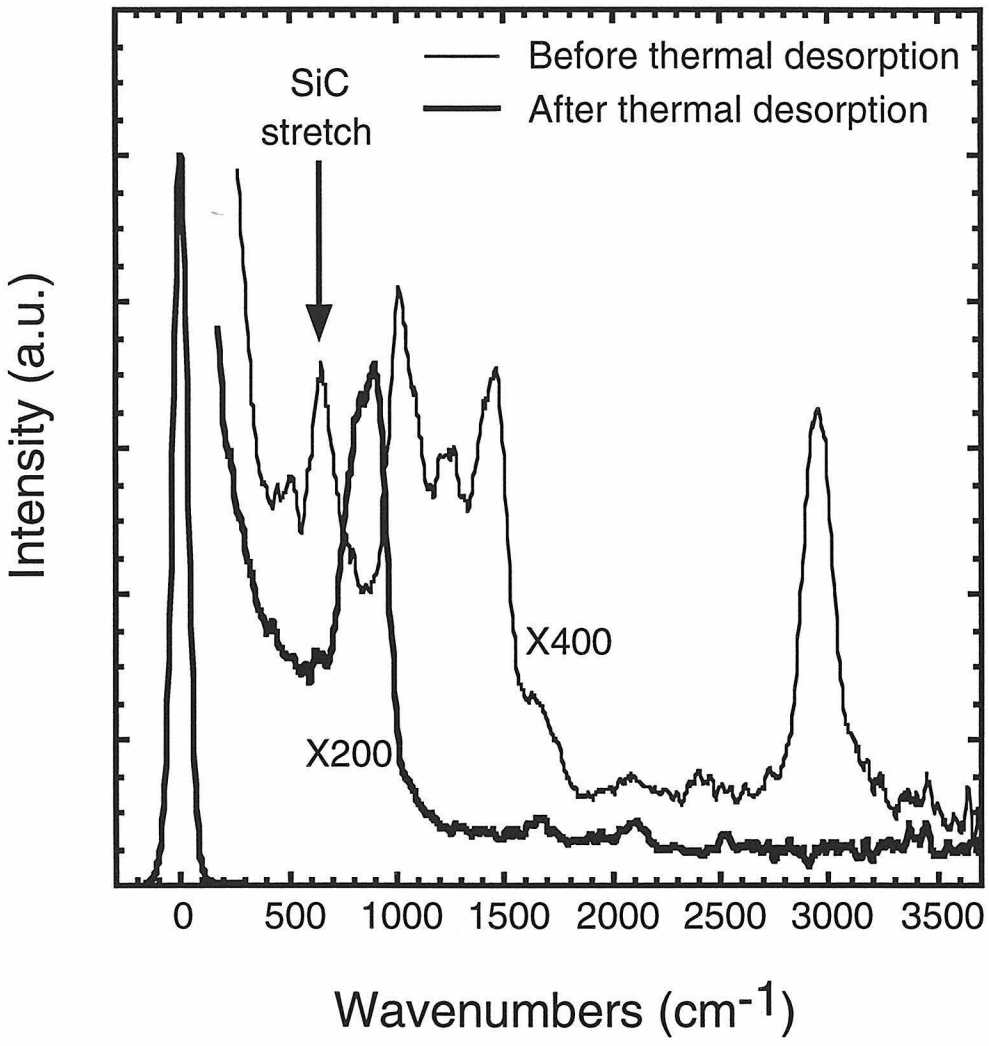
Before thermal desorption
After thermal desorption
SiC
stretch
X400
X200
Intensity (a.u.)
0
500
1000
1500
2000
2500
3000
3500
Wavenumbers (cm-1)

verified, it was made, nonetheless, based on the precedence of its use in previous investigations of alkanethiol monolayers on gold[76,101,102] and alkyl monolayers on silicon.[3,4] An index of refraction $N_C = 1.46$ and $K_C = 0$ was used for the alkane films in these studies as it was within the range of values previously used for saturated hydrocarbon phases.[76,101,102]

Ellipsometric measurements of the alkylated surfaces gave effective thicknesses that increased monotonically with the length of the alkane chain used in the reactant molecules (Figure 14; Table II). The observed thickness scaled linearly with the thickness calculated by the XPS overlayer method, providing some confidence in the use of the above values for the films' refractive indices. When the observed ellipsometric thicknesses were compared with the ideally expected values, it was found that for the short chains ($n \leq 6$) the measured thicknesses were consistently ~3 Å higher than the calculated values. This observation did not hold for the long chains ($10 \leq n \leq 18$), suggesting that the packing in the longer chains was different from that for the shorter chains. Ellipsometry measurements nevertheless clearly indicated that alkane chains of varying lengths could be successfully used to reproducibly create very thin overlayers.

(b) Contact Angle Goniometry

Contact angle measurements are sensitive indicators of the surface properties of a monolayer. Although the wettability of a monolayer should be determined only by its surface properties and not by the properties of the bulk medium, the bulk is indirectly expected to affect the surface properties by affecting the order, packing and tilt of the surface functional groups. In practice, therefore, contact angle measurements are not only sensitive to the surface but also to the properties of the interfacial region.[45] The technique can thus provide a rapid assessment of the surface quality of monolayer films.

Contact angle measurements were performed with water and hexadecane to elucidate the nature of the free surface of the alkylated silicon. In studies involving alkanethiol monolayers on gold[101,102] and alkyl monolayers prepared from 1-alkenes on

Figure 14. Ellipsometric thicknesses of alkyl monolayers prepared with alkyl chains of different lengths. The solid circles denote the observed thicknesses and the open circles denote their ideally expected thicknesses. The observed ellipsometric thickness is a monotonic function of the alkyl chain length. For n = 10, the higher value corresponds to surface prepared with $C_{10}H_{21}Li$ and the lower value corresponds to surfaces prepared from $C_{10}H_{21}MgBr$. The difference between the observed value and the ideally expected value can be attributed to contributions from the presence of adventitious species and to the varying packing density for chains of different lengths (see text). The solid square and the open square denote the observed and ideally expected thickness for the fluorocarbon alkane chain ($-(CH_2)_3CF_3$).

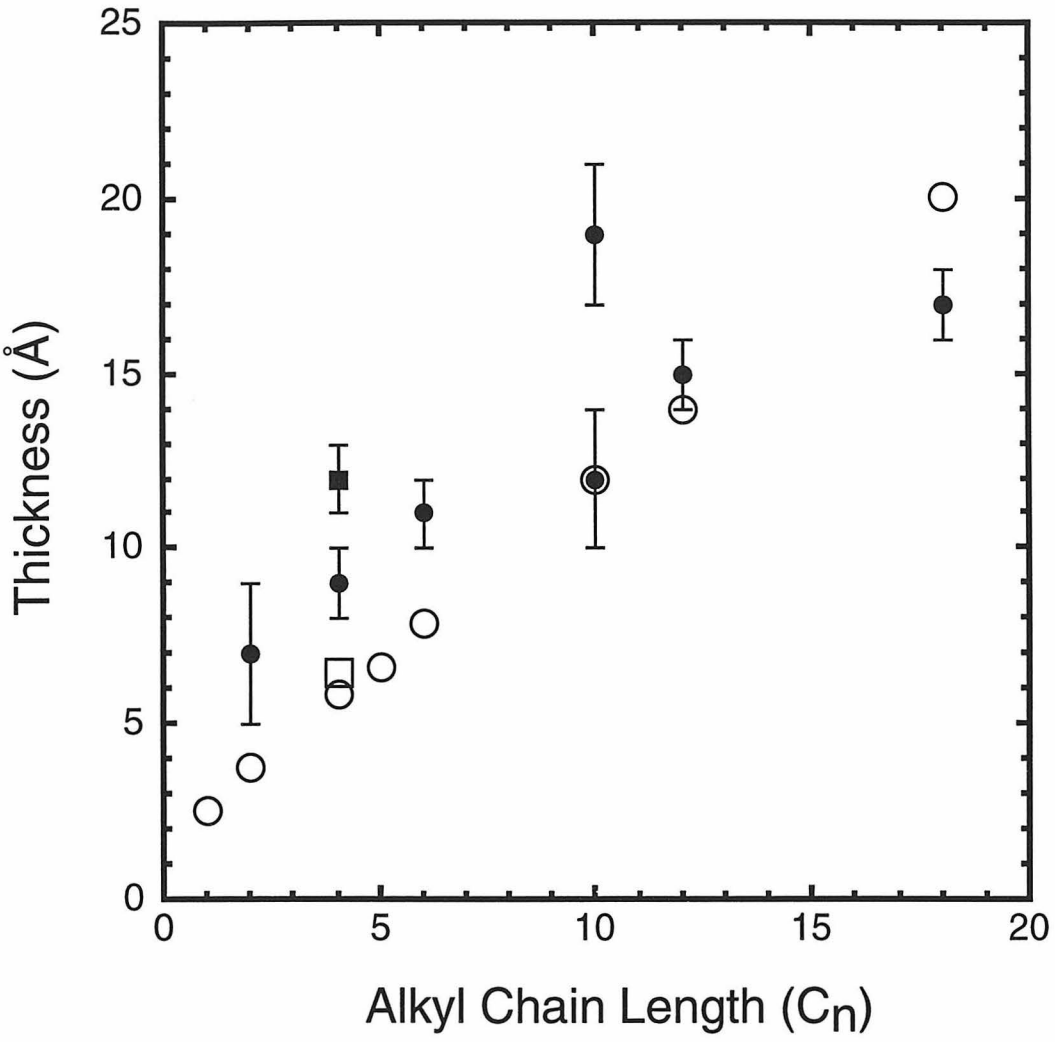
25
20
15
10
5
0
0
5
10
15
20
Thickness (Å)
Alkyl Chain Length (C_n)

Table II. Physical properties of alkyl-terminated Si(111) surfaces.

Alkyl Chain Length (C_n)[a]	Observed Ellipsometric Thickness (Å)	Calculated Film Thickness[b] (Å)	Air Stability[c] (x t_{SiH})	Contact Angle Water (°)	Contact Angle Hexadecane (°)
2	7 ±2	3.82	8	85 ±3	< 10
4	9 ±1	5.85	> 35	95 ±2	< 10
6	11±1	7.89	> 35	100 ±2	30 ±1
10	12 ±2	11.95	12	93 ±2	< 10
12	15 ±1	13.98	7	104 ±2	27 ±1
18	17 ±1	20.08	> 36	99 ±2	37 ±1

a) $C_n = -C_nH_{2n+1}$. b) The calculation assumes that the alkyl groups are rigidly bound to the surface of silicon and the Si-C bond is normal to the surface. The numbers do not correspond to the length of the alkyl chain. c) The numbers represent the ratio of the time taken by alkyl-terminated surface to oxidize the same amount as a H-terminated surface. t_{SiH} is about 2 hours 30 minutes for half a monolayer of oxide as measured by XPS.

silicon,[3,4] contact angles for water in the range 110°-115° and for hexadecane in the range 45°-50° have been taken to indicate a tightly packed alkyl monolayer with a free surface terminated by methyl groups. Lower contact angles, it has been suggested,[3,4,101,102] indicate the presence of exposed methylene groups at the surface. As shown in Table II, contact angle measurements on our alkyl-terminated surfaces gave angles between 85° and 105° for water and 37° or lower for hexadecane. This suggested that the surface contained some amount of exposed methylene units at the surface. The methylene units could have been exposed either due to less than optimal (dense) packing of the alkyl chains or due to significant tilting of the alkyl chains from surface normal. Both of these conditions would be consistent with the IR data as well as with the approximately half monolayer packing that was determined from the XPS data (*vide infra*).

3. Chemical Stability of Alkyl-Terminated Surfaces

The chemical stability of the alkyl-terminated surface was determined by exposing it to air and to various wet chemical environments. The robustness of the alkyl overlayer was measured by exposing an alkyl-terminated surface to boiling chloroform for 30 min. XPS survey spectra of the butyl-terminated surface, taken before and after this treatment, showed virtually identical intensity of the C 1s signals from the surface (Figure 15). This observation indicated that the alkyl moieties were tightly bound at the silicon surface and could not be easily desorbed.

The ability of the alkyl overlayers in significantly decreasing any interaction between the silicon surface and a chemically reactive environment was evaluated by exposing the alkyl-terminated surfaces to acidic and basic aqueous solutions. When a hydrogen-terminated surface and a $C_{12}H_{37}$-terminated surface were exposed to an aqueous KOH (pH=13) solution, for 2.5 hours at room temperature, the former showed significant "pock marks" on the surface, indicating the progress of an etching reaction at the surface. In contrast, no such marks were observed on the butyl-terminated surface when it was

Figure 15. XPS survey spectra of a butyl-terminated silicon surface before and after exposure of the surface to boiling chloroform for 30 minutes. The same intensity of the C 1s signal on the two spectra indicates that the alkyl groups are chemisorbed, rather than physisorbed, at the surface.

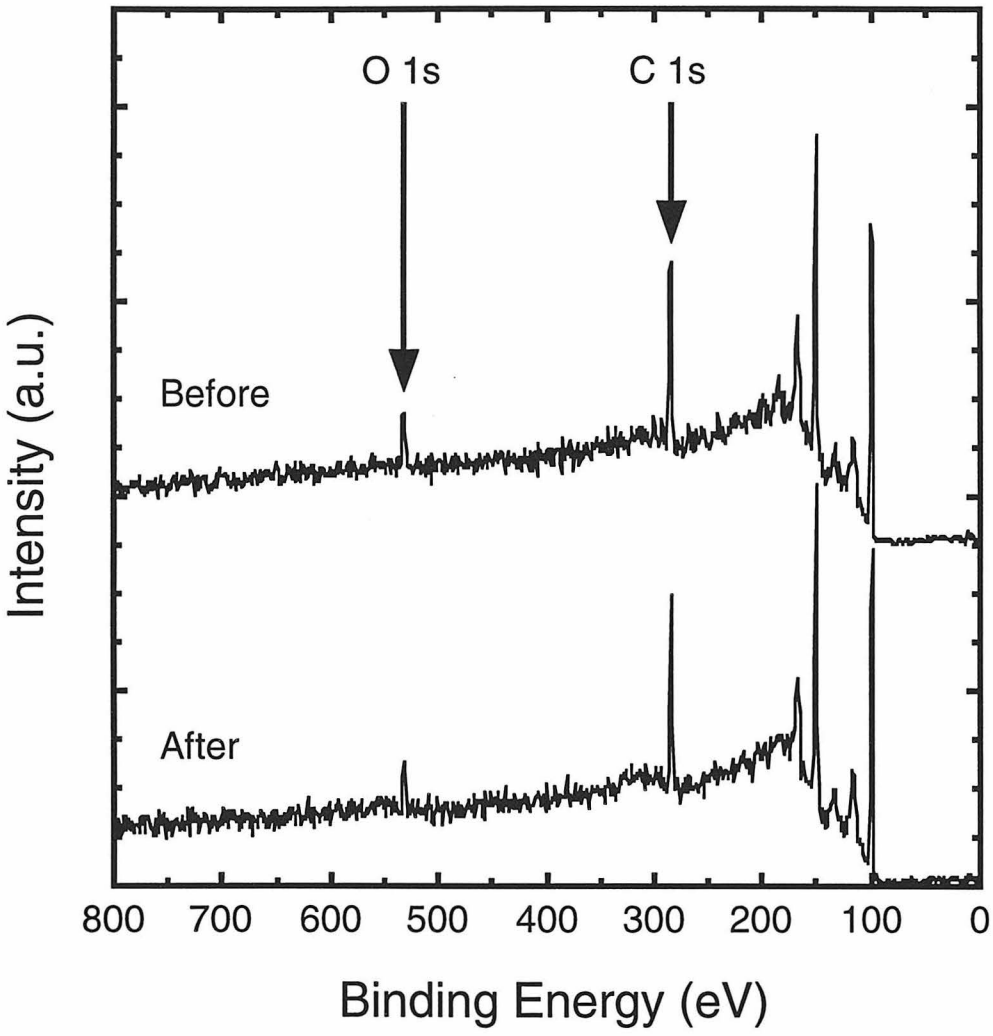
O 1s
C 1s
Before
After
Intensity (a.u.)
800
700
600
500
400
300
200
100
0
Binding Energy (eV)

immersed in the same solution for the same duration. Furthermore, when a H-terminated and a $C_{12}H_{37}$-terminated surface were exposed to an aqueous H_2SO_4 (pH=1) solution, for 2.5 hours at room temperature, the H-terminated surface showed approximately half monolayer oxide coverage, as observed in the high resolution XPS spectra of the Si 2p region. In contrast, negligible oxidation was observed for the alkyl terminated surface when it was immersed in the same solution for the same duration (Figure 16). These results indicate that the alkyl overlayers can successfully protect the silicon surface against reactive chemical environments.

The stability of the alkylated silicon surfaces towards oxidation in air ambient was measured by observing the growth of the silicon oxide peak in the Si 2p high resolution XP spectra as a function of the time of exposure of the derivatized silicon surface to air. All alkylated surfaces (of different chain lengths) prepared in this work were found to be more resistant to oxidation than the hydrogen-terminated silicon surface (Table II). For example, the hydrogen-terminated silicon surface required about 3 hours to form half a monolayer of oxide, but a $-CH_3$ terminated surface required 5 hours to form about the same amount of oxide. Silicon surfaces derivatized with longer alkyl chains were even more resistant to oxidation, and some did not reach half a monolayer oxide coverage even after 2 days of exposure to air. This result was significant because it is known that unintentional oxidation of H-terminated silicon degrades the electrical properties of the silicon surface.[10]

IV. DISCUSSION

The two-step reaction sequence described above, radical initiated chlorination followed by reaction with Grignard or organolithium reagents, provided a simple, general approach to functionalization of H-terminated silicon surfaces. As observed by infrared spectroscopy, ideally monohydride-terminated surfaces were obtained by etching Si(111) surfaces with HF and NH_4F. High resolution XPS data of the Si 2p region showed that the etched surfaces were free of silicon oxide (< 0.2 monolayers), indicating that the C and

Figure 16. High resolution XPS spectra of the Si 2p regions of a H-terminated and a $C_{12}H_{37}$-terminated silicon surface after exposure to an aqueous acidic solution (pH=1) for 30 minutes at room temperature. While the H-terminated surface showed approximately a half monolayer of oxide on the surface, negligible oxidation was observed for the $C_{12}H_{37}$-terminated surface.

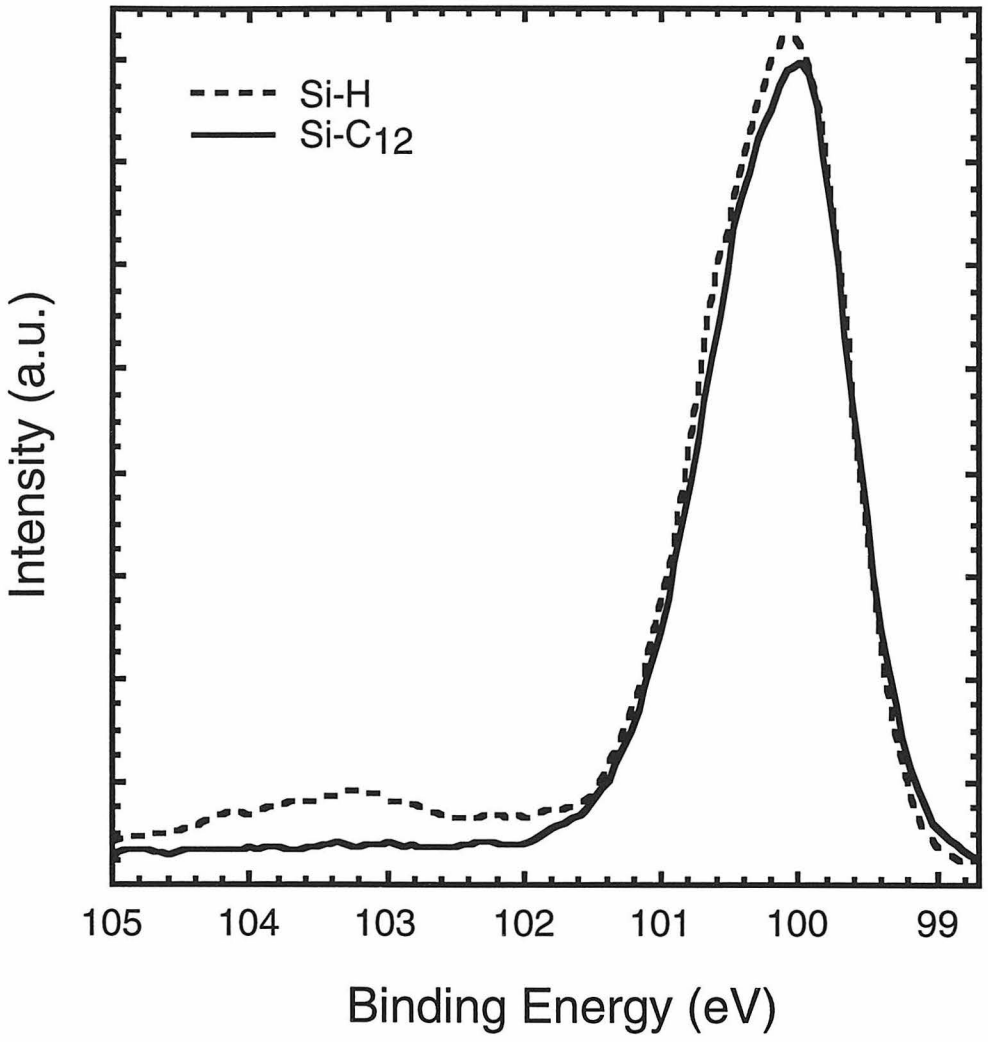
Si-H
Si-C12
Intensity (a.u.)
105
104
103
102
101
100
99
Binding Energy (eV)

O signals seen in the XPS survey scan and in the AES data were due to adventitious material on the surface. Additional support for the presence of adventitious material on the silicon surface came from the empirical observation that, in the survey scan, the raw area ratio of O 1s/C 1s peaks, averaged over more than 50 samples, remained constant at 0.95±0.15. The constant O 1s/C 1s ratio and a lack of signal in the 101 to 104 eV region of the Si 2p high resolution XPS data suggested that the oxygen signal from the surface was not due to silicon oxides or alkoxides and that the O and C peaks were due to adventitious carbonaceous material. This observation of adventitious C and O was also consistent with earlier published reports for HF-etched silicon samples exposed to ambient and/or organic solutions.[74,81] However, even though the adventitious coverage was small, it was sufficiently large by UHV standards to preclude the observation of Si-H signal by HREELS or H_2 (mass 2) signal by TPD.

Radical-initiated chlorination of the H-terminated surface resulted in the replacement of surface hydrogen by chlorine atoms. The presence of chlorine on the surface was indicated by the Cl 2s and Cl 2p peaks in the XP survey spectra, by the presence of Cl peak in the Auger spectra, and by the presence of a Si-Cl stretch in the HREEL spectra. The peak in the HREEL spectra also indicated that the surface chlorine was covalently bound to the surface silicon. This result was also supported by the high resolution XP spectra of the Si 2p region, where the wider peak, when deconvoluted to include a third component corresponding to surface silicon atoms bound to chlorine (Si_{Cl}), resulted in a peak at 1.09±0.09 eV higher in binding energy than the Si $2p_{3/2}$ peak consistent with chlorine bound surface silicon atoms.[96]

Quantitative analysis of the chlorine coverage from XPS survey spectra and high resolution spectra gave slightly varying results, primarily due to a number of assumptions involved in the calculations. Three different methods were used for the quantification - two of which estimated the number of chlorine atoms present on the surface and the third estimated the number of surface silicon atoms that were bound to the chlorine atoms. In the

first set of calculations, the ratio of the peak areas of the Cl 2p peak to the Si 2p peak in the survey spectra were used in the overlayer-substrate model. For lack of relevant values in the literature, the escape depth of Si 2p electrons through Cl overlayer and the thickness of the Cl monolayer were calculated using equations (3) and (4), respectively. For these calculations, the surface density of Cl atoms was taken to be equal to the density of liquid chlorine.[70] Applying equation (3), the chlorine monolayer thickness was calculated to be 3.4 Å. Using the Cl 2p/Si 2p ratio from the survey scan and applying the overlayer substrate model,[68] the effective thickness of the chlorine overlayer was calculated to be 5.0±0.4 Å. Ratioing this to the calculated thickness of the monolayer, the coverage was estimated at 1.5±0.1 monolayers.[106] An identical calculation using the Cl 2s/Si 2p ratio from the survey scan gave a coverage of 1.28±0.09 monolayer (4.3±0.3 Å). In the second method, employing the high resolution scans, the total integrated peak area for the Cl 2p high resolution peak was divided by the total integrated peak area for the Si 2p high resolution peak, both having been normalized for their respective data collection durations. This intensity ratio gave an effective layer thickness of 4.3±0.2 Å, equivalent to a coverage of 1.28±0.06 monolayers. The third method evaluated the number of silicon surface atoms (Si_{Cl}) that were bound to Cl atoms. The ratio of $Si_{Cl}/(2p_{1/2}+2p_{3/2})$ was used in the overlayer-substrate model to calculate the coverage of the chlorinated silicon atoms. Assuming the density of the chlorinated Si atoms forming a monolayer to be the same as that of the bulk silicon atoms, this calculation gave an effective overlayer thickness of 1.0±0.3 Å which corresponded to 0.66±0.20 monolayers. By geometric arguments, it is expected that each surface silicon atom can bind to a Cl atom to form a saturated monolayer. Therefore, ideally on an unreconstructed surface, the number of chlorine bound surface silicon atoms should be equal to the number of Cl atoms present on the surface. An observed ratio of Cl:Si of 2 suggests that the real surface is likely rougher than the ideal surface, which is assumed to be flat. The greater than one ratio is, however, consistent with the TPD results which show two peaks, indicating the presence of di- or tri-

chloride species on the surface,[96,99] and also with prior literature reports for other chlorinated silicon surfaces.[71,96]

Reaction of the chlorine-terminated surface with alkyl Grignard or alkyl lithium reagents provided a convenient way to alkylate the silicon surface. This procedure allowed the formation of important surface functionalities, such as methyl-terminated silicon surfaces (see Chapter 4),[2] that are not available through any other currently known routes.[3,4] XPS data showed that this procedure removed the surface chlorine and replaced it with an alkyl group, as evidenced by the disappearance of the Cl 2s and Cl 2p peaks and an increase in the C 1s signal in the XP survey spectra. Concomitantly, the high resolution spectra of the Si 2p region also showed the disappearance of the Si_{Cl} component. IR data showed that while the surface silicon hydride was not reformed in this process, alkylation resulted in a large increase in the intensity of the C-H stretching peaks, supporting the XPS results that indicated the presence of a large amount of hydrocarbon on the surface. Conclusive evidence for the formation of surface Si-C bonds, however, came from HREELS data, which showed a peak at 650 cm^{-1} indicating covalent surface binding of the alkyl moieties.

Figure 17 shows the C 1s/Si 2p ratio observed in the XP survey and high resolution scans. The carbon signal was found to increase monotonically when the chemistry was performed with alkyl reagents of increasing chain lengths ($-C_nH_{2n+1}$: $1 \leq n \leq 18$). Also shown for comparison is the C/Si ratio expected for a monolayer with uniform ideal coverage (*vide infra*) of each given chain length. In general, the observed ratios were found to be higher than the ideal values and the difference was found to decrease (and even become negative) as the surface was derivatized with longer chain lengths. There are two parameters that can account for the deviation of the observed C/Si ratio from the ideal value for any given chain length. On one hand, the presence of adventitious carbon causes the observed ratio to be higher than the ideal value. On the other hand, less than optimal density of the overlayer, either due to incomplete overlayer formation or due to significant

Figure 17. Raw ratio of the C 1s to Si 2p peaks for alkyl-terminated surfaces of different chain lengths ($-C_nH_{2n+1}$). Solid circles denote the ratio of the two peaks in the survey scan and solid triangles denote the ratio calculated from the high resolution scans of the two individual regions. Open circles denote the expected ratio for an ideal monolayer which was calculated for $n \geq 2$ assuming a half monolayer coverage (see text) and no contributions from adventitious sources. For $n = 1$, geometric factors permit the formation of one monolayer and this has been assumed in the figure. The solid square and the solid diamond denote the observed ratio of C 1s to Si 2p peak areas for the $-(CH_2)_3CF_3$ terminated surface in the survey and high resolution scans, respectively. The open square denotes the ideally expected ratio for the fluorocarbon alkane chain ($-(CH_2)_3CF_3$).

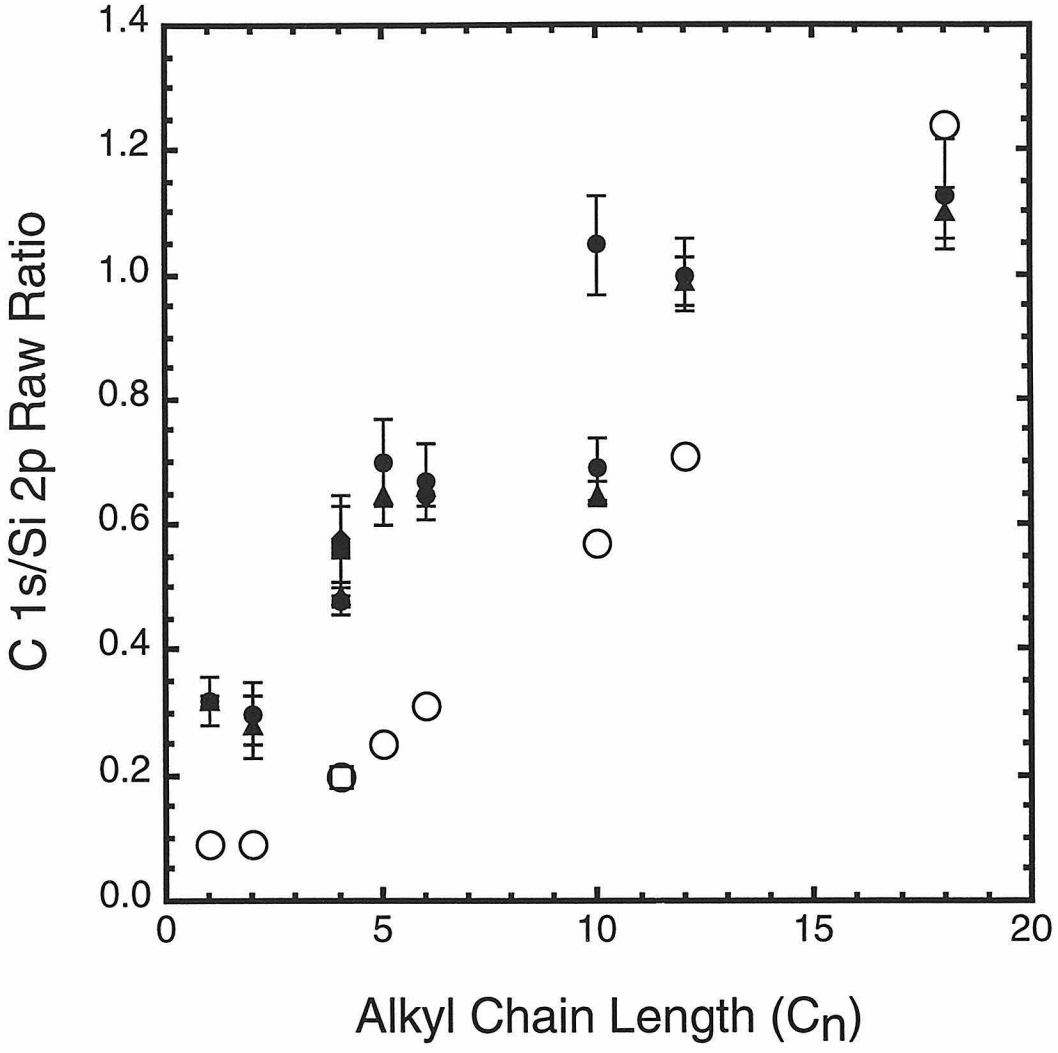
C 1s/Si 2p Raw Ratio
1.4
1.2
1.0
0.8
0.6
0.4
0.2
0.0
0
5
10
15
20
Alkyl Chain Length (Cn)

tilt of the alkane chains, causes a decrease in the observed ratio as compared to the ideally expected value. The observed ratio thus contains both these factors in different proportions for each chain length. We hypothesize that while short chains ($n \leq 6$) formed near complete overlayers with very similar contributions from adventitious sources, longer chains ($10 \leq n \leq 18$) did not form as complete overlayers, and in some cases, in spite of contributions from adventitious carbon, exhibited C/Si ratio lower than the ideally expected value.

In order to estimate the areal coverage of alkyl species on the silicon surface, the chlorinated Si(111) surface was derivatized with $CF_3(CH_2)_3MgBr$ and CF_3CH_2OLi. The unique F 1s signal from the alkane chains was used as an XPS tag. The overlayer thickness was calculated by assuming that the $-CF_3$ groups were at the solid-vacuum interface, being positioned there by the underlying methylene groups which were anchored rigidly to the silicon surface by covalent Si-C and Si-O bonds.[107] Using F 1s/Si 2p ratios from the survey spectra, the overlayer-substrate model gave a coverage of 0.43±0.05 monolayers for surfaces derivatized with $CF_3(CH_2)_3MgBr$ and of 0.51±0.01 monolayers for surfaces derivatized with CF_3CH_2OLi. Analysis of the ratio of the high resolution peaks of F 1s and Si 2p for surfaces derivatized with $CF_3(CH_2)_3MgBr$ gave a coverage of 0.48±0.09 monolayers.

It is known form earlier studies of crystalline long chain hydrocarbons that the diameter of an alkyl chain is ~4.85 Å.[108] For comparison, the Si-Si distance in the (111) plane of silicon is only 3.84 Å.[15] This clearly suggests that two alkane chains cannot bind to two neighboring surface silicon atoms. This situation is different from that of alkanethiol monolayers on Au, where optimally dense packing of alkyl chains and maximization of inter-chain interaction is possible due to lack of covalent bonding between the Au atoms and the sulfur head groups.[45] Therefore, on silicon, the densest packing available for the alkane chains, which maximizes interchain interactions, is for them to bind to every second silicon atom, leading to half a monolayer coverage. Such a 2x1 unit cell on

the surface has also been hypothesized in prior studies of alkanes on Si(111), even though the covalent bonding of individual alkyl chains to the surface silicon atoms has not been established spectroscopically.[3,4] The experimental data on alkyl coverage, presented above, is in complete agreement with the ideally expected coverage for an alkyl overlayer in which the constituent alkyl groups are covalently bound to the surface silicon atoms.

A caveat to this generalization is the methyl-terminated Si(111) surface. Due to the small size of the methyl group and due to a lack of a C-C bond which would otherwise interfere with the binding at the neighboring silicon atom, two methyl groups can be bound to two neighboring surface silicon atoms. Thus only for the methyl group, an ideal coverage is one monolayer and not a half monolayer. This uniqueness can be exploited in cases where propensity to oxidation is strongly influenced by the number of surface silicon atoms that are not bound to a carbon atom (see Chapter 4).

As described above, only half the atoms on the Si(111) surface are bound to alkane chains. At this time we are not aware of the identity of the species that occupies the second half of the surface silicon atoms. While the XPS survey data and Auger data rule out any species other than O, C or H, XPS data from the high resolution spectra of the Si 2p region as well as IR do not support the hypothesis of silicon atoms being bound to oxygen. Although the IR data of the alkyl-terminated surface also do not show the reformation of Si-H bonds at the surface, presence of a very broad silicon hydride peak cannot be ruled out. The only other possibility is that the second half-monolayer of surface silicon atoms is bound to a carbon atom coming from an unidentified source. This hypothesis is neither supported nor denied by the current data. Qualitative spectroscopic data cannot distinguish between the formation of Si-C bonds from the unidentified source, from the Si-C bonds of the surface attached alkyl chains. Quantitative XPS data cannot identify the nature of the unknown carbon substrate due to interference from contributions from adventitious sources. More experiments are needed to resolve this issue.

Further analysis of the alkyl coverage indicates that the area of the 2 x 1 unit cell on the Si(111) surface, 25.54 $Å^2$, is significantly larger than the minimum area required for an alkyl chain, 18.5 $Å^2$, in a tightly packed crystalline environment.[108] This suggests that for a half-monolayer coverage, the alkyl overlayer can be expected to be quite porous. This hypothesis is supported by our infrared spectroscopy data for $-C_{18}H_{37}$ and $-C_{12}H_{25}$ terminated surfaces, for which the ATR spectra yielded asymmetric methylene C-H stretching peaks at 2923 and 2922 cm^{-1}, respectively. These peak positions for alkanethiol monolayers on gold have been interpreted to indicate a semi-amorphous environment of the alkyl chains.[101,102] Lower contact angles of water and hexadecane on the alkylated surfaces also indicated that these monolayers are not tightly packed and methyl-terminated as the densely packed alkanethiol monolayers on Au, which show higher contact angles for both solvents.[3,4,101,102] We thus believe that, for an alkyl overlayer in which the molecules are covalently bound to the silicon surface, a half monolayer coverage with a semi-amorphous environment of the alkyl chains *should* be expected. The data presented in this chapter is consistent with this argument.

V. CONCLUSIONS

The general picture that emerges from the results described above is of a silicon(111) surface covered with an alkyl overlayer that is one molecule thick and in which the molecules are covalently attached directly to the silicon surface without the presence of an anchoring layer of oxide. Quantification of the alkyl coverage gives a half monolayer coverage in which the alkyl chains are attached to every second surface silicon atom in a 2 x 1 unit cell. At this time it is not clear what species occupies the silicon atoms that are not bound to alkane chains. The alkyl overlayers are chemically robust and are not easily degraded. The high stability of these overlayers is further indicative of a chemically attached monolayer as opposed to a physisorbed layer. The chlorination/alkylation procedure thus provides a facile pathway to introduce chemical functionality to the silicon

surface by attaching alkane molecules with different functional groups at the free end. The procedure opens an avenue to tailor the surface properties of silicon towards possible applications in catalysis, lubrication, adhesion, sensing etc.

As compared to the H-terminated surface, the alkyl-terminated surfaces are found to be more stable towards oxidation in air and in contact with various wet chemical environments. These properties of the alkyl overlayers can have important ramifications in applications where oxidation of the silicon surface is undesirable. A case in point is the inability of H-terminated silicon surface to form a stable semiconductor/liquid junction solar cell in contact with aqueous electrolyte. Modification of silicon surfaces with alkyl monolayers can decrease the propensity to form an oxide by not only providing a barrier to water from reaching the silicon surface but also by binding the surface silicon atoms into stable covalent silicon-carbon bonds and thus decreasing their ability to oxidize. Experiments aimed at taking advantage of this property of the alkyl overlayers are described in the next chapter, as are experiments aimed at understanding how these alkyl monolayers, prepared by the two-step chlorination/alkylation procedure, affect the electrical properties of the silicon surface.

VI. FUTURE DIRECTIONS

The work described herein is only the beginning of a project that can expand in different directions depending on the goal one is trying to achieve. The quality of the alkyl modified silicon surface and its attributes can be tailored to suit the particular use. An exhaustive list of variations on the theme of "covalently bound alkyl chains on silicon surfaces", is endless and beyond the scope of this thesis. It is left to the reader to envisage the uses depending on the requirements of a particular application for these surfaces. Given below are only a few suggestions for immediately feasible projects.

1. RLi is Better than RMgX

During the course of these experiments it became obvious that for a given chain alkyl length, surfaces prepared from RLi as the alkylating reagent were more completely formed than surfaces prepared by RMgX. Surfaces prepared with RLi consistently gave higher XPS (C 1s) signals than surfaces prepared from RMgX with the same alkyl chain length. The difference became more pronounced as the length of the alkyl chain increased. A case in point is the derivatization of silicon surfaces with three different chain lengths, viz. $-C_4H_9$, $-C_6H_{13}$ and $-C_{10}H_{21}$. While almost identical coverages were observed when the modification was done with either C_4H_9MgCl or C_4H_9Li, only a slight difference was seen between surfaces derivatized with $C_6H_{13}MgBr$ and $C_6H_{13}Li$, with the latter showing a slightly higher coverage. The difference became pronounced when the chain length was increased to 10 carbons. Surfaces derivatized with $C_{10}H_{21}Li$ showed almost 1.5 times higher coverage than their counterparts derivatized with $C_{10}H_{21}MgBr$ (Figure 15). The observed surface coverage of $C_{10}H_{21}Li$ derivatized surfaces was also closer to the ideally expected value, after correcting for adventitious carbon coverage.

This observation is also in agreement with results from molecular analogs of the silicon surface in which reactions of $SiCl_4$ were studied with RLi and RMgBr.[65,66,109,110] While RMgBr reagents are quite effective in replacing three out of the four chlorine atoms on the silicon atom, RLi reagents can successfully remove all four chlorine atoms.[110] Experimentally it was observed that surfaces derivatized with longer chain alkyl Grignard ($n > 10$) often exhibited large amounts of residual chlorine even after long exposures of the chlorinated surfaces to these reagents. Based on molecular analogs and on the observations on the Si(111) surface, it can be predicted that longer chain alkanes will make more complete monolayers if the reactant is RLi rather than RMgBr.

2. Derivatization with Fluoroalkanes

For applications where the barrier property of the alkane overlayers is required, it is necessary to decrease the porosity of the overlayer film. It was shown above that if the

silicon surface was to be derivatized with alkane molecules that were covalently bound to the surface, a certain amount of porosity would be inevitable. One alternative to solve this problem is to derivatize the surface with linear fluorocarbon chains. While the cross section area of a hydrocarbon chain is 18.5 $Å^2$,[101,108] that for a fluorocarbon chain is 24.63 $Å^2$.[101,111] This implies that derivatizing the Si(111) surface by fluorocarbon chains will increase the area covered by the adsorbate from 72% to 96%, for a 2 x 1 unit cell of 25.54 $Å^2$ area.

Derivatization with fluorocarbons can especially have significant ramifications for two particular applications where either the barrier layer is required to keep water away from the silicon surface, e.g., in Si/water (liquid) junction solar cells, or where thin insulator layer are required for applications in solid-state devices such as diodes, transistors etc.[112] In a situation where it is desirable to keep water away from the silicon surface, the reduced porosity of the fluorocarbon overlayer will be complemented by the increased hydrophobicity of the monolayer. Silicon modified by such a monolayer would make a more stable Si/water junction solar cell, a feat that as only been partially achieved with the alkyl overlayers (see Chapter 4). Such a surface would also be expected to be less affected by strong acidic and basic environments. Less porous fluorocarbon monolayers (dielectric constant = 2.1 (from Teflon))[113] would also be expected to fare better as thin layer dielectrics as compared to their more porous hydrocarbon counterparts (dielectric constant = 2.4 (polyethylene)).[113]

Molecular analogs of a fluorocarbon terminated silicon surface exist in the literature.[110,114-116] Boutevin et al. have shown that $SiCl_4$ can be derivatized with moieties of the general form $CF_3(CF_2)_n(CH_2)_2$- ($1 \leq n \leq 6$) to produce $Si((CH_2)_2(CF_2)_nCF_3)_4$, using alkyl lithium and alkyl Grignard prepared from their respective fluoroalkyl halides.[110,115] These procedures are thus completely analogous with the methods described in this chapter.

3. Other Alternatives

Derivatization of silicon with linear alkane chains is not the only alternative to modifying silicon surfaces. One can potentially imagine variations in the structure of the molecular backbone forming the overlayer, nature of the free end of the overlayer molecule and the nature of reaction resulting in the formation of covalent Si-C bond. Leads can be taken from the work on alkyl thiol monolayers on Au where phenyl rings, double and triple bonds, and other structural moieties have been included in the backbone to form these overlayers.[45] The properties of these and of other linear alkyl overlayers on Au are well documented[45] and the comparison can be extended (with due consideration of the differences of the Au and silicon case) to the expected overlayers on silicon. The fact that the free end of the overlayer molecules can be varied as long as it is consistent with the reaction chemistry has already been demonstrated for alkyl overlayers on silicon.[4]. This approach to modifying the terminal groups can be extended to include redox active molecules,[47-49] for applications in charge transfer studies at semiconductor/liquid interfaces[17] and for stabilization of the semiconductor surface in aqueous media,[47-49] or to include special head groups for applications in sensors.[26,27] Depending on the chemical requirements of the unique head groups, the nature of the reaction forming the Si-C bond can also be varied. Two non-oxidative approaches to forming surface bound overlayers have already been published in the literature.[2-4] An alternate approach, recently proposed,[117] involves the use of Langmuir Blodgett films of 1-alkenes to form the monolayers. In this approach, the desired monolayer is first formed at a liquid air interface, then transferred to the silicon surface and subsequently covalently bound to the surface by means of UV light or γ-radiation. The added beauty of this approach is that any likely rearrangement of the film during surface binding can result in purification of the monolayer of impurities and the lack of reaction initiating chemical or products can be expected to result in more homogeneous overlayers.

VII. REFERENCES

(1) Wolf, S.; Tauber, R. N. *Silicon Processing for the VLSI Era*; Lattice Press: Sunset Beach, 1986.

(2) Bansal, A.; Li, X.; Lauermann, I.; Lewis, N. S.; Yi, S. I.; Weinberg, W. H. *J. Am. Chem. Soc.* **1996**, *118*, 7225.

(3) Linford, M. R.; Chidsey, C. E. D. *J. Am. Chem. Soc.* **1993**, *115*, 12631.

(4) Linford, M. R.; Fenter, P.; Eisenberger, P. M.; Chidsey, C. E. D. *J. Am. Chem. Soc.* **1995**, *117*, 3145.

(5) Lauerhaas, J. M.; Sailor, M. J. *Science* **1993**, *261*, 1567.

(6) Lee, E. J.; Ha, J. S.; Sailor, M. J. *J. Am. Chem. Soc.* **1995**, *117*, 8295.

(7) Allongue, P.; Kieling, V.; Gerischer, H. *J. Phys. Chem.* **1995**, *99*, 9472.

(8) Ando, A.; Miki, K.; Matsumoto, K.; Shimizu, T.; Morita, Y.; Tokumoto, H. *Jpn. J. Appl. Phys.* **1996**, *35*, 1064.

(9) Lei, J. A.; Bai, Y. B.; Wang, D. J.; Li, T. J.; Tian, K. E. *Thin Solid Films* **1994**, *243*, 459.

(10) Hsu, J. W. P.; Bahr, C. C.; vom Felde, A.; Downey, S. W.; Higashi, G. S.; Cardillo, M. J. *J. Appl. Phys.* **1992**, *71*, 4983.

(11) Myamlin, V. A.; Pleskov, Y. V. *Electrochemistry of Semiconductors*; Plenum Press: New York, 1967.

(12) Kumar, A.; Lewis, N. S. *J. Phys. Chem.* **1991**, *95*, 7021.

(13) Brattain, W. H.; Garrett, C. G. B. *Bell Syst. Tech. J.* **1955**, *34*, 129.

(14) Bolts, J. M.; Bocarsly, A. B.; Palazzotto, M. C.; Walton, E. G.; Lewis, N. S.; Wrighton, M. S. *J. Am. Chem. Soc.* **1979**, *101*, 1378.

(15) Sze, S. M. *The Physics of Semiconductor Devices;* 2nd ed.; Wiley: New York, 1981.

(16) Buczkowski, A.; Radzimski, Z. J.; Rozgonyi, G. A.; Shimura, F. *J. Appl. Phys.* **1991**, *69*, 6495.

(17) Lewis, N. S. *Ann. Rev. Phys. Chem.* **1991**, *42*, 543.

(18) Murray, R. *Electroanalytical Chemistry*; Marcel Dekker: New York, 1984; Vol. 13, pp 191.

(19) Somorjai, G. A. *Chemistry in Two Dimensions: Surfaces*; Cornell University Press: Ithaca, NY, 1981.

(20) Durand, R. R.; Bencosme, C. S.; Collman, J. P.; Anson, F. C. *J. Am. Chem. Soc.* **1983**, *105*, 2710.

(21) Yamamoto, Y.; Nishihara, H.; Aramaki, K. *J. Electrochem. Soc.* **1993**, *140*, 436.

(22) Notoya, T.; Poling, G. W. *Corrosion* **1979**, *35*, 193.

(23) Bowden, F. P.; Tabor, D. *The Friction and Lubrication of Solids*; Oxford University Press: London, 1968.

(24) Zisman, W. A. *Friction and Wear*; Elsevier: New York, 1959.

(25) Kaelble, D. H. *Physical Chemistry of Adhesion*; Wiley-Interscience: New York, 1971.

(26) Leyden, D. E.; Collinus, W. *Silylated Surfaces*; Gordon and Breach, Science Publishers Inc.: New York, 1980.

(27) *Silanes, Surfaces, and Interfaces*; Leyden, D. E., Ed.; Gordon, Breach and Harwood: Snowmass, Colorado, 1986; Vol. 1.

(28) Barraud, A.; Rosilio, C.; Teixier, A. R. *J. Coll. Interf. Sci.* **1977**, *62*, 509.

(29) Barraud, A.; Rosilio, C.; Tiexier, A. R. *Solid State Technol.* **1979**, 120.

(30) Barraud, A.; Rosilio, C.; Teixier, A. R. *Thin Solid Films* **1980**, *68*, 91.

(31) Barraud, A. *Thin Solid Films* **1983**, *99*, 317.

(32) Calvert, J. M. *Organic Thin Films and Surfaces*; Academic Press: San Diego, CA, 1993.

(33) Staring, E. G. J. *Rec. Trav. Chim.* **1991**, *110*, 492.

(34) Derose, J. A.; Leblanc, R. M. *Surf. Sci. Rep.* **1995**, *22*, 73.

(35) Geddes, N. J.; Sambles, J. R.; Martin, A. S. *Adv. Mater. Opt. Electron.* **1995**, *5*, 305.

(36) Simon, R. A.; Wrighton, M. S. *Appl. Phys. Lett.* **1984**, *44*, 930.

(37) Serpone, N.; Borgarello, E.; Pelizzetti, E. In *Photocatalysis and Environment* ; M. Schiavello, Ed.; Kluwer Academic Publishers: Dordrecht, 1988; Vol. 237; pp 499.

(38) Ollis, D.; Pelizzetti, E.; Serpone, N. In *Photocatalysis: Fundamentals and Applications* ; N. Serpone and E. Pelizzetti, Ed.; John Wiley & Sons: New York, 1989; pp 603.

(39) Ollis, D. F. *Environ. Sci. Technol.* **1985**, *19*, 480.

(40) Matthews, R. W. *J. Phys. Chem.* **1987**, *91*, 3328.

(41) Kormann, C.; Bahnemann, D. W.; Hoffmann, M. R. *Environ. Sci. Technol.* **1991**, *25*, 494.

(42) Fox, M. A. In *Photocatalysis and Environment: Trends and Applications* ; M. Schiavello, Ed.; Kluwer Academic Publishers: Dordrecht, 1988; Vol. 237; pp 445.

(43) Furtak, T. E.; Canfield, D. C.; Parkinson, B. A. *J. Appl. Phys.* **1980**, *51*, 6018.

(44) Lunt, S. R.; Casagrande, L. G.; Tufts, B. J.; Lewis, N. S. *J. Phys. Chem.* **1988**, *92*, 5766.

(45) Ulman, A. *An Introduction to Ultrathin Organic Films*; Academic: San Diego, CA, 1991.

(46) Roberts, G. *Langmuir-Blodgett Films*; Plenum Press: New York, 1990.

(47) Bocarsly, A. B.; Walton, E. G.; Wrighton, M. S. *J. Am. Chem. Soc.* **1980**, *102*, 3390.

(48) Bocarsly, A. B.; Walton, E. G.; Bradley, M. G.; Wrighton, M. S. *J. Electroanal. Chem.* **1979**, *100*, 283.

(49) Wrighton, M. S.; Austin, R. G.; Bocarsly, A. B.; Bolts, J. M.; Haas, O.; Legg, K. D.; Nadjo, L.; Palazzotto, M. C. *J. Am. Chem. Soc.* **1978**, *100*, 1602.

(50) Angst, D. L.; Simmons, G. W. *Langmuir* **1991**, *7*, 2236.

(51) Wasserman, S. R.; Tao, Y. T.; Whitesides, G. M. *Langmuir* **1989**, *5*, 1074.

(52) Wasserman, S. R.; Whitesides, G. M.; Tidswell, I. M.; Ocko, B. M.; Pershan, P. S.; Axe, J. D. *J. Am. Chem. Soc.* **1989**, *111*, 5852.

(53) Maoz, R.; Sagiv, J. *J. Colloid Interface Sci.* **1984**, *100*, 465.

(54) Pomerantz, M.; Segmuller, A.; Netzer, L.; Sagiv, J. *Thin Solid Films* **1985**, *132*, 153.

(55) Dulcey, C. S.; Georger, J. H.; Krauthamer, V.; Fare, T. L.; Stenger, D. A.; Calvert, J. M. *Science* **1991**, *252*, 551.

(56) Silberzan, P.; Leger, L.; Aussere, D.; Benattar, J. J. *Langmuir* **1991**, *7*, 1647.

(57) Davies, G., H,; Yarwood, J. Y. *Spectrochim. Acta* **1987**, *43A*, 1619.

(58) Gilman, H.; Ingham, R. K.; Moore *J. Am. Chem. Soc.* **1940**, *62*, 2327.

(59) Gilman, H.; Moore; Bain *J. Am. Chem. Soc.* **1941**, *63*, 2479.

(60) Vogel, A. I. *Vogel's Textbook of Practical Organic Chemistry;* 5th. ed.; Longman: New York, 1989.

(61) Etching silicon samples in 40% NH_4F solution, that had been prepared by dissolving 99.99+% pure NH_4F (Aldrich) in filtered de-ionized water, did not give the desired hydrophobic silicon surface. A high resolution XP spectra of this surface, exhibited a broad low intensity peak in the Si 2p region at a position approx. 2.5 eV higher in binding energy than the bulk silicon peak. This peak was suggestive of presence of silicon oxide on the surface. Surprisingly, this suboxide could not be removed when this surface was immersed in HF/NH_4F solution. However, as suggested by Dr. Yves Chabal of AT&T Bell Labs (Lucent Technologies), etching the silicon surfaces in 40% NH_4F solution obtained from Transene company gave the desired hydrophobic, monohydride-terminated silicon surface. Also, towards obtaining hydrophobic monohydride-terminated silicon surfaces, flash-photolysed water gave better results than 18 Megaohm cm water obtained from a Barnstead E-Pure 4 element filter. The length of the water rinse also

seemed to affect the extent of monohydride termination. A brief rinse of 2-5 seconds followed by drying in a stream of nitrogen gave the best results.

(62) Higashi, G. S.; Chabal, G. W.; Trucks, G. W.; Raghavachari, K. *Appl. Phys. Lett.* **1990**, *56*, 656.

(63) Hassler, K.; Koll, W. *J. Organomet. Chem.* **1995**, *487*, 223.

(64) Wyman, D. P.; Wang, J. Y. C.; Freeman, W. R. *J. Org. Chem.* **1963**, *28*, 3173.

(65) Meen, R. H.; Gilman, H. *J. Org. Chem.* **1958**, *23*, 314.

(66) Rosenberg, H.; Groves, J. D.; Tamborski, C. *J. Org. Chem.* **1960**, *25*, 243.

(67) Occasionally if Mg or halide signals were seen in XPS after sonication, the surface was rinsed briefly with water and methanol and then characterized.

(68) Seah, M. P. In *Practical Surface Analysis ;* 2nd ed.; D. Briggs and M. P. Seah, Ed.; John Wiley & Sons: Chichester, 1990; Vol. 1; pp 201.

(69) Scofield, J. H. *J. Electron Spectrosc. Relat. Phenom.* **1976**, *8*, 129.

(70) Sconce, J. S. *Chlorine, its Manufacture, Properties and Uses.*; Reinhold Pub. Corp.: New York, 1962.

(71) Durbin, T. D.; Simpson, W. C.; Chakarian, V.; Shuh, D. K.; Varekamp, P. R.; Lo, C. W.; Yarmoff, J. A. *Surf. Sci.* **1994**, *316*, 257.

(72) Schnell, R. D.; Rieger, D.; Bogen, A.; Himpsel, F. J.; Wandelt, K.; Steinmann, W. *Phys. Rev. B* **1985**, *32*, 8057.

(73) Yarmoff, J. A.; Shuh, D. K.; Durbin, T. D.; Lo, C. W.; Lapiano-Smith, D. A.; McFeely, F. R.; Himpsel, F. J. *J. Vac. Sci. Technol.* **1992**, *A10*, 2303.

(74) Tufts, B. J.; Kumar, A.; Bansal, A.; Lewis, N. S. *J. Phys. Chem.* **1992**, *96*, 4581.

(75) Laibinis, P. E.; Bain, C. D.; Whitesides, G. M. *J. Phys. Chem.* **1991**, *95*, 7017.

(76) Tillman, N.; Ulman, A.; Schildkraut, J. S.; Penner, T. L. *J. Am. Chem. Soc.* **1988**, *110*, 6136.

(77) Widdra, W.; Huang, C.; Yi, S. I.; Weinberg, W. H. *J. Chem. Phys.* **1996**, *105*, 5605.

(78) In *Annual Book of ASTM Standards* 1990; pp F 576.

(79) Cheng, K. L. *Japan. J. Appl. Phys.* **1995**, *34*, 5527.

(80) Stinespring, C. D.; Wormhoudt, J. C. *J. Appl. Phys.* **1989**, *65*, 1733.

(81) Mende, G.; Finster, J.; Flamm, D.; Schulze, D. *Surf. Sci.* **1983**, *128*, 169.

(82) Burrows, V. A.; Chabal, Y. J.; Higashi, G. S.; Raghavachari, K.; Christman, S. B. *Appl. Phys. Lett.* **1988**, *53*, 998.

(83) Yablonovitch, E.; Allara, D. L.; Chang, C. C.; Gmitter, T.; Bright, T. B. *Phys. Rev. Lett.* **1986**, *57*, 249.

(84) Grunthaner, F. J.; Grunthaner, P. J.; Vasquez, R. P.; Lewis, B. F.; Maserjian, J.; madhukar, A. *Phys. Rev. Lett.* **1979**, *43*, 1683.

(85) Grunthaner, P. J.; Grunthaner, F. J.; Fathauer, R. W.; Lin, T. L.; Hecht, M. H.; Bell, L. D.; Kaiser, W. J.; Schowengerdt, F. D.; Mazur, J. H. *Thin Solid Films* **1989**, *183*, 197.

(86) Grunthaner, P. J.; Hecht, M. H.; Grunthaner, F. J.; Johnson, N. M. *J. Appl. Phys.* **1987**, *61*, 629.

(87) Himpsel, F. J.; Meyerson, B. S.; McFeely, F. R.; Morar, J. F.; Taleb-Ibrahimi, A.; Yarmoff, J. A. In *Photoemission and Absorption Spectroscopy of Solids and Interfaces with Synchrotron Radiation* ; M. Campagna and R. Rosei, Ed.; North-Holland Elsevier Science Publishers B.V.: Amsterdam, 1990.

(88) Himpsel, F. J. *Acta Phys. Polon. A* **1994**, *86*, 771.

(89) Higashi, G. S.; Becker, R. S.; Chabal, Y. J.; Becker, A. J. *Appl. Phys. Lett* **1991**, *58*, 1656.

(90) Chabal, Y. J.; Harris, A. L.; Raghavachari, K.; Tully, J. C. *Int. J. Mod. Phys. B* **1993**, *7*, 1031.

(91) Dumas, P.; Chabal, Y. J.; Jakob, P. *Appl. Surf. Sci.* **1993**, *65/66*, 580.

(92) Pietsch, G. J.; Higashi, G. S.; Chabal, Y. J. *Appl. Phys. Lett.* **1994**, *64*, 3115.

(93) Widdra, W.; Huang, C.; Briggs, G. A. D.; Wienberg, W. H. *J. Electron. Spec. Rel. Phenom.* **1993**, *64-5*, 129.

(94) Schulze, G.; Henzler, M. *Surf. Sci.* **1983**, *124*, 336.

(95) Sonication of the chlorinated samples in anhydrous methanol or dichloromethane did not result in any decrease in the coverage of adventitious C or O. The sonication process, also, did not result in a decrease in the chlorine coverage or an increase in surface oxidation.

(96) Whitman, L. J.; Joyce, S. A.; Yarmoff, J. A.; McFeely, F. R.; Terminello, L. J. *Surf. Sci.* **1990**, *232*, 297.

(97) Florio, J. V.; Robertson, W. D. *Surf. Sci.* **1969**, *18*, 398.

(98) Gao, Q.; Cheng, C. C.; Chen, P. J.; Choyke, W. J.; Yates Jr., J. T. *Thin Solid Films* **1993**, *225*, 140.

(99) Gupta, P.; Coon, P. A.; Koehler, B. G.; George, S. M. *Surf. Sci.* **1991**, *249*, 92.

(100) For these surfaces the lack of signal due to Cl in the XP spectra could be due to the lower sensitivity of the XPS technique.

(101) Chidsey, C. E. D.; Loiacono, D. N. *Langmuir* **1990**, *6*, 682.

(102) Porter, M. D.; Bright, T. B.; Allara, D. L.; Chidsey, C. E. D. *J. Am. Chem. Soc.* **1987**, *109*, 3559.

(103) Socrates, G. *Infrared Characteristic Group Frequencies;* 2nd ed.; John Wiley & Sons: Middlesex, U.K., 1994.

(104) Huang, C.; Widdra, W.; Wang, X. S.; Weinberg, W. H. *J. Vac. Sci. Technol.* **1993**, *A11*, 2250.

(105) Yoshinobu, J.; Tsuda, H.; Onchi, M.; Nishijima, M. *Solid State commun.* **1986**, *60*, 801.

(106) The slightly larger effective coverage calculated from Cl 2p peak in the survey scan could be due to additional contribution to the Cl 2p peak intensity from the third harmonic of the Si 2s plasmon loss peak.

(107) This assumption was not necessary to obtain an areal coverage of 0.5 monolayer. Assuming that the chains were not held rigidly and that the F atoms were randomly (uniformly) distributed in the overlayer, the coverage values obtained were 0.50±0.06 and 0.57±0.10 for the survey and high resolution data, respectively, of $CF_3(CH_2)_3MgBr$ and 0.51±0.01 from the survey data of CF_3CH_2OLi.

(108) Ewen, B.; Strobl, G. R.; Richter, D. *Faraday Discuss. Chem. Soc.* **1980**, *69*, 19.

(109) Gilman, H.; Ingham, R. K. *J. Am. Chem. Soc.* **1955**, *77*, 1680.

(110) Boutevin, B.; Guida-Pietrasanta, F.; Ratsimihety, A. *J. Fluorine Chem.* **1993**, *60*, 211.

(111) Wunderlich, B. *Macromolecular Physics*; Academic Press: New York, 1973; Vol. 1.

(112) Nakagawa, O. S.; Ashok, S.; Sheen, C. W.; Märtensson, J.; Allara, D. L. *Jpn. J. Appl. Phys.* **1991**, *30*, 3759.

(113) Weast, R. C.; Astle, M. J.; Bayer, W. H. *Handbook of Chemistry and Physics;* 71^{th} ed.; CRC Press: Boca Baton, FL., 1991.

(114) Boutevin, B.; Guida-Pietrasanta, F.; Ratsimihety, A.; Caporiccio, G. *J. Fluorine Chem.* **1994**, *68*,

(115) Boutevin, B.; Guida-Pietrasanta, F.; Ratsimihety, A.; Caporiccio, G. *J. Fluorine Chem.* **1995**, *70*, 53.

(116) Boutevin, B.; Guidapietrasanta, F.; Ratsimihety, A.; Caporiccio, G. *J. Fluorine Chem.* **1995**, *75*, 75.

(117) Bansal, A. "Research Proposal: Modification of Silicon Surface by Covalently Attached Langmuir-Blodgett Film," California Institute of Technology, 1996.

Chapter 4

Electrical Properties of n-Si(111) Surfaces Derivatized with Covalently Attached Alkane Chains

Abstract

The electrical properties of alkyl-terminated n-Si(111) surfaces, prepared via the two-step halogenation/alkylation procedure, were analyzed in contact with CH_3OH-$Me_2Fc^{+/0}$ solution and in contact with Au. Current-voltage and capacitance-voltage measurements of these surfaces in CH_3OH-$Me_2Fc^{+/0}$ solution indicated that the electrical properties of the alkyl-terminated surfaces were very similar to those of a H-terminated surface. The alkyl overlayers did not shift the band edges or induce additional surface recombination but they did provide a small resistance to charge transfer across the Si/liquid interface. I-V characteristics of n-Si/alkyl/Au MIS devices indicated that these junctions, as prepared, behaved largely like n-Si/Au Schottky junctions. The efficacy of alkyl overlayers in preventing photooxidation and photocorrosion of n-silicon surfaces was measured in contact with $Fe(CN)_6^{3-/4-}$(aq) solution and with $Me_2Fc^{+/0}$ solutions to which a known amount of water had been added. The alkyl-terminated surfaces consistently showed better I-V characteristics and lower oxidation rates than the H-terminated surface, indicating that stability to oxidation had been achieved without any significant compromise in the electrical quality of the silicon surface.

I. INTRODUCTION

Although almost all contemporary microelectronic devices based on silicon have their origin in the hydrogen-terminated silicon surface,[1,2] the outstanding electrical properties of these surfaces are short lived due to oxidation in air even on the time scale of hours.[3] These H-terminated surfaces are also unstable in contact with aqueous media and photooxidize or photocorrode rapidly under illumination.[4-7] Functionalization of the semiconductor surface without partial oxidation and/or formation of electrical defects is one approach towards achieving control over the chemical, physical and electrical properties of the surface.[8-10] Such modifications can be potentially important in fabricating improved electronic devices[2,11] as well as in measurement of charge transfer rate constants at semiconductor/liquid contacts.[12]

The formation of monomolecular assemblies at semiconductor surfaces provides a rational approach for fabricating interfaces with a well-defined composition, structure and properties.[13-17] Earlier work on modification of the silicon surface using this approach has emphasized attachment of various molecules to the surface using silanization chemistry.[6,13-15,18-27] This step unavoidably introduces a non-optimal Si/SiO_2 interface as the anchoring layer, compromising the electrical properties of the resulting surface. Only recently it has been demonstrated that modification of silicon surface is also possible by attaching molecules directly to the surface silicon atoms without concomitant oxidation of the surface.[8-10] These modified surfaces were found to have superior physical and chemical qualities compared to a H-terminated surface. In particular, the derivatized surfaces were found to be more resistant to oxidation in air and in contact with wet chemical environments.[8-10] However, it was not clear whether the improvements in the physical and chemical properties were achieved at a cost of inferior electrical properties, or if the electrical properties of the derivatized silicon surfaces were at par with, or even better than, the excellent electrical properties of a freshly etched silicon surface.[3] Although a

major application of silicon surfaces is in electronic devices, no study on the electrical characterization of such systems yet exists in the literature.

This chapter describes the results of electrochemical experiments performed to evaluate the electrical properties of silicon surfaces that have been chemically modified with alkyl groups, via the two-step halogenation/alkylation procedure, reported recently in the literature.[8] A large body of literature available on the behavior of H-terminated silicon surfaces in contact with various redox couples provides a ready reference point against which the properties of the alkyl derivatized surfaces can be evaluated.[28-42]

It is known that hydrogen-terminated n-silicon photoelectrodes in contact with non-aqueous electrolytes make extremely stable and efficient photoelectrochemical cells.[38,43] In fact, the hydrogen-terminated silicon surface is so electrically perfect that less than 1 in 10^6 surface atoms acts as a recombination site.[31,44] The electrical properties of this system are limited only by recombination of photogenerated charge carriers in the bulk of the silicon.[31,44] Functionalization of the silicon surface would thus be of limited use if the chemical modifications resulted in defects which mediated recombination and degraded the electrical properties. The electrical properties of the modified silicon surfaces were therefore evaluated by steady-state current voltage (I-V) measurements and capacitance voltage (C-V) measurements in contact with methanol-dimethylferrocene$^{+/0}$ (CH_3OH-$Me_2Fc^{+/0}$) solution. In each case, the electrical properties of a hydrogen-terminated surface, under identical conditions, were used as a benchmark.

It is well known that silicon/metal Schottky junctions exhibit Fermi level pinning and display low open circuit voltages due to formation of metal silicides.[2,45-47] One successful technique to avoid these drawbacks is to create a metal-insulator-semiconductor junction (MIS).[48-51] An extremely thin insulator (typically 5-20 Å silicon oxide) layer interposed between the metal and silicon prevents the formation of metal silicides and thus prevents Fermi level pinning. The requirements on this insulator layer are stringent. It should be thick enough to prevent silicide formation and yet it should be thin enough as not

to add significant series resistance to the junction. In addition, the insulator should not introduce recombination centers or trap fixed or mobile charges (or at least do so in a known, time independent way) that can alter the properties of the device over time. Lastly the layer should be amenable to being formed uniformly and reproducibly. It has already been shown in Chapter 3 that the thickness of the alkyl overlayer can be controlled accurately on a 2-20 Å scale and that the monolayers can be formed uniformly and reproducibly.[8] The ability of alkyl monolayers to act as a thin insulator layer was therefore evaluated by making Si/alkyl/Au MIS solid-state devices. The electrical characteristics of this device were compared with MIS devices made from thin oxide layers.[48]

Another important goal of the electrical characterization was to measure the efficacy of the alkyl layers in preventing photooxidation of silicon in aqueous environments. Stabilization of silicon surface towards photooxidation is one of the "holy grails" of semiconductor-liquid junction photoelectrochemistry, and it is well known that H-terminated n-silicon surfaces undergo rapid photooxidation and photocorrosion in aqueous environments upon illumination.[4-7] The alkyl overlayers were expected to impart stability by either acting as a barrier layer or by virtue of the formation of strong Si-C bonds. If the alkyl monolayers behave primarily as a barrier, the propensity towards oxidation is expected to reduce when the derivatization is performed with increasing alkyl chain lengths. On the other hand, if stability is achieved due to formation of Si-C bonds, the alkyl-terminated surfaces are expected to be more stable than the H-terminated surface, but any increase in the alkyl chain length would not impart any additional stability. The stability of alkyl-modified surfaces was therefore evaluated by deliberately destabilizing the n-Si/$Me_2Fc^{+/0}$ junction by adding a known amount of water to the CH_3OH-$Me_2Fc^{+/0}$ solution, running the cell under illumination at short circuit, and then measuring the extent of oxidation by X-ray photoelectron spectroscopy (XPS). Finally, the stability of alkyl-terminated surfaces was also evaluated in contact with $Fe(CN)_6^{3-/4-}$(aq) solution in which the H-terminated surface is known to be unstable.[7]

II. EXPERIMENTAL

1. Silicon Samples

The silicon samples used in the electrochemical studies were phosphorus doped n-type, single crystal Si(111) wafers of 100 mm diameter and polished on one side (Wafernet Inc). They were either 500±50 μm thick and of 1.5-3.0 ohm cm resistivity or 575±20 μm thick and of 3-6 ohm cm resistivity. The wafers were cut into small pieces and either derivatized as described in the literature[8] (see Chapter 3) or etched and characterized.

2. Chemicals and Redox Couples

Buffered hydrofluoric acid (b-HF) and 40% ammonium fluoride (NH_4F) were obtained from Transene Co. (Rowland, MA). Dimethylferrocene (Me_2Fc) (Strem Chemicals) was purified by vacuum sublimation. Dimethylferrocenium hexafluoro phosphate ($Me_2Fc^+PF_6^-$) was prepared by oxidizing dimethylferrocene with benzoquinone in HPF_6(aq).[43] $LiClO_4$ (Aldrich) and methanol (EM Science) were used as such. As outlined in the results section, different amounts of the dimethylferrocenium/ dimethylferrocene ($Me_2Fc^{+/0}$) were used depending upon the unique requirements of the experiments. $K_4Fe(CN)_6$ (J.T. Baker) and $K_3Fe(CN)_6$ (J.T. Baker) were used as such. 99.99% Au (Materials Research Corp.) was used for making metal-insulator-semiconductor (MIS) devices.

3. Electrochemical Cell Assembly

The current-voltage (I-V), capacitance-voltage (C-V) and electrode stability measurements were conducted in a custom-made cell of 50 ml total volume that was made of Delrin (Figure 1). The exposed area of the electrode was 2.4 cm^2 (1.25 cm x 1.9 cm). The samples were illuminated through a window in the front of the cell that had an area of ~6 cm^2 (1.9 cm x 3.15 cm), ensuring that the entire electrode surface was uniformly illuminated. The front window, which was made from 10 Ω° LOF conducting glass (provided by Mr. Fred Millet, Toledo, OH), was coated on one side (facing the cell) with F

Figure 1. Schematic of a custom-made electrochemical cell fabricated from Delrin. The semiconductor working electrode was sealed onto the cell body by means of a Viton O-ring. The conducting glass acted as the front window and as a counter electrode. The platinum wire served as the pseudo-reference electrode. To form a two compartment, four electrode cell, the Delrin cell was modified, by inserting a test-tube modified at one end with a Vycor frit, through the larger hole in the top cover to form the second compartment that held the counter electrode. The front tin oxide window now served as the second working electrode.

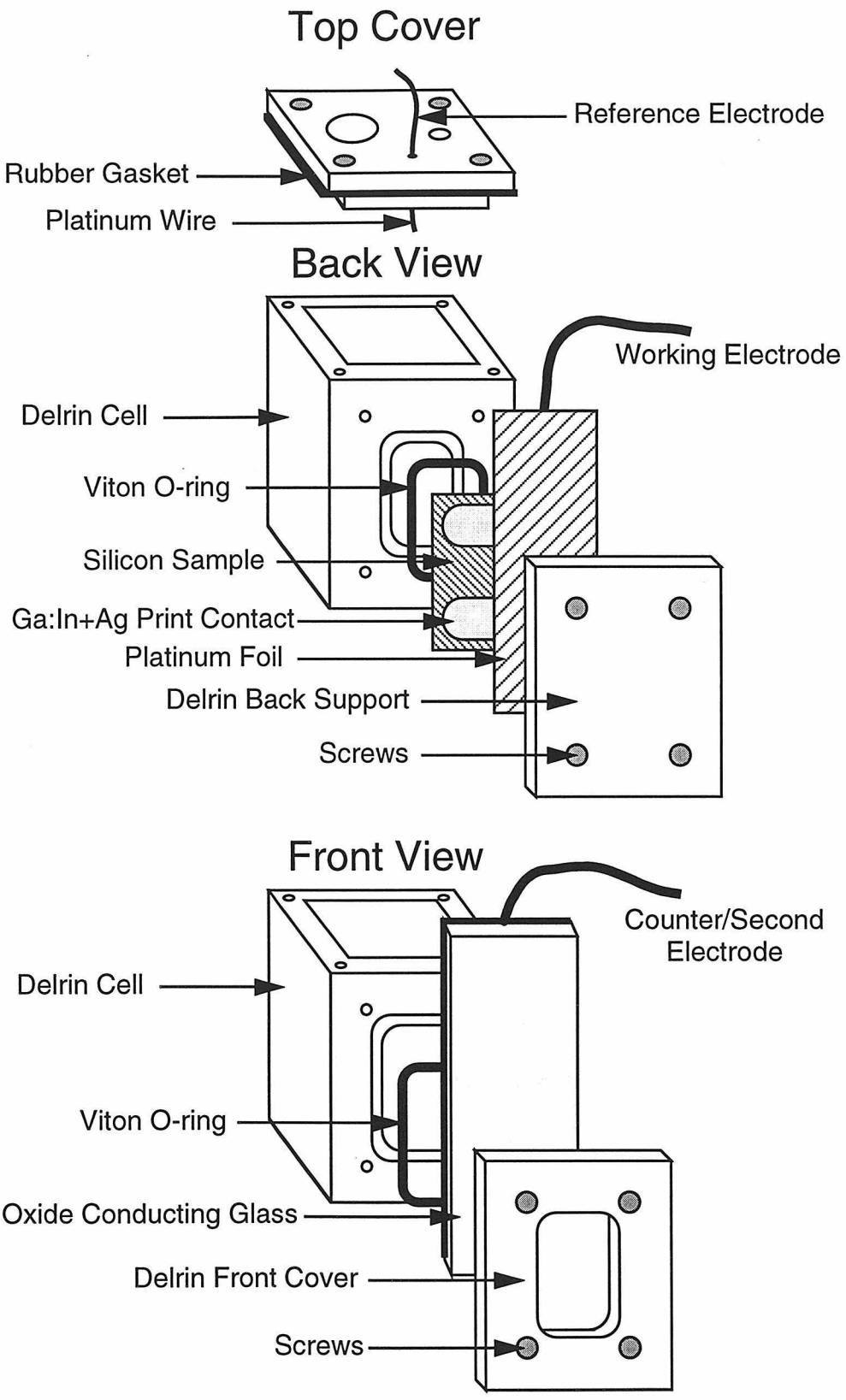
Top Cover
Reference Electrode
Rubber Gasket
Platinum Wire
Back View
Working Electrode
Delrin Cell
Viton O-ring
Silicon Sample
Ga:In+Ag Print Contact
Platinum Foil
Delrin Back Support
Screws
Front View
Counter/Second Electrode
Delrin Cell
Viton O-ring
Tin Oxide Conducting Glass
Delrin Front Cover
Screws

doped tin oxide and also served either as the counter electrode or as a second working electrode (*vide infra*). I-V characteristics of a platinum foil working electrode were found to be identical whether the counter electrode was the tin oxide window or another Pt electrode, indicating that the use of the more convenient tin oxide counter electrode did not add any significant series resistance to the cell. The silicon sample and the counter electrode were sealed onto the cell casing by means of Viton O-rings. The sample was scratched on the back with Ga:In eutectic mixture, a dab of conductive Ag print (GC electronics) was applied, and the sample was contacted with a long piece of 0.05 mm thick Pt foil (Aldrich 99.9+%). A flat piece of Delrin was then used at the back to press the silicon and the contact against the O-ring, by means of four screws that could be finger tightened. A thin platinum wire of 0.5 mm diameter was inserted through a small hole in the top cover of the cell, epoxied with Epoxi-Patch Kit 1C white epoxy (Dexter Corp.), and was positioned adjacent to the semiconductor electrode. During the experiment the Pt wire stayed immersed in the redox solution and served as the reference electrode. The redox/electrolyte solution could be added to the assembled cell through a small hole in the top cover. The top cover also contained another larger hole through which a thermometer, a saturated calomel electrode (SCE) or a fritted second compartment could be inserted into the cell. The solution was stirred with a Teflon coated magnetic stir bar placed inside the cell.

For experiments that required the use of a two compartment, four electrode cell, the Delrin cell was modified by inserting a test-tube modified at one end with a Vycor frit through the top cover to form the second compartment that held the counter electrode immersed in a solution of $Me_2Fc^{+/0}$. The front tin oxide window now served as the second working electrode. The semiconductor electrode and the reference electrode were set up as described above.

4. Electrochemical Techniques and Measurements

(a) Current-Voltage (I-V) Measurements

I-V characteristics of H-terminated and alkyl-terminated silicon electrodes were determined in contact with CH_3OH-50 mM Me_2Fc-1 to 2 mM $Me_2Fc^+PF_6^-$ solutions containing 1.0 M $LiClO_4$ as electrolyte. The I-V curves were plotted on a Houston Instruments Model 2000 X-Y recorder at a scan rate of 50 mV/s. Potential control was accomplished with a Princeton Applied Research model 173 potentiostat and model 175 universal programmer. Samples were illuminated by ELH or ENH type tungsten-halogen bulbs.[43] All potentials were recorded vs. a Pt wire poised at the Nernstian potential of the redox couple (cell potential). The limiting photocurrent density, J_{ph}, was measured at +0.050 V vs. the cell potential. Occasionally at the end of the experiment, a methanolic standard calomel electrode (SCE)[39] was used to measure the redox potential of the solution vs. the SCE. I-V characteristics of the H-terminated and alkyl-terminated electrodes were determined in contact with 0.35 M $K_4Fe(CN)_6$-0.05 M $K_3Fe(CN)_6$ (aq) in a similar manner.

I-V measurements on the H-terminated and alkyl-terminated silicon surfaces were also done in a metal-insulator-semiconductor (MIS) configuration. A front mask with an exposed circular area of 0.8 cm^2 was used to define the front contact. The back contact, along with the sample, was pressed against the mask to ensure a good electrical contact at the rear. The whole assembly was put in an evaporator and 210±5 Å of Au was evaporated at a pressure of $(1\text{-}5)\times10^{-6}$ Torr.[48] The assembly was then taken out of the evaporator and the front contact to the sample was achieved using a custom-made probe station employing a gold wire.

(b) Capacitance-Voltage Measurements

The barrier height of a semiconductor/liquid junction in contact with a redox couple can be calculated based on the Mott-Schottky equation, which describes the dependence of

the differential capacitance of the semiconductor space charge layer on the applied bias.[2,52] The semiconductor-liquid junction can be described by three capacitances, the semiconductor space charge capacitance (C_{sc}), the liquid Helmholtz capacitance (C_H) and the ionic diffuse layer capacitance (C_d), which are in series with each other. Since $C_{sc} << C_H$ and $C_{sc} << C_d$, the equivalent circuit of the junction can be reduced to a single capacitor (C_{sc}), with a resistor (R_{sc}) in parallel to it and another resistor (R_s) in series with the two.[36,39] In this model, R_{sc} represents the voltage dependent resistance of the semiconductor space charge layer and R_s accounts for all the other resistances in the cell that are in series with the semiconductor-liquid junction.

The C_{sc} values can be determined from the experimental impedance data using the equation

$$\omega C_{sc} = \frac{1+\left(1-4\left(\frac{Z_{im}}{R_{sc}}\right)^2\right)^{1/2}}{2\,Z_{im}} \qquad (1)$$

where Z_{im} is the imaginary component of the complex impedance at a given frequency and $\omega = 2\pi f$.[2,52] According to the Mott-Schottky equation,

$$C_{sc}^{-2} = \frac{2}{q\varepsilon\varepsilon_0 N_D A_s^2}\left(V - V_{fb} - \frac{kT}{q}\right) \qquad (2)$$

where ε is the relative permittivity of silicon, ε_0 is the permittivity of free space, N_D is the dopant density of the semiconductor, A_s is the area of the electrode, V is the applied bias and V_{fb} is the flat-band potential. A plot of C_{sc}^{-2} vs. V should give a straight line with $(2/(q\varepsilon\varepsilon_0 N_D A_s^2))$ as the slope and an x-intercept of $(V_{fb}+(kT/q))$.

Impedance data for the H-terminated and alkyl-terminated surfaces in contact with CH_3OH-1.0 M $LiClO_4$-0.100 M Me_2Fc-5 mM $Me_2Fc^+PF_6^-$ solution were obtained on a Schlumberger model 1260 frequency response analyzer equipped with a Schlumberger model 1286 electrochemical interface. An impedance measurement consisted of 13 frequency sweeps, from 10^5 to 10^2 Hz, in the dark, each with a 10 mV peak ac amplitude,

taken at 0.050 V intervals of DC reverse bias ranging from 0.000 V to 0.600 V applied to the electrode vs. the Nernstian cell potential. The actual range of frequency that was analyzed (typically 40 KHz-400 Hz) was only that for which the phase angle of the complex impedance was greater than 80°, i.e. for which the system behaved primarily as a capacitor.[2,52] The space charge resistance (R_{sc}) was calculated for each dc bias by fitting the plot of the negative of the imaginary component of the impedance vs. the real component of the impedance (Nyquist plot) to a semicircle and taking the diameter of the semicircle to be R_{sc}.[2,52] C_{sc}^{-2} was then plotted as a function of the reverse DC bias applied to the semiconductor according to the Mott-Schottky equation for a semiconductor-liquid contact in depletion.[2,52] Straight line fits to the data were extrapolated to infinite C_{sc} (C_{sc}^{-2} = 0), which corresponds to the situation at flat band. The voltage axis intercept of the plot gave the flat-band potential (V_{fb}) of the junction.[2,52] The barrier height of the junction was then calculated by adding the potential difference between the Fermi level and the bottom of the conduction band (V_n) to $|V_{fb}|$.[2,52]

(c) Electrode Stability Measurements

The stability of the derivatized electrode towards photooxidation in the presence of water was measured in contact with $Me_2Fc^{+/0}$ solution to which a known amount of water had been added. Two different methods were used to compare the stability of derivatized electrodes with that of the H-terminated electrodes. In the first method, H-terminated or alkyl derivatized electrodes were first exposed to a CH_3OH-1.0 **M** $LiClO_4$-50 m**M** Me_2Fc-1-5 m**M** $Me_2Fc^+PF_6^-$ solution. The electrodes were stabilized in contact with this solution, in the dark, by cycling the potential between -0.80 V and +0.50 V vs. the Nernstian cell potential for ~30 minutes. It is known that in contact with the $Me_2Fc^{+/0}$ solution, this procedure yields improved and stable I-V curves for H-terminated electrodes.[39] The stabilization procedure did not significantly affect the dark I-V characteristics of the alkyl-terminated electrodes. I-V scans were then taken between -0.70 V and +0.20 V at a few different levels of illumination and plots of $\ln(J_{ph})$ vs. V were

analyzed to ensure that the cell was behaving as expected according to literature.[31,53] A 5.0 ml aliquot (out of the 50 ml cell volume) of the solution was then withdrawn from the cell and replaced by 5.0 ml of deionized water. An I-V scan was then taken at J_{ph} = 4.0 mA/cm^2 in this solution and the cell was then held at short circuit. The illumination of the cell was occasionally adjusted to maintain a short circuit photocurrent density of 4.0 mA/cm^2. After 20 minutes, another I-V curve was recorded and the cell was dismantled. The silicon wafer was then rinsed with methanol and broken into three parts. The middle third of the sample was again rinsed with methanol, then sonicated in methanol for 2 min and subsequently analyzed by XPS for oxide coverage.

In the second, more stringent, test of stability, the Delrin cell was modified to form a two compartment, four electrode cell. A Pine Instruments RDE-3 bipotentiostat was used to control the potential of the semiconductor and of the tin oxide electrode. Due to the limitations on the potential achievable by the RDE-3 bipotentiostat, the front window of the cell was masked off to leave only an approximately square opening of 0.69 cm^2 through which the center of the semiconductor electrode was illuminated. In a typical experiment, the cell was setup and the semiconductor electrode was stabilized as described above. A 10.0 ml aliquot (out of the 50 ml cell volume) of the CH_3OH-1.0 **M** $LiClO_4$-50 m**M** Me_2Fc-1 m**M** $Me_2Fc^+PF_6^-$ solution was then withdrawn from the cell and replaced by 10.0 ml of 1.0 **M** $LiClO_4$(aq) solution. As before, the short circuit illumination intensity was then set to 4.0 mA/cm^2 (with respect to the exposed area) and an I-V scan was taken. The working electrode was then held between +0.10 V and +0.40 V vs. the Nernstian cell potential and the light intensity was adjusted occasionally to maintain 4.0 mA/cm^2. In order to ensure that the composition of the working compartment was not significantly affected by the above procedure, the tin oxide electrode was biased opposite to the silicon electrode to pass the same amount of cathodic current through the cell. The experiment was terminated either after the cell displayed significantly resistive I-V characteristics or after

22-25 hours of illumination. As described above, the cell was then dismantled and the illuminated portion of the silicon electrode was analyzed for oxide coverage.

5. X-ray Photoelectron Spectroscopy (XPS)

Details of the XPS instrument have been provided in Chapter 3. The core electrons in the silicon samples were excited using monochromatic Al K_α x-rays (1486.6 eV) incident at 35° from horizontal. The emitted electrons were collected by a hemispherical analyzer also positioned at a take off angle of 35° from horizontal. The axis of the incident x-rays and the analyzer axis were in vertical planes that were at right angles to each other. The silicon samples were mounted on custom-made stainless steel or aluminum sample stubs with the help of gold-plated molybdenum clips or gold-plated screws which also served to ground the samples. Since all samples were sufficiently conducting, all energy measurements are reported referenced to the spectrometer Fermi level.

Data collection and analysis were performed using M-probe package software version 3.4, details of which are provided in Chapter 3. High resolution scans of the Si 2p region were used to evaluate the extent of oxidation of the samples after exposure to the various electrochemical solutions. Data were collected with an elliptic spot of size 800 μm x 1500 μm at two different resolutions. The pass energies corresponding to the two resolutions were 104.67 eV and 53.98 eV, respectively. The corresponding energy windows in which the electrons were collected were 13.95 and 6.85 eV, respectively. This instrument had a resolution (FWHM for Au $4f_{7/2}$ peak) of 1.25±0.01 eV and 1.00±0.01 eV, respectively, for the two different data sets.

Peak analysis routines provided by the M-Probe package software were used to analyze the data. In a typical analysis, the Si 2p high resolution peak was smoothed by a 3 point smoothing routine and then deconvoluted into $2p_{1/2}$ and $2p_{3/2}$ components arising from bulk silicon atoms, as well as a third, usually well separated, component corresponding to the oxidized silicon atoms. In the deconvolution procedure, the starting values for the peak FWHM were often adjusted (and sometimes fixed for the Si $2p_{1/2}$

component) so as to get final results which minimised the difference between the FWHM values for the two peaks. The overall spectra were best fit by using 95% Gaussian/5% Lorentzian and 15% asymmetric lineshapes for the bulk silicon peaks while the oxide peak was best fit by using 95% Gaussian/5% Lorentzian and a symmetric lineshape.

The surface coverage of oxide on the silicon substrate was estimated using the overlayer-substrate model.[54] The thickness of the oxide layer was calculated using the equation

$$d_{ox} = \lambda \sin\theta \ln\left(1 + \left(\frac{I_{ox}}{I_{Si}} \cdot \frac{\rho_{Si}}{\rho_{ox}}\right)\right) \qquad (3)$$

where d_{ox} is the oxide thickness in Å, λ(Å) is the escape depth of Si 2p electrons through the oxide layer, θ is the take off angle from the horizontal, I_{ox}/I_{Si} is the raw intensity ratio of the oxide peak area to the Si $2p_{(1/2+3/2)}$ peak area and ρ_{Si} and ρ_{ox} are *atomic* densities of silicon atoms in the substrate and in the oxide layer. The values used in the above calculations were λ = 26 Å,[43] θ = 35°, $\rho_{Si} = 5 \times 10^{22}$ atoms cm^{-3},[2] and $\rho_{ox} = 2.28 \times 10^{22}$ atoms cm^{-3}.[43]

III. RESULTS

1. Electrical Characteristics of Alkyl-Terminated Silicon Surfaces

(a) Current-Voltage (I-V) Characteristics of Alkyl-Terminated Silicon Surfaces in Contact with Dimethylferrocene$^{+/0}$ ($Me_2Fc^{+/0}$) Solutions

Since H-terminated silicon electrodes are extremely stable in $Me_2Fc^{+/0}$ solution[38,43] and the I-V characteristics of this junction are well characterized,[28-42] the n-Si/$Me_2Fc^{+/0}$ contact was used as a benchmark against which the behavior of alkyl-terminated surfaces was determined. Figure 2 shows the steady-state current density-voltage curves for a hydrogen-terminated silicon surface and for alkyl-terminated silicon surfaces in contact with CH_3OH-1.0 **M** $LiClO_4$-0.050 **M** Me_2Fc-1 to 2 m**M** $Me_2Fc^+PF_6^-$ solution, taken at a

Figure 2. Current density-voltage characteristics of H-terminated and alkyl-terminated surfaces in contact with CH_3OH-1.0 **M** $LiClO_4$-0.050 **M** Me_2Fc-1 to 2 m**M** $Me_2Fc^+PF_6^-$ solution. As compared to the H-terminated surface, the alkyl groups provided some resistance to charge transfer across the semiconductor/liquid interface. Surfaces derivatized with short chain alkyl groups ($n \leq 6$), exhibited a trend of increasing resistance to charge transfer as a function of increasing alkyl chain length. For alkyl chain lengths with $10 \leq n \leq 18$, no correlation was observed between the length of the alkyl group and the resistance offered by the overlayer.

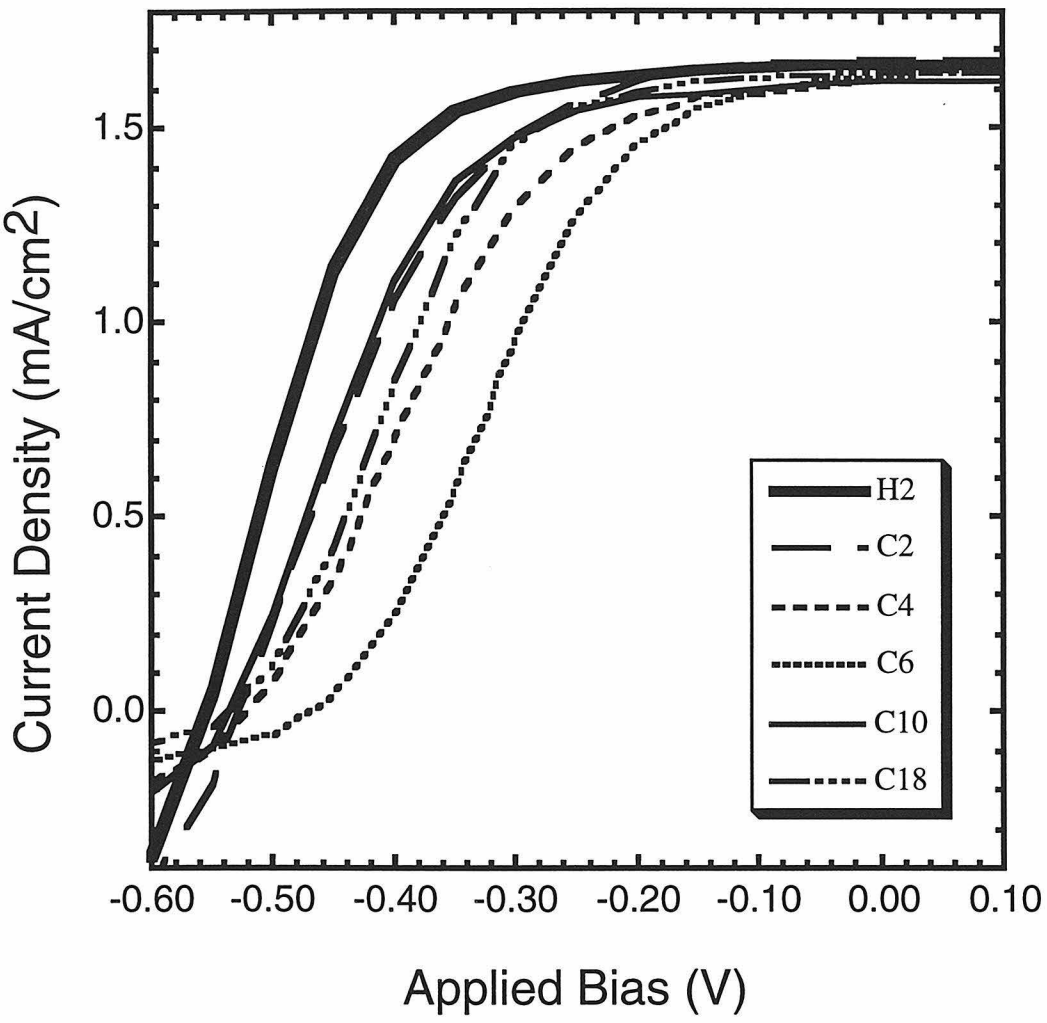
Current Density (mA/cm2)
1.5
1.0
0.5
0.0
-0.60
-0.50
-0.40
-0.30
-0.20
-0.10
0.00
0.10
Applied Bias (V)
H2
C2
C4
C6
C10
C18

short circuit photocurrent density of 1.66 mA/cm^2. As compared to the H-terminated surface, the alkyl groups provided some resistance to charge transfer across the semiconductor/ liquid interface. Surfaces derivatized with short chain alkyl groups ($n \leq 6$) exhibited a trend of increasing resistance to charge transfer as a function of increasing alkyl chain length. As the length of the alkane chain was increased further ($10 \leq n \leq 18$), the resistance to charge transfer was observed to decrease, although it was always greater than for the H-terminated surface. For alkyl chain lengths with $10 \leq n \leq 18$, no correlation was observed between the length of the alkyl group and the resistance offered by the overlayer to charge transfer across the semiconductor/liquid junction.

To measure the extent of recombination induced by the alkylation procedure at the silicon/liquid interface, the open circuit voltages (V_{oc}) of hydrogen and alkyl-terminated surfaces were determined in contact with the $Me_2Fc^{+/0}$ solution. It is known that for an n-Si-H/$Me_2Fc^{+/0}$ junction, less than 1 in 10^6 atoms acts as a recombination center and the I-V characteristics are determined only by the recombination of photogenerated carriers in the bulk of the semiconductor.[31,44] Any increase in the recombination at the alkylated surface would thus result in a decrease in the observed V_{oc}.[2] This measurement would be independent of the resistance of the overlayer because it is made when no current is flowing through the junction.

Table I compares the open circuit voltages (V_{oc}) observed for the alkyl-terminated surfaces with that observed on a H-terminated surface, at a photocurrent density of 1.66 mA/cm^2. For many samples of each of the surfaces, current-voltage data were also collected at several different levels of illumination, and plots of $\ln(J_{ph})$ vs. V_{oc} were made. From these plots the diode quality factor (A) and the dark equilibrium exchange current density (J_0) were calculated. Table I also displays the average A and J_0 values calculated for these surfaces. The tabulated results clearly showed that the chlorination/alkylation procedure did not result in any significant increase in the surface recombination at the n-Si/alkyl/$Me_2Fc^{+/0}$ solution junction.

Table I. Current-voltage and capacitance-voltage properties of H-terminated and alkyl-terminated surfaces in contact with CH_3OH-$Me_2Fc^{+/0}$ solution. Current-voltage properties of H-terminated and alkyl-terminated surfaces in contact with Au.

Alkyl Chain Length (C_n)	I-V properties in CH_3OH-$Me_2Fc^{+/0}$			C-V properties in CH_3OH-$Me_2Fc^{+/0}$		I-V properties of Au MIS	
	V_{oc}[a] (V)	A	J_o (mA/cm^2)	Nd (cm^{-3})	V_{fb}[b] (V)	A	Jo (mA/cm^2)
H	0.56	1.05	$1x10^{-8}$	4.0±1.0	0.72±0.05	1.01	$6x10^{-5}$
2	0.53	1.18	$5x10^{-8}$	4.3±0.1	0.69±0.03		
4	0.52	1.08	$3x10^{-8}$	4.7±0.2	0.69±0.03	1.01	$6x10^{-5}$
6	0.47	1.07	$6x10^{-8}$	3.9±0.3	0.66±0.05	0.62	$6x10^{-8}$
10	0.54	1.06	$5x10^{-8}$	4.2±0.4	0.69±0.03		
12		1.05	$1x10^{-8}$			1.06	$1x10^{-4}$
18	0.54	0.95	$9x10^{-10}$	4.1±0.2	0.71±0.04	0.90	$5x10^{-6}$

a) $J_{ph} = 1.66 \pm 0.04$ mA/cm^2. All V_{oc} data are ±0.03V. b) Barrier height = $|V_{fb}| + V_n$. V_n = 0.245 V for these samples.

(b) Capacitance-Voltage (C-V) Characteristics of Alkyl-Terminated Silicon Surfaces in Contact with Dimethylferrocene$^{+/0}$ ($Me_2Fc^{+/0}$) Solutions

Capacitance-voltage measurements were undertaken for the alkyl-terminated surfaces in contact with $Me_2Fc^{+/0}$ solution to determine if the two-step modification procedure resulted in any shift in the band edge positions, as compared to those of a hydrogen-terminated silicon surface in contact with the same solution. Using the Mott-Schottky equation (2), flat-band potentials were calculated for the H-terminated and alkyl-terminated surfaces. Figure 3 plots the inverse square of the measured differential capacitances of these junctions as a function of the bias applied to the junction (Mott-Schottky plots). The flat band potential for each junction was determined by extrapolating the data to infinite capacitance ($C_{sc}^{-2} = 0$) (Figure 3b). The results of these measurements are summarized in Table I. For the alkyl-terminated surfaces, the sample resistivity calculated from the slopes of the C_{sc}^{-2} vs. V plots gave a dopant density value of (4-5)x10^{15} cm^{-3}, consistent with resistivity values measured using a four point probe[2] (3x10^{15} cm^{-3}). The excellent quality of the data was evident by a lack of frequency dispersion, excellent linearity of the data as a function of bias for a given frequency, and good agreement of the calculated dopant density with that measured by four point probe experiments. The difference between the Fermi level and the edge of the conduction band (0.245 V) was added to the observed flat-band potentials to obtain the barrier heights. The barrier heights measured for the alkyl-terminated surfaces were similar to that observed for H-terminated Si(111) surface. This result indicated that derivatization with alkyl chains did not shift the band edges of silicon, as expected for a neutral adsorbate.[55-58]

(c) Current-Voltage (I-V) Characteristics of Alkyl-Terminated Silicon Surfaces in Contact with Gold

It is well known that the problem of Fermi level pinning, observed at a metal/semiconductor (Schottky) junction, can be alleviated by interposing a thin layer of oxide to form a metal-insulator-semiconductor (MIS) junction.[48-51] The alkyl overlayers

Figure 3. (a) C_{sc}^{-2} vs. V (Mott-Schottky) plots of H-terminated and alkyl-terminated surfaces in contact with CH_3OH-1.0 **M** $LiClO_4$-0.100 **M** Me_2Fc-~5 m**M** $Me_2Fc^+PF_6^-$ solution. Data from 17 different frequencies ranging from 16 KHz to 400 Hz are shown. (b) Linear fits to the data are extrapolated to the x-axis to obtain flat-band potentials. Barrier height for these Si/liquid junctions are obtained by adding 0.245 V to the observed flat-band potentials.

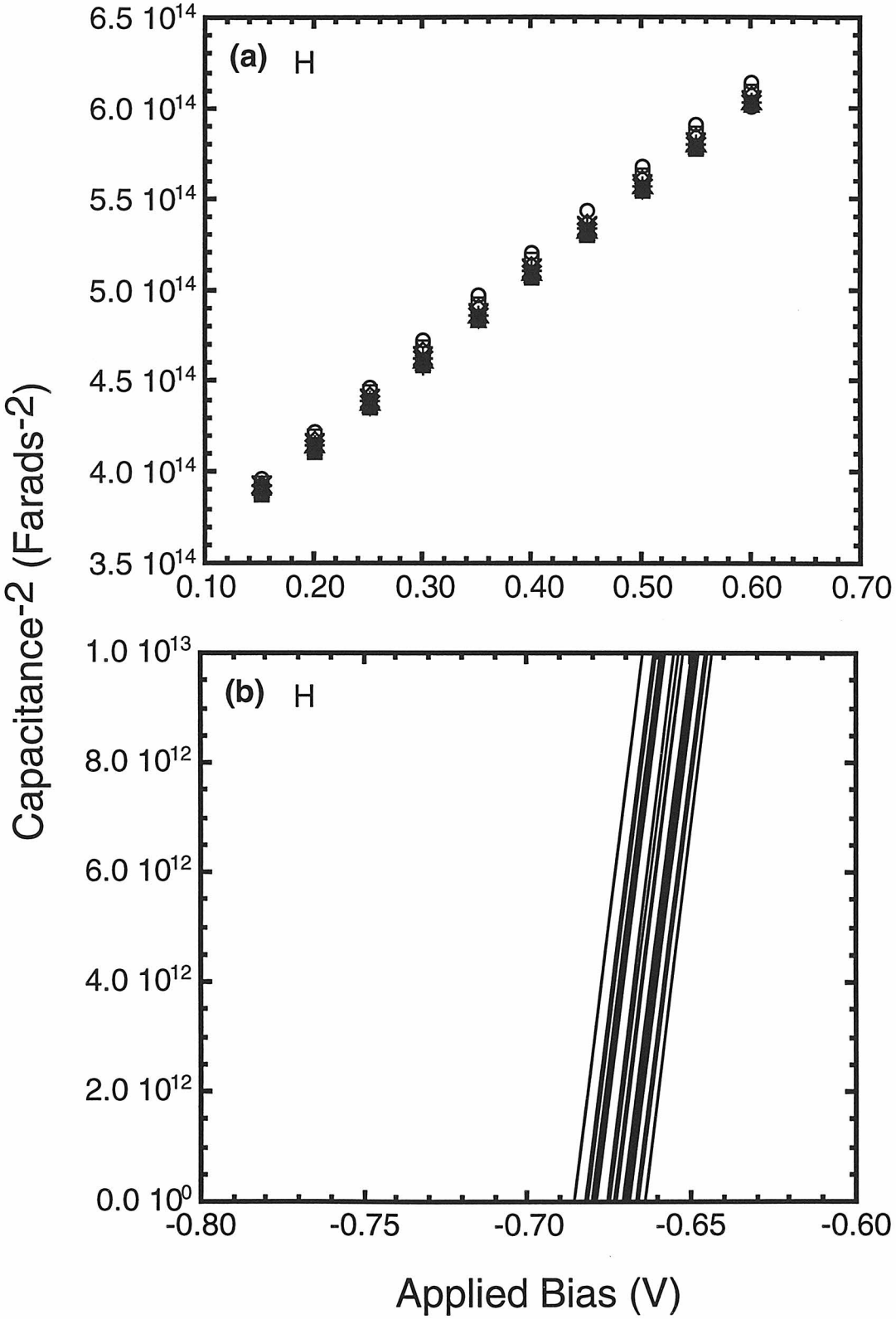
(a) H
(b) H
Capacitance-2 (Farads-2)
Applied Bias (V)
6.5 10^14
6.0 10^14
5.5 10^14
5.0 10^14
4.5 10^14
4.0 10^14
3.5 10^14
0.10
0.20
0.30
0.40
0.50
0.60
0.70
1.0 10^13
8.0 10^12
6.0 10^12
4.0 10^12
2.0 10^12
0.0 10^0
-0.80
-0.75
-0.70
-0.65
-0.60

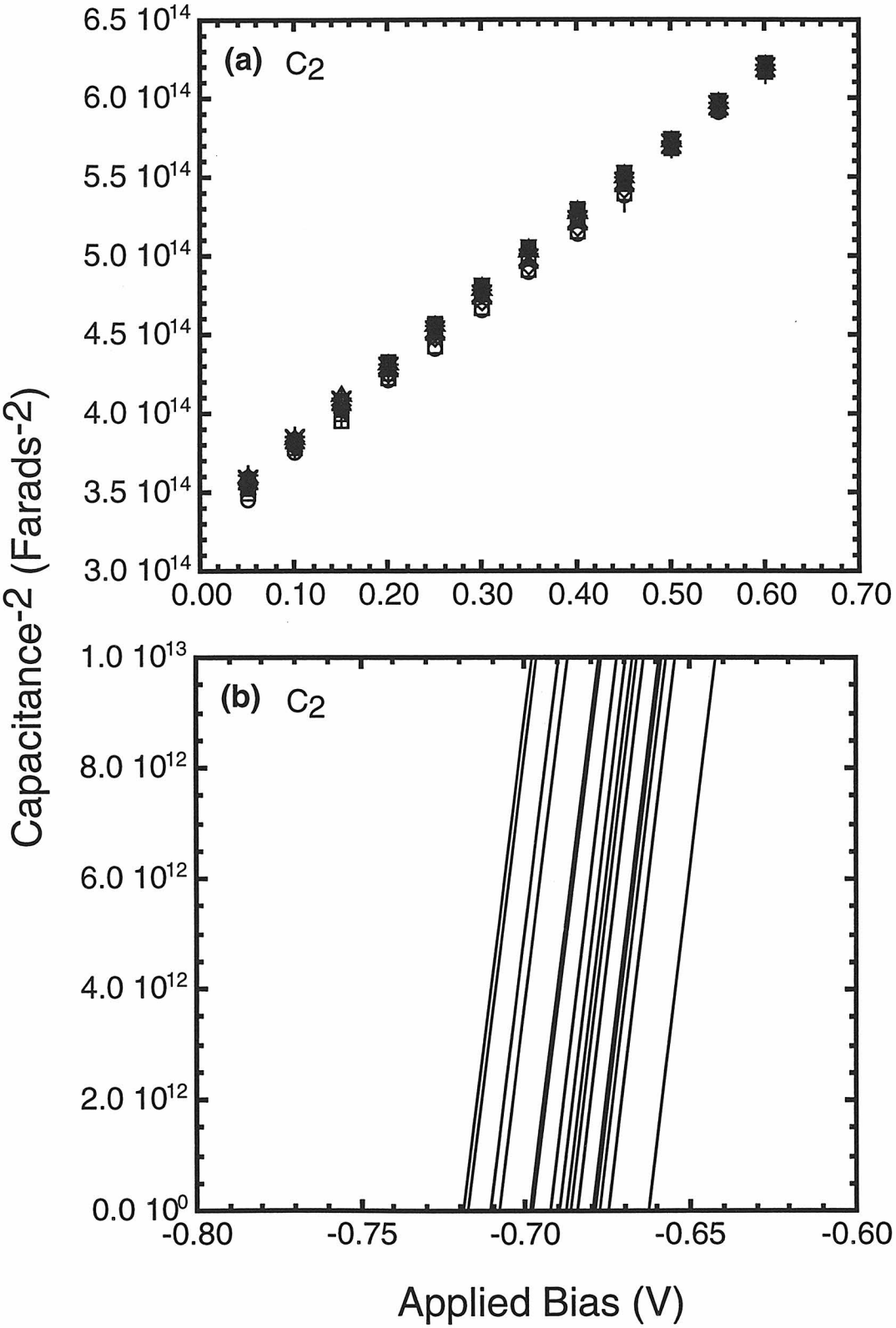
(a) C2
(b) C2
Capacitance-2 (Farads-2)
Applied Bias (V)
6.5 10^14
6.0 10^14
5.5 10^14
5.0 10^14
4.5 10^14
4.0 10^14
3.5 10^14
3.0 10^14
0.00
0.10
0.20
0.30
0.40
0.50
0.60
0.70
1.0 10^13
8.0 10^12
6.0 10^12
4.0 10^12
2.0 10^12
0.0 10^0
-0.80
-0.75
-0.70
-0.65
-0.60

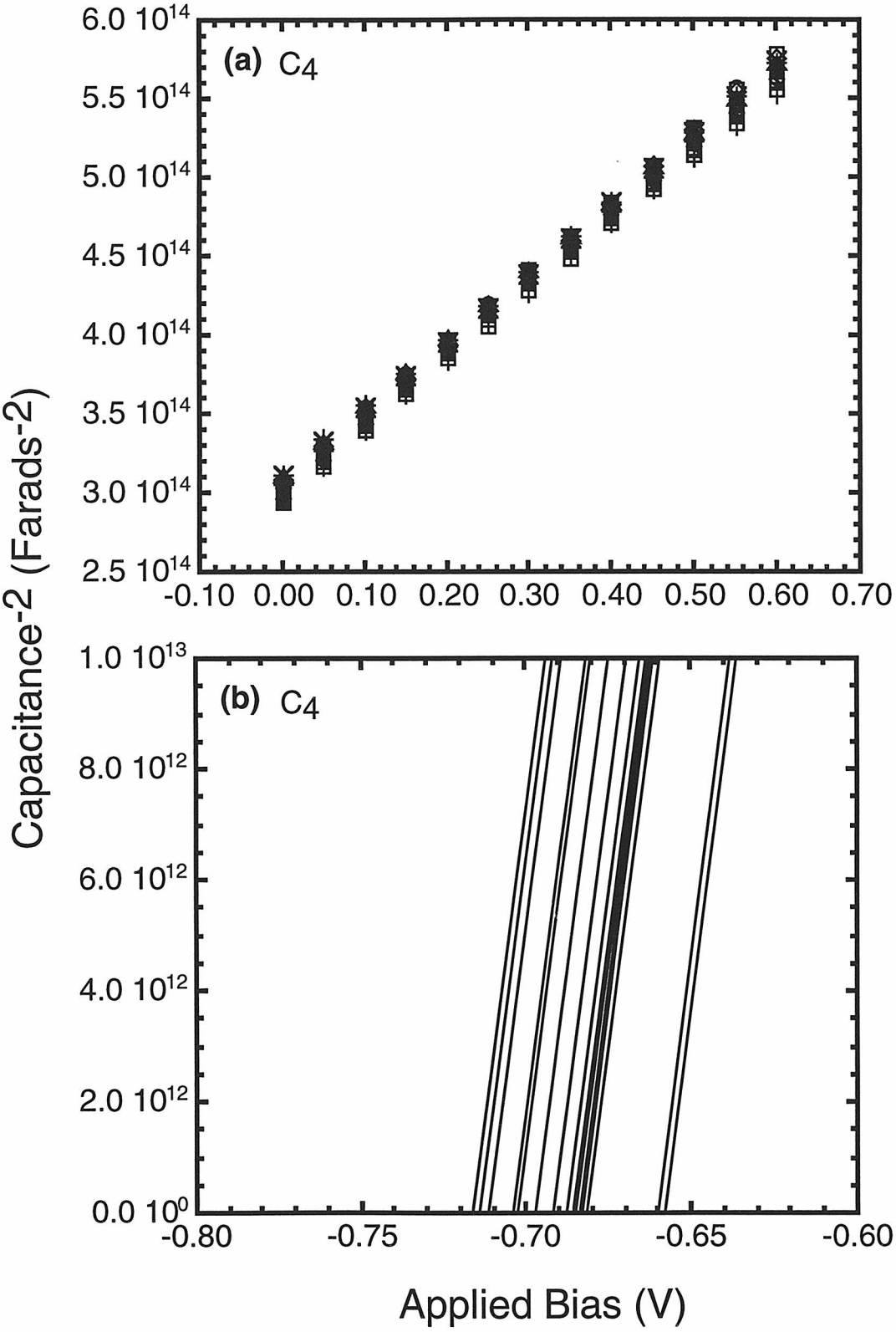
(a) C4
(b) C4
Capacitance-2 (Farads-2)
Applied Bias (V)
6.0 10^14
5.5 10^14
5.0 10^14
4.5 10^14
4.0 10^14
3.5 10^14
3.0 10^14
2.5 10^14
-0.10 0.00 0.10 0.20 0.30 0.40 0.50 0.60 0.70
1.0 10^13
8.0 10^12
6.0 10^12
4.0 10^12
2.0 10^12
0.0 10^0
-0.80 -0.75 -0.70 -0.65 -0.60

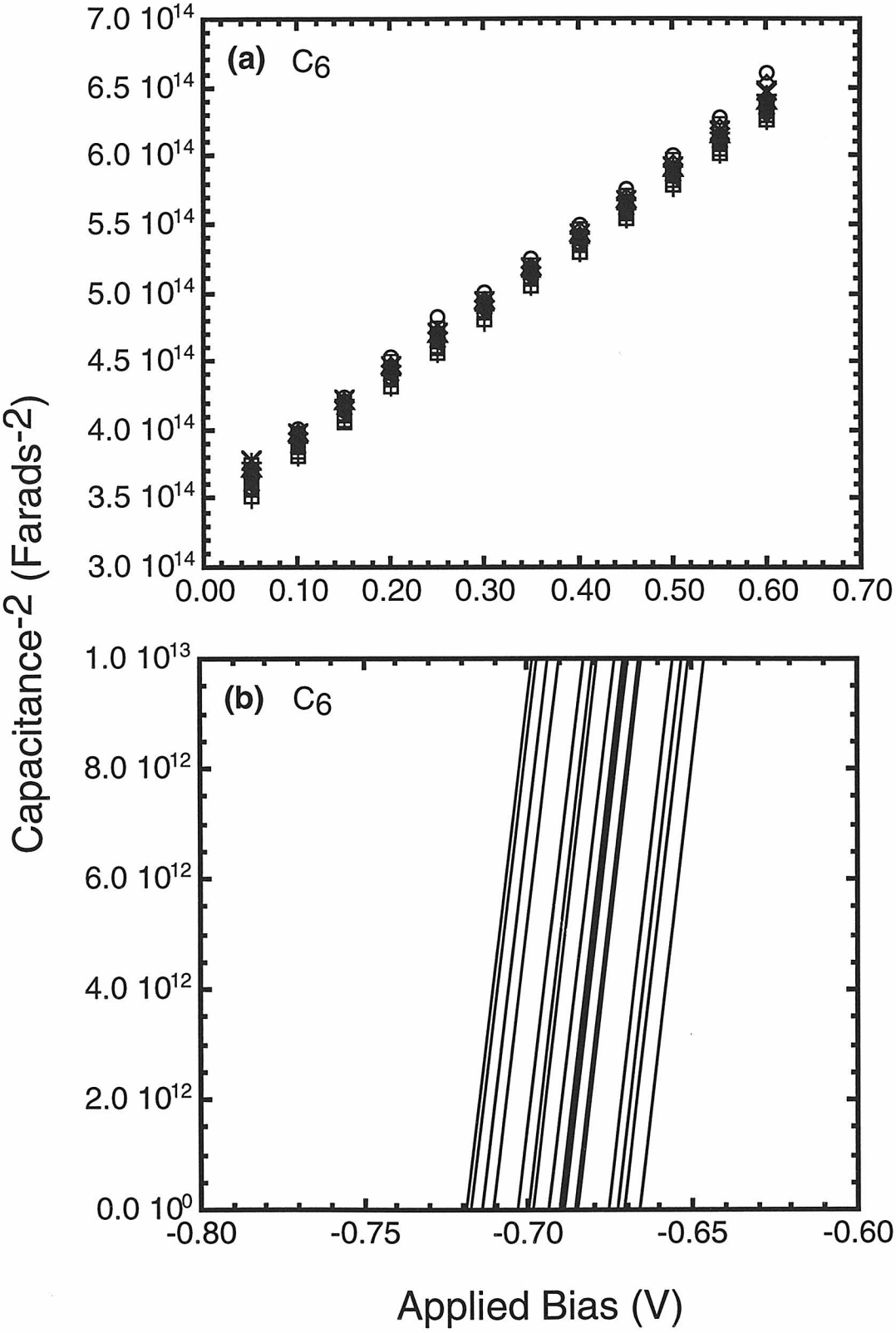
(a) C6
(b) C6
Capacitance-2 (Farads-2)
Applied Bias (V)
7.0 10^14
6.5 10^14
6.0 10^14
5.5 10^14
5.0 10^14
4.5 10^14
4.0 10^14
3.5 10^14
3.0 10^14
0.00
0.10
0.20
0.30
0.40
0.50
0.60
0.70
1.0 10^13
8.0 10^12
6.0 10^12
4.0 10^12
2.0 10^12
0.0 10^0
-0.80
-0.75
-0.70
-0.65
-0.60

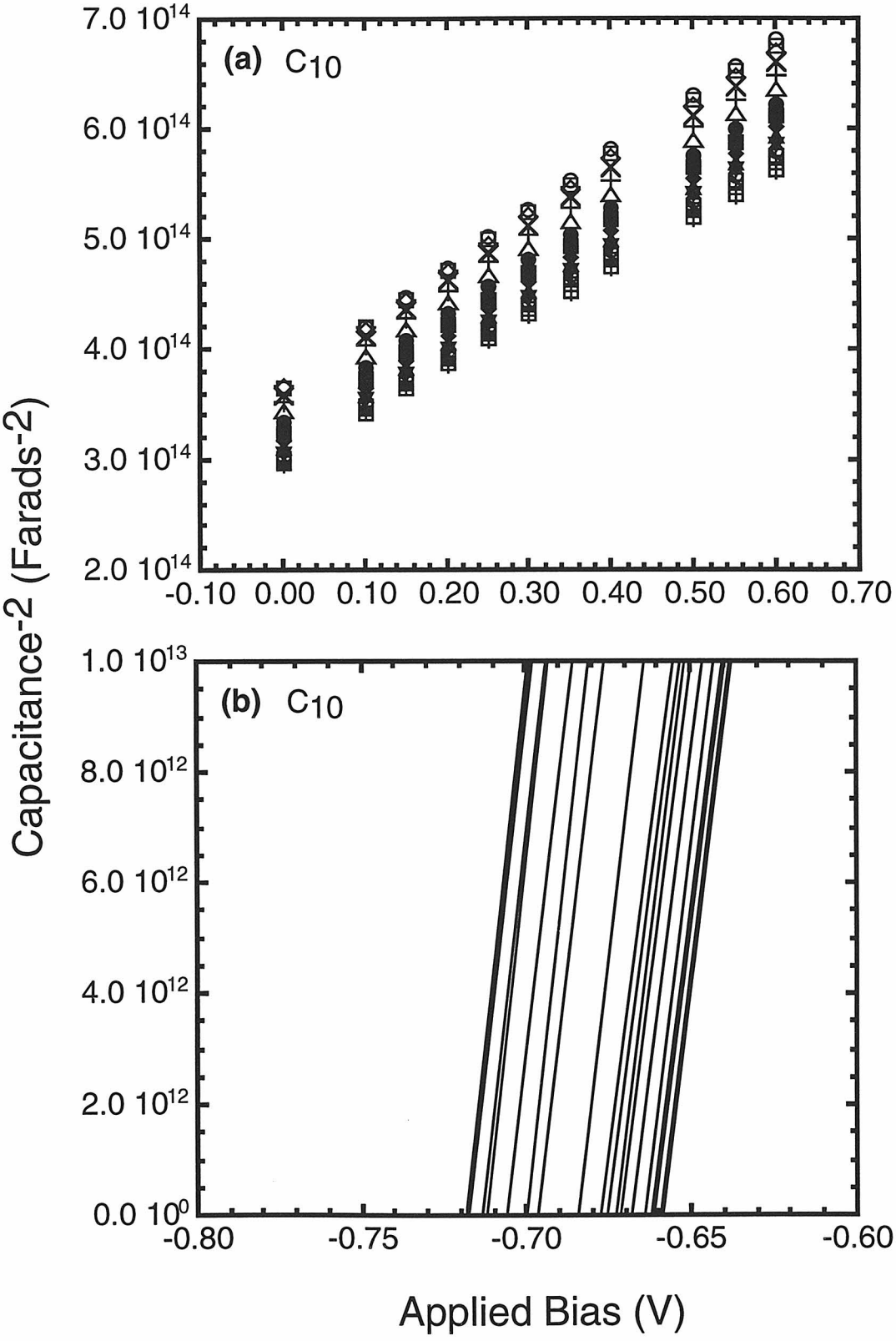
(a) C10
(b) C10
Capacitance-2 (Farads-2)
Applied Bias (V)
7.0 10^14
6.0 10^14
5.0 10^14
4.0 10^14
3.0 10^14
2.0 10^14
-0.10 0.00 0.10 0.20 0.30 0.40 0.50 0.60 0.70
1.0 10^13
8.0 10^12
6.0 10^12
4.0 10^12
2.0 10^12
0.0 10^0
-0.80 -0.75 -0.70 -0.65 -0.60

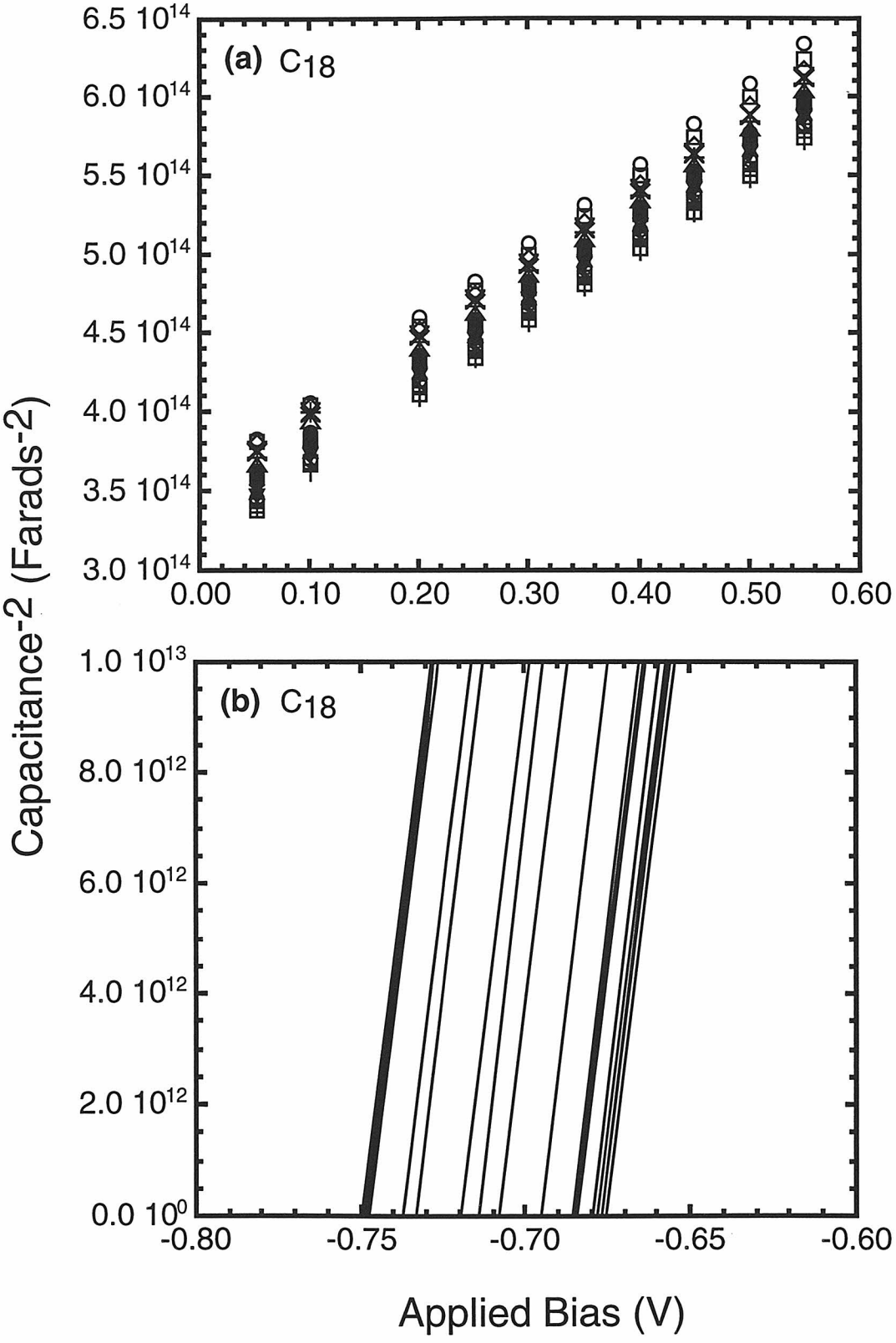
(a) C18
(b) C18
Capacitance-2 (Farads-2)
Applied Bias (V)
6.5 10^14
6.0 10^14
5.5 10^14
5.0 10^14
4.5 10^14
4.0 10^14
3.5 10^14
3.0 10^14
0.00
0.10
0.20
0.30
0.40
0.50
0.60
1.0 10^13
8.0 10^12
6.0 10^12
4.0 10^12
2.0 10^12
0.0 10^0
-0.80
-0.75
-0.70
-0.65
-0.60

were tested as an alternative to the thin oxide layer in an MIS configuration employing Au as the gate metal. Figure 4 shows the current density-voltage plots for H-terminated and alkyl-terminated n-Si(111) surfaces in contact with a 200 Å gold overlayer. As expected for a bare silicon-gold Schottky junction, a V_{oc} of approximately 0.29 V was observed for a photocurrent density of 9 mA/cm^2. At similar photocurrent densities, the alkyl-terminated surfaces showed V_{oc} values between 0.31 V and 0.36 V. In contrast, an ideal MIS was expected to give a V_{oc} of 0.56 V for the same current density. Table I lists the diode quality factors and the dark equilibrium exchange current densities calculated for ln(Jph) vs. V plots of n-Si/Au junctions formed from H-terminated and alkyl-terminated silicon surfaces. The results indicate that despite the presence of alkyl overlayer on the silicon surface, these surfaces largely behaved like a metal/semiconductor Schottky junction.

2. Stability of Alkyl-Terminated Surfaces in Aqueous Environments

(a) Current-Voltage (I-V) Characteristics of Alkyl-Terminated Silicon Surfaces in Contact with Dimethylferrocene$^{+/0}$ ($Me_2Fc^{+/0}$) Solutions Containing Water

The efficacy of alkyl overlayers in preventing photooxidation and photocorrosion of n-silicon surfaces was measured in contact with $Me_2Fc^{+/0}$ solutions to which a known amount of water had been added. Two slightly different criteria were used to compare the stability of derivatized electrodes with that of H-terminated Si electrodes.

In the first method, stabilized hydrogen-terminated or alkyl-terminated electrodes were exposed, under illumination, to CH_3OH-1.0 **M** $LiClO_4$-0.050 **M** Me_2Fc-~1 m**M** $Me_2Fc^+PF_6^-$ solution containing 10% (v/v) water. The cell was held at short circuit at a light limited current density of J_{ph} = 4.0 mA/cm^2 for 20 minutes. After 20 minutes, the silicon surface was analyzed for oxide coverage by XPS. Figure 5 shows the current density-voltage curves for these electrodes, that were observed immediately after adding water and after 20 minutes of charge transfer at short circuit. All the electrodes showed

Figure 4. Current density-voltage characteristics for n-Si/alkyl/Au MIS devices. The thin solid line denotes the J-V characteristics of n-Si-H/Au semiconductor/metal (Schottky) junction. The thick solid line denotes the J-V characteristics of silicon surfaces derivatized with (a) $-C_2H_5$, (b) $-C_4H_9$, (c) $-C_6H_{13}$, (d) $-C_8H_{17}$, (e) $-C_{10}H_{21}$, (f) $-C_{12}H_{25}$, (g) $-C_{18}H_{37}$.

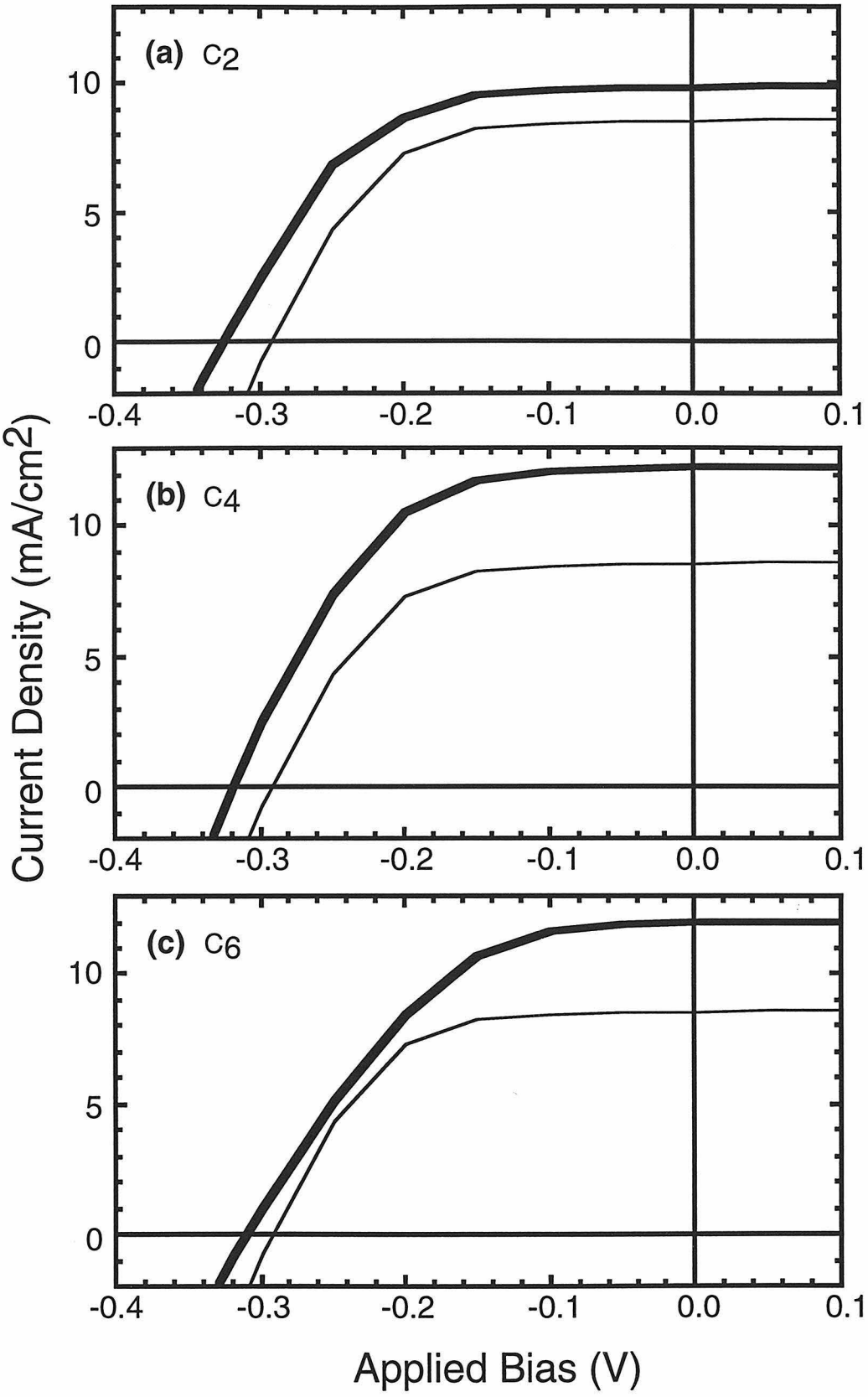
(a) C2
(b) C4
(c) C6
10
5
0
-0.4
-0.3
-0.2
-0.1
0.0
0.1
Current Density (mA/cm2)
Applied Bias (V)

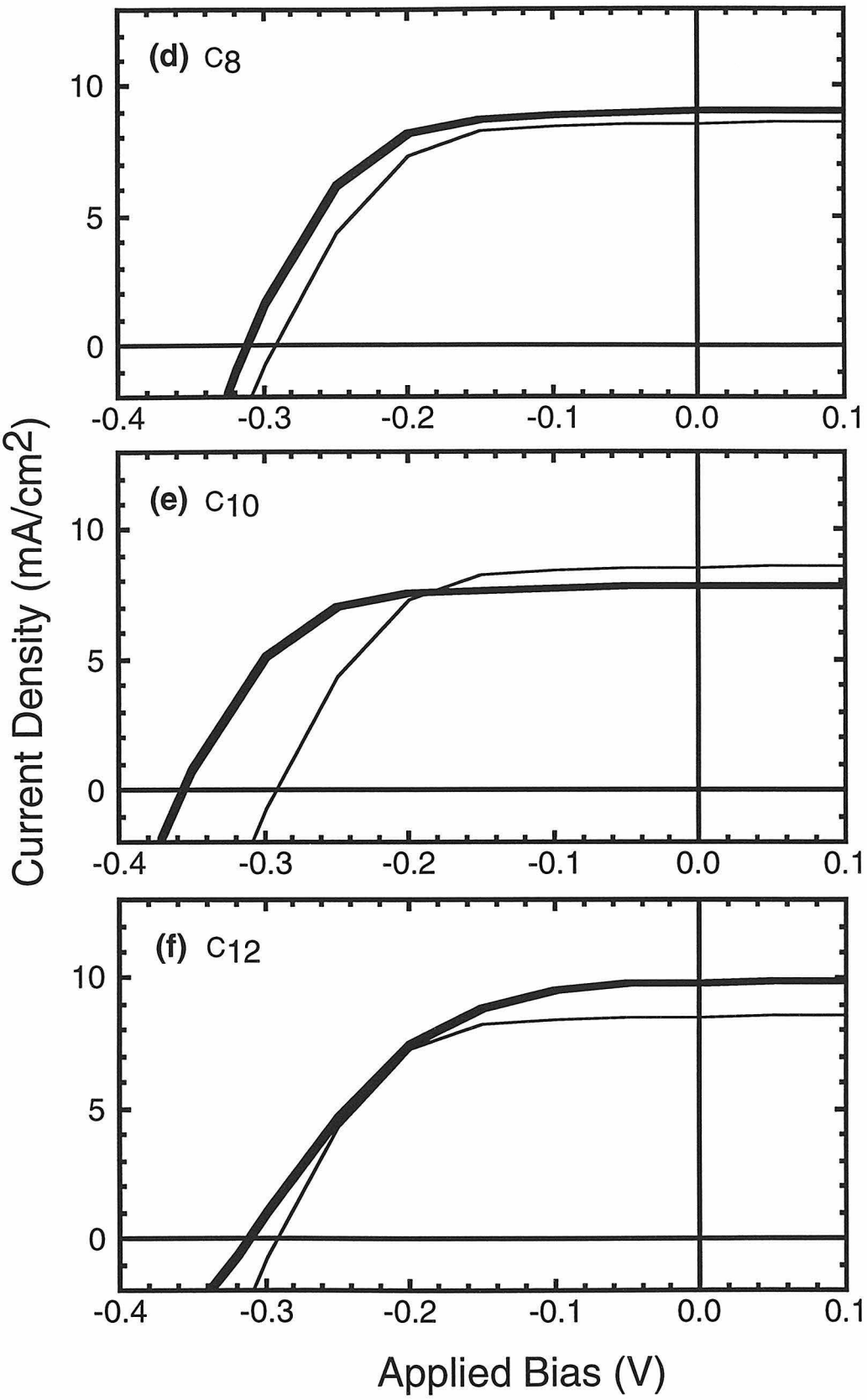
(d) C8
(e) C10
(f) C12
10
5
0
-0.4
-0.3
-0.2
-0.1
0.0
0.1
Current Density (mA/cm2)
Applied Bias (V)

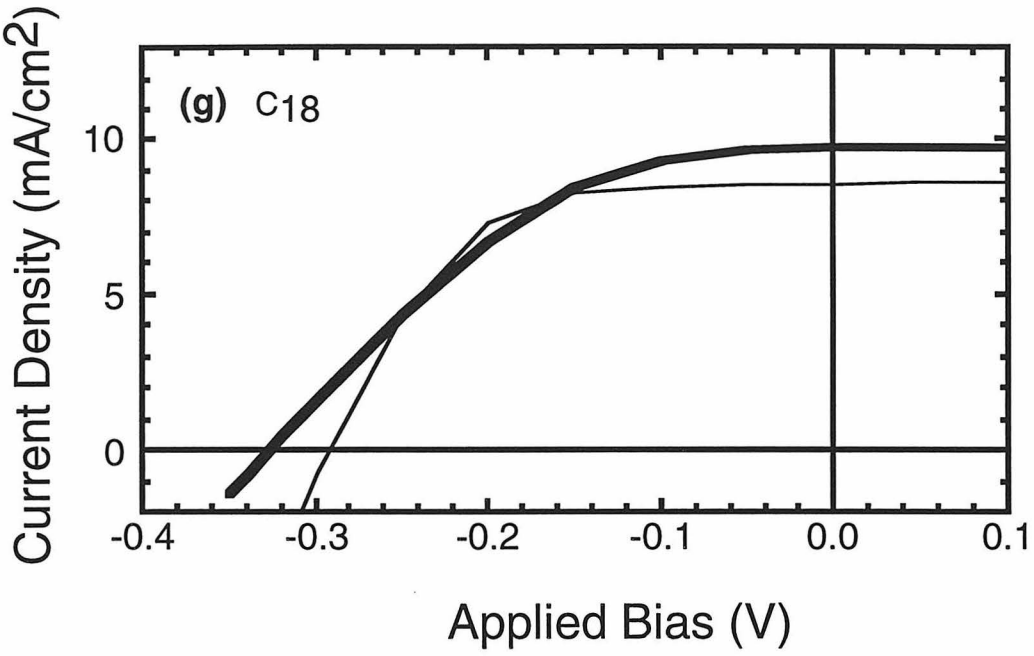
(g) C18
Current Density (mA/cm2)
10
5
0
-0.4
-0.3
-0.2
-0.1
0.0
0.1
Applied Bias (V)

Figure 5. Current density-voltage characteristics of silicon surfaces in contact with CH_3OH-1.0 **M** $LiClO_4$-0.050 **M** Me_2Fc-~1 m**M** $Me_2Fc^+PF_6^-$ solution containing 10% (v/v) water. The thin solid line denotes the J-V curved observed immediately after adding water. The thick solid line denotes the J-V characteristics after 20 minutes of illumination at a short circuit current density of 4.0 mA/cm^2. The surfaces shown are terminated in (a) -H, (b) $-C_2H_5$, (c) $-C_4H_9$, (d) $-C_6H_{13}$, (e) $-C_{10}H_{21}$, (f) $-C_{12}H_{25}$, (g) $-C_{18}H_{37}$.

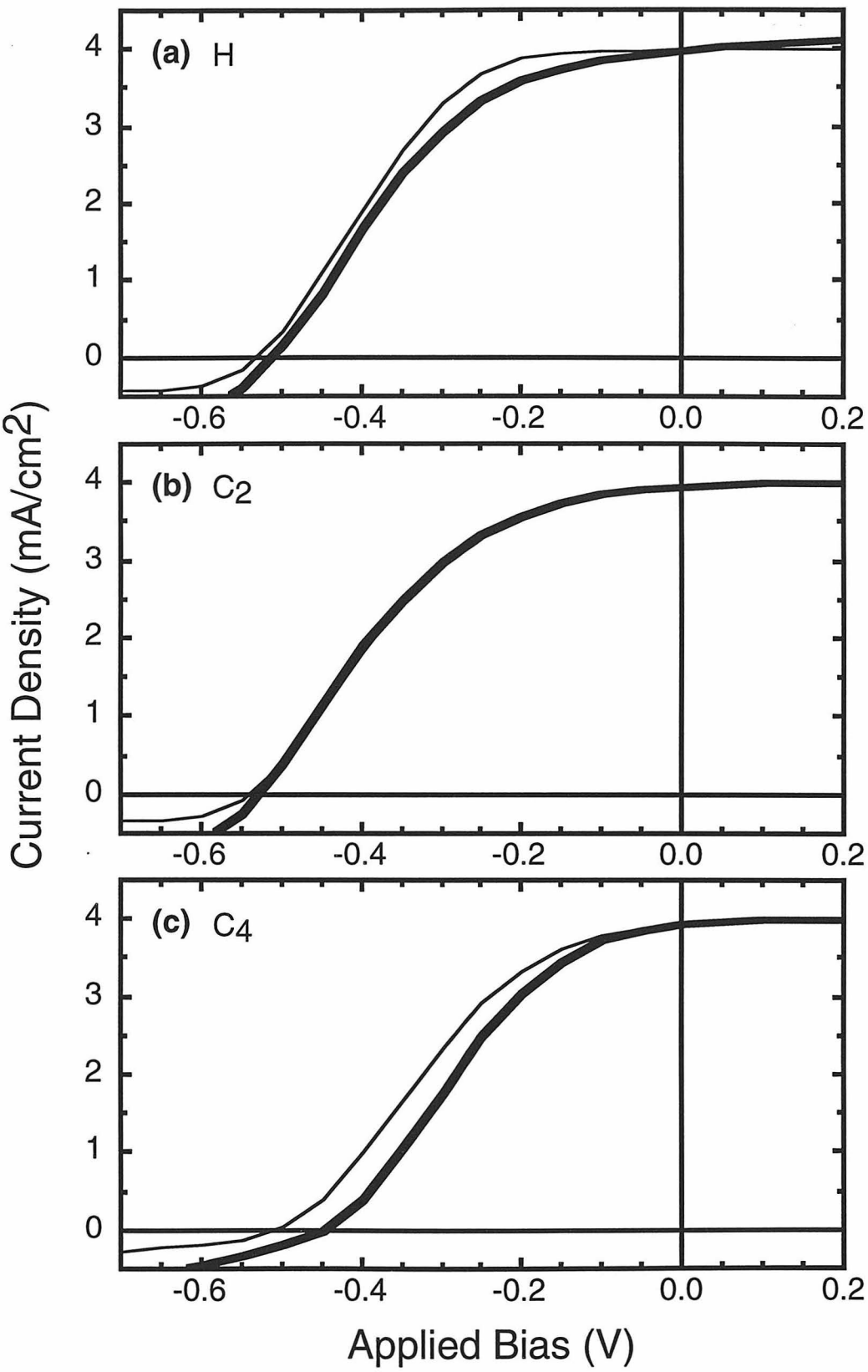
(a) H
(b) C2
(c) C4
Current Density (mA/cm2)
Applied Bias (V)
4
3
2
1
0
-0.6
-0.4
-0.2
0.0
0.2

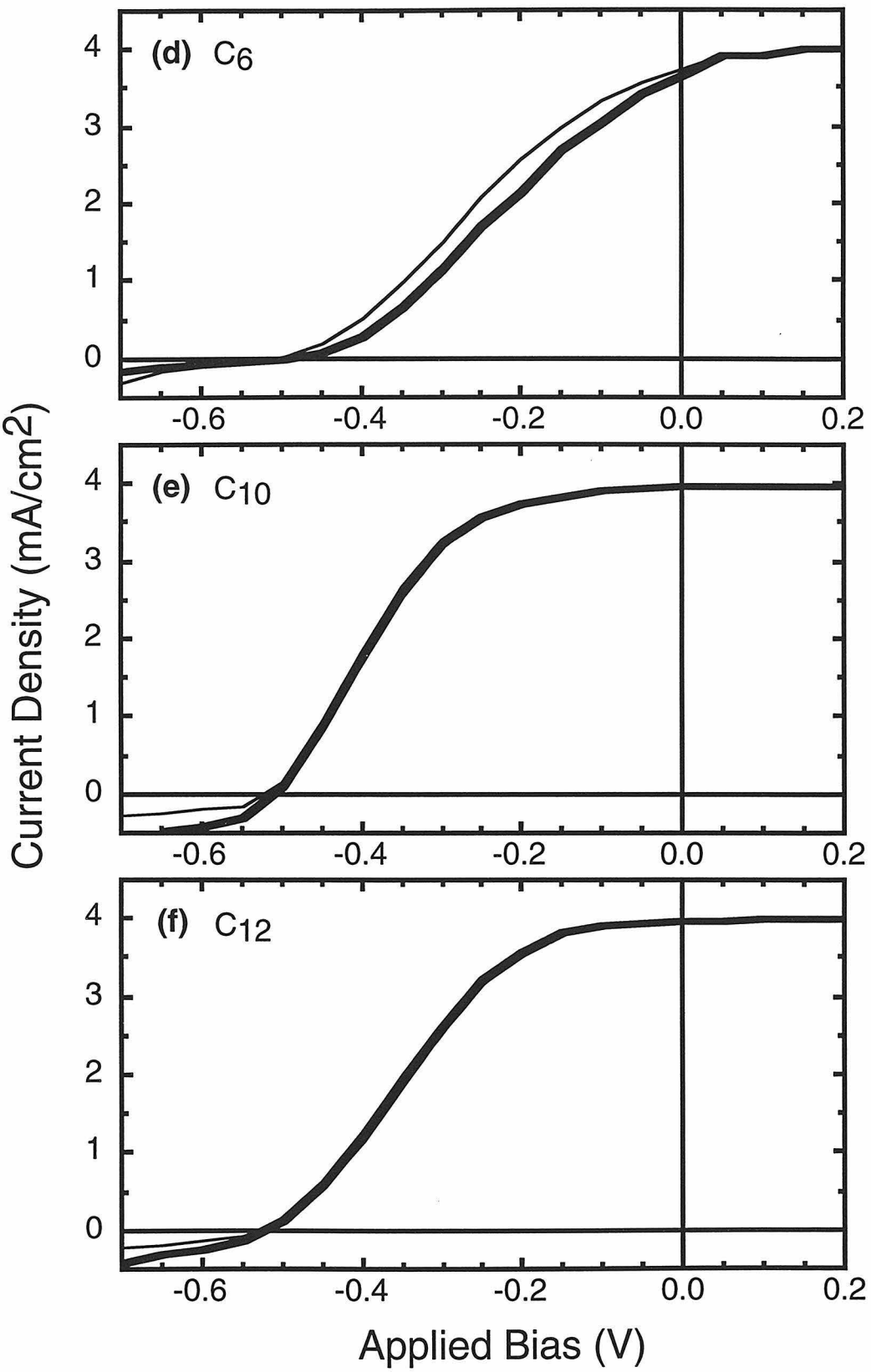
(d) C6
(e) C10
(f) C12
Current Density (mA/cm2)
Applied Bias (V)
4
3
2
1
0
-0.6
-0.4
-0.2
0.0
0.2

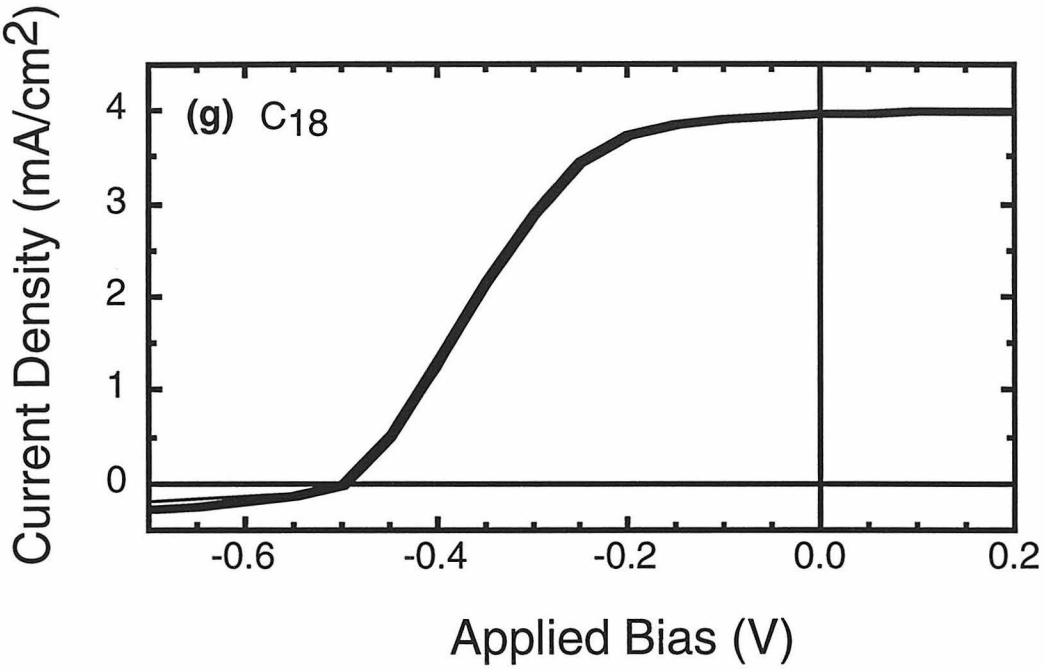
(g) C18
Current Density (mA/cm2)
Applied Bias (V)
4
3
2
1
0
-0.6
-0.4
-0.2
0.0
0.2

negligible change in V_{oc} or fill factor over this time period. Table II shows the oxide coverage observed by XPS for H-terminated and alkyl-terminated silicon surfaces. While the H-terminated surface showed 2.4±0.1 monolayers of oxide in 20 minutes, the most oxidized of the derivatized surfaces showed less than 0.6±0.2 monolayers of oxide. More typically however, the amount of oxidation was below the quantification limit of 0.3 monolayers, and for some chain lengths, no oxidation could be detected at all. These results clearly indicated that the alkylation procedure suppressed the photooxidation of silicon in the presence of water.

A more stringent test of the stability imparted by alkylation was performed on fresh samples by increasing the water concentration to 20% (v/v) and holding the electrode at a small reverse bias at a light limited current density of 4.0 mA/cm^2. The experiment was terminated either when the cell displayed significantly resistive I-V characteristics or after 22-25 hours of illumination at short circuit. Figure 6 shows the J-V curves for a H-terminated surface and for alkyl-terminated surfaces immediately after immersion, after 90 minutes of illumination, and, for the alkyl-terminated surfaces, after ~24 hours of illumination. The I-V characteristics of the H-terminated surface deteriorated rapidly upon illumination and the experiment was stopped after 90 minutes because the level of illumination could not be increased any further without significantly increasing the temperature of the cell. In contrast, the alkylated surfaces exhibited high fill factors even after 20-25 hours of illumination at 4.0 mA/cm^2, with only minimal decay in fill factors, most of which occurred within the first 15 minutes of exposure to the solution.

XPS analysis of the illuminated region of the H-terminated surface after a 90 minute exposure to the cell above showed approximately 4 monolayers of oxide on the silicon surface. In contrast, alkylated surfaces showed much lower oxidation levels (<1 monolayer) even though these surfaces were analyzed after 20-25 hours of illumination. The lack of oxidation of the alkylated surface was also consistent with the negligible change observed in the I-V characteristics of these surfaces in the electrochemical experiments.

Table II. Current-voltage properties of H-terminated and alkyl-terminated surfaces in contact with CH_3OH-$Me_2Fc^{+/0}$ solutions containing known amounts of water. For these measurements the current density was maintained at 4.0 mA/cm^2.

Alkyl Chain Length (C_n)	10% H_2O Oxide (ML)[a]	Current-voltage properties in CH_3OH-$Me_2Fc^{+/0}$ with 20% H_2O @ t = 0 min V_{oc} (V)	ff	@ t = 90 min V_{oc} (V)	ff	@ t = t_{max} t_{max}(min)	V_{oc} (V)	ff
H	2.4	0.48	0.55	0.43	0.31	b	b	b
2	< 0.3	0.48	0.50	0.47	0.54	1500	0.43	0.52
4	< 0.3	0.47	0.45	0.43	0.42	1410	0.41	0.40
6	< 0.3	0.44	0.33	0.39	0.29	1350	0.38	0.28
10	< 0.3	0.48	0.50	0.47	0.50	1350	0.45	0.50
12	< 0.3	0.45	0.44	0.45	0.44	1465	0.43	0.42
18	0.6							

a) ML = monolayers. b) The I-V characteristics of the H-terminated surface deteriorated rapidly upon illumination and the experiment was stopped after 90 minutes because the level of illumination could not be increased any further without significantly increasing the temperature of the cell.

Figure 6. Current density-voltage characteristics of silicon surfaces in contact with CH_3OH-1.0 **M** $LiClO_4$-0.050 **M** Me_2Fc-~1 m**M** $Me_2Fc^+PF_6^-$ solution containing 20% (v/v) water. The thin solid line denotes the J-V curved observed immediately after adding water. The thick solid line denotes the J-V characteristics after 90 minutes of illumination at a short circuit current density of 4.0 mA/cm^2. The dashed line denotes the J-V characteristics after ~24 hours of illumination. The exact duration of illumination for each surface is given in Table II. The surfaces shown are terminated in (a) -H, (b) -C_2H_5, (c) -C_4H_9, (d) -C_6H_{13}, (e) -$C_{10}H_{21}$, (f) -$C_{12}H_{25}$.

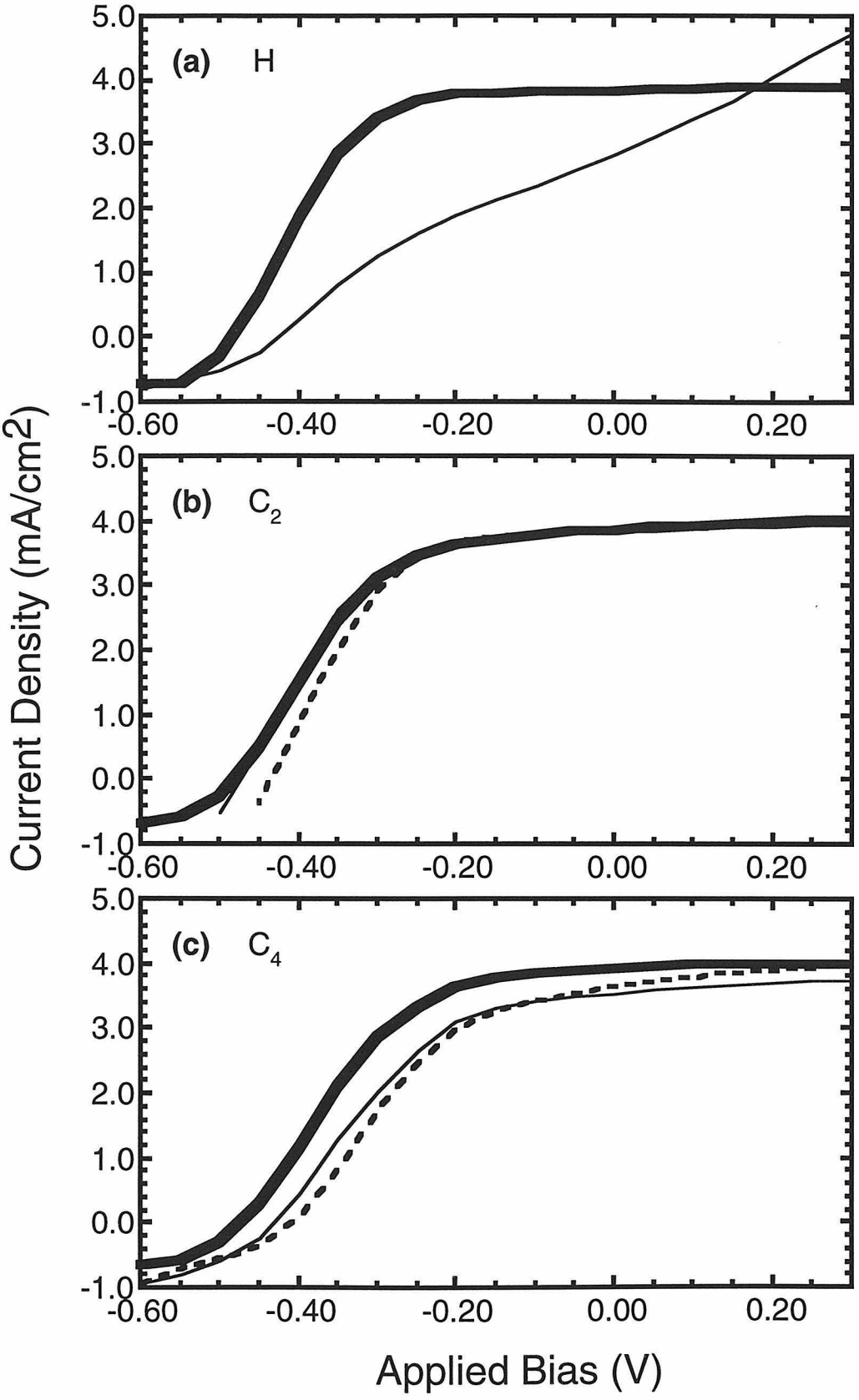
(a) H
(b) C2
(c) C4
Current Density (mA/cm2)
Applied Bias (V)
5.0
4.0
3.0
2.0
1.0
0.0
-1.0
-0.60
-0.40
-0.20
0.00
0.20

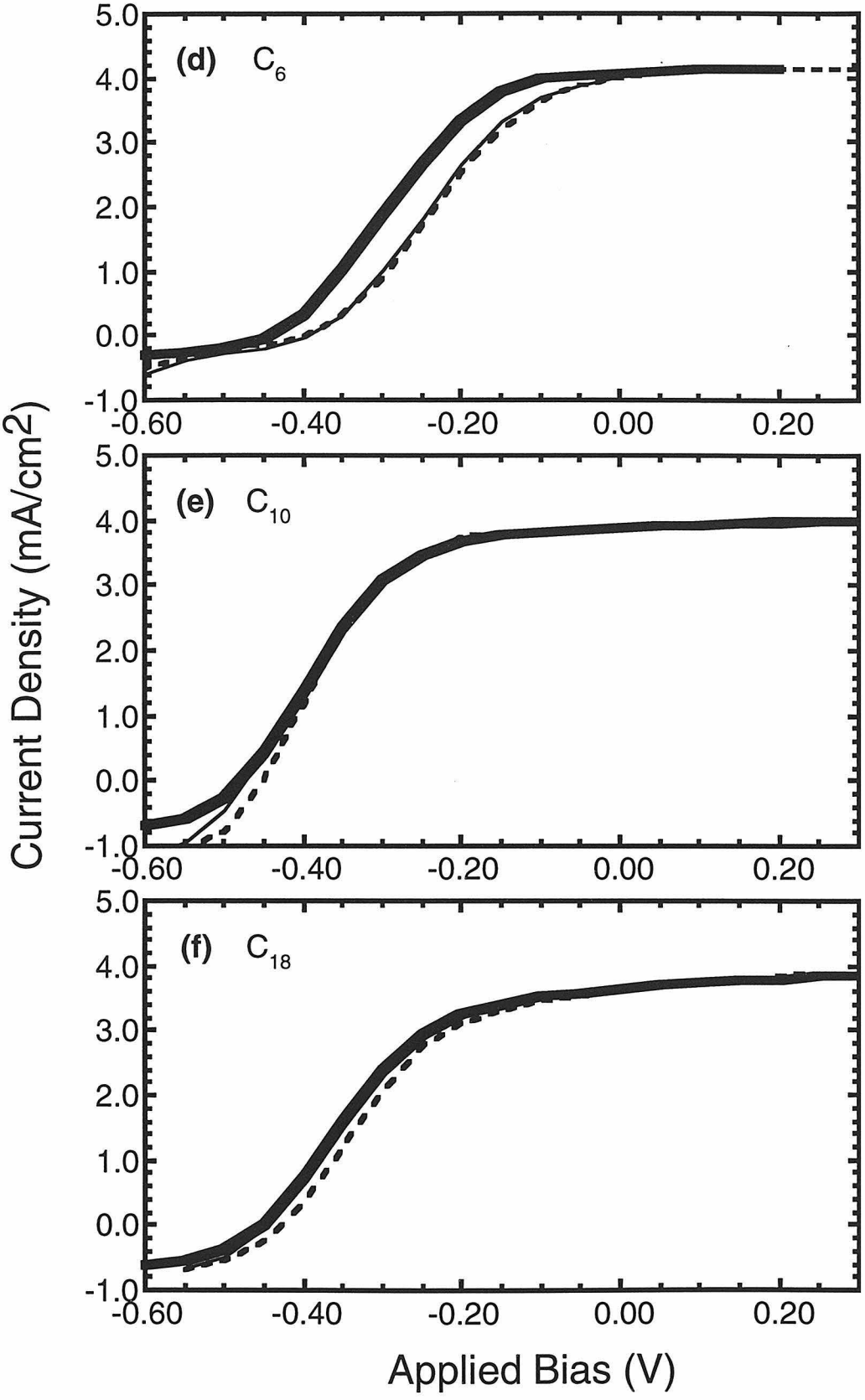
(d) C6
(e) C10
(f) C18
Current Density (mA/cm2)
Applied Bias (V)
5.0
4.0
3.0
2.0
1.0
0.0
-1.0
-0.60
-0.40
-0.20
0.00
0.20

(b) Current-Voltage (I-V) Characteristics of Alkyl-Terminated Silicon Surfaces in Contact with Potassium Ferro-Ferricyanide ($Fe(CN)_6^{3-/4-}$) Solutions

Since the concentration of water in the CH_3OH-$Me_2Fc^{+/0}$ cell could not be increased beyond 20% due to precipitation of the redox couple from the solution, an even more compelling test of stability of alkyl covered Si surfaces towards photooxidation was performed in contact with 0.35 **M** $Fe(CN)_6^{4-}$-0.05 **M** $Fe(CN)_6^{3-}$(aq) solution. As compared to CH_3OH-$Me_2Fc^{+/0}$/water solutions (~11 **M** H_2O), a much higher concentration of water (~55 **M** H_2O) was expected to more fully oxidize the surfaces. Figure 7a shows the J-V characteristics of a H-terminated and some alkyl-terminated surfaces in contact with $Fe(CN)_6^{3-/4-}$(aq) solution immediately after immersion. Consistent with literature reports, a resistive I-V curve was observed for the H-terminated surface in contact with the $Fe(CN)_6^{3-/4-}$(aq) solution.[7] In contrast, silicon surfaces derivatized with two of the shortest possible carbon chains, $-CH_3$ and $-C_2H_5$, gave V_{oc} values and fill factors that were significantly higher than for the H-terminated surface. On the other hand, surfaces derivatized with $-C_4H_9$ and $-C_6H_{13}$ gave lower V_{oc} and lower fill factors than the H-terminated surface.

This trend can be understood on the basis of a second observation: when a H-terminated and a $-CH_3$ terminated silicon surface were simply immersed in the $Fe(CN)_6^{3-/4-}$(aq) solution for 10 minutes and subsequently analyzed for oxide coverage by XPS, the H-terminated surface exhibited ~3 monolayers of oxide whereas the alkyl-terminated surface showed less than one monolayer of oxide. The ~3 monolayer thick oxide was thus mimicking a series resistance to the junction that was equivalent to approximately a 3 carbon long alkane chain.

As was done in experiments with the CH_3OH-$Me_2Fc^{+/0}$/water solutions, the silicon surfaces were held in the $Fe(CN)_6^{3-/4-}$(aq) solution at a photocurrent density of 1.0 mA/cm^2. The electrode was biased just enough into reverse bias to hold the semiconductor

Figure 7. Current density-voltage characteristics of silicon surfaces in contact with 0.35 **M** $Fe(CN)_6^{4-}$-0.05 **M** $Fe(CN)_6^{3-}$(aq) solution. (a) Immediately after exposure of the surface to the solution, the $-CH_3$ and $-C_2H_5$ terminated surfaces exhibit higher V_{oc} and fill factor while the $-C_4H_9$ and $-C_6H_{13}$ terminated surfaces exhibit lower V_{oc} and fill factor, than the H-terminated surface. (b) After 60 minute of illumination at 4.0 mA/cm^2, the H-terminated surface shows a very large decrease in Voc and fill factor whereas the $-CH_3$ and $-C_2H_5$ surfaces exhibit only a small decrease. The $-C_4H_9$ and $-C_6H_{13}$ terminated surfaces decayed very rapidly under illumination and light limited curves (at 1.0 mA/cm^2) could not be recorded for them after 60 minutes.

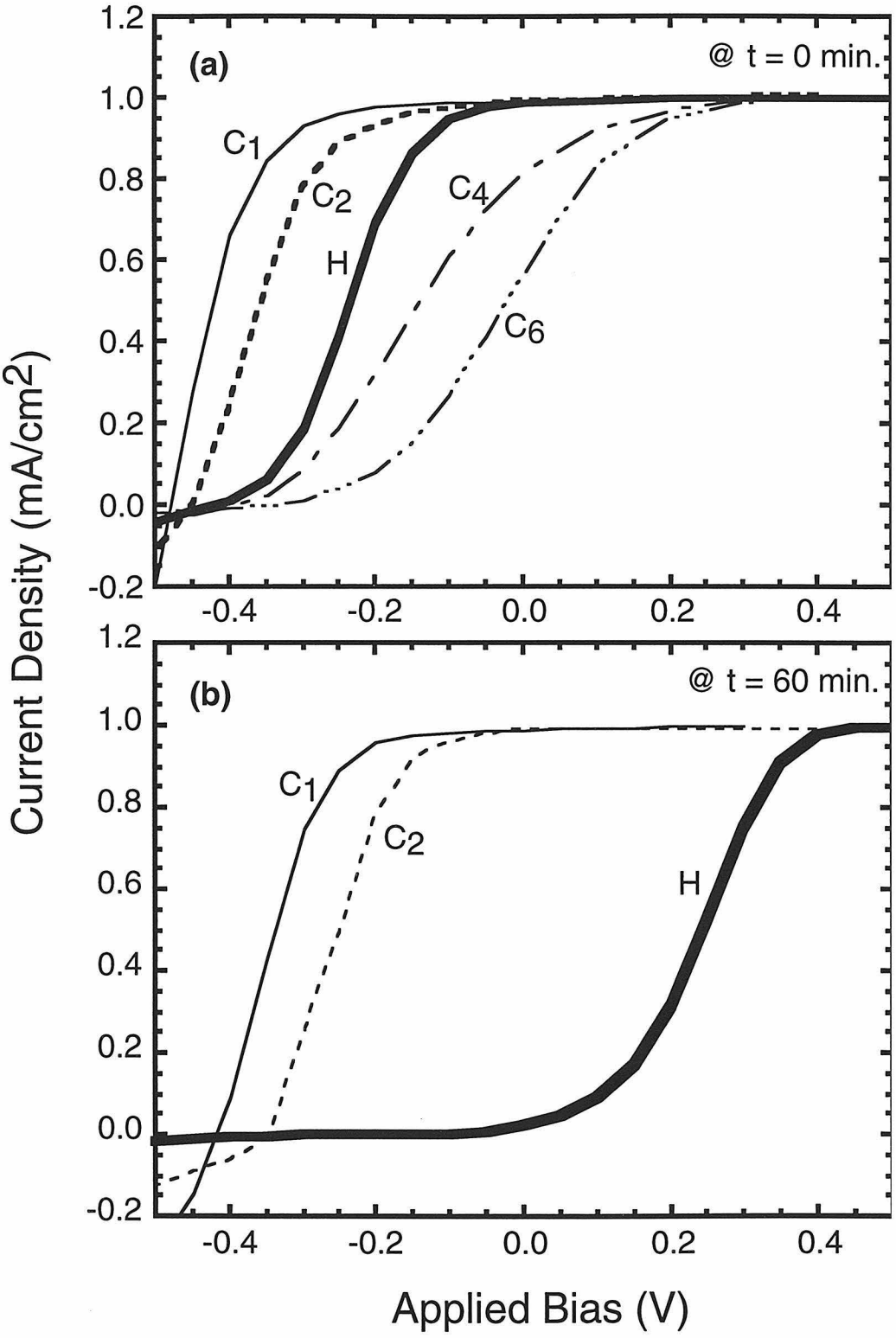
(a)
@ t = 0 min.
C1
C2
C4
H
C6
(b)
@ t = 60 min.
C1
C2
H
Current Density (mA/cm2)
Applied Bias (V)
1.2
1.0
0.8
0.6
0.4
0.2
0.0
-0.2
-0.4
-0.2
0.0
0.2
0.4

electrode at the light limited photocurrent. Figure 7b shows the J-V curves for three of the above electrodes after 60 minutes of illumination. The $-C_4H_9$ and $-C_6H_{13}$ terminated surfaces decayed very rapidly under illumination and light-limited curves (at 1.0 mA/cm^2) could not be recorded for them after 60 minutes. Table III lists the V_{oc} and fill factors observed for the silicon surfaces immediately after immersion in the $Fe(CN)_6^{3-/4-}(aq)$ solution and after 60 minutes of illumination. The results showed that while the V_{oc} and fill factor of the H-terminated surface decayed significantly in 60 minutes, the V_{oc} and fill factor of $-CH_3$ and $-C_2H_5$ terminated surfaces decreased very little over the same time period. This result, along with the results observed in the CH_3OH-$Me_2Fc^{+/0}$/water solutions, clearly indicates that alkyl chains can significantly impede the rate of oxidation of Si surfaces in contact with an aqueous environment.

IV. DISCUSSION

Recent studies of alkyl-terminated Si(111) surfaces showed that these surfaces were resistant to oxidation in air and in wet chemical environments.[8-10] The results described above complement these studies and show that the stability towards oxidation can be extended to aqueous electrochemical environments. Furthermore, this stability is not achieved at the cost of inferior electrical characteristics. Steady-state I-V and C-V measurements show that the electrical properties of these alkyl derivatized surfaces, prepared by the halogenation/alkylation method, are similar to those of H-terminated silicon surfaces. While the alkyl monolayers introduce a small series resistance for the charge transfer across the semiconductor-liquid interface, they do not introduce any significant amount of additional recombination centers at the Si-alkyl interface or mobile charges in the alkyl layer. The neutral character of these overlayers also does not induce any shift in the conduction and valence bands of the semiconductor.

The trend (or lack thereof) observed in the resistance of the alkyl overlayer to charge transfer across the semiconductor/liquid junction can be qualitatively explained as

Table III. Current-voltage properties of H-terminated and alkyl-terminated surfaces in contact with $Fe(CN)_6^{3-/4-}(aq)$ solutions.

Alkyl Chain Length (C_n)	I-V properties in $Fe(CN)_6^{3-/4-}(aq)$[a] @ t = 0 min		@ t = 60 min	
	V_{oc} (V)	ff	V_{oc} (V)	ff
H	0.42	0.34	0.22	0.08
1	0.48	0.64	0.42	0.57
2	0.45	0.53	0.35	0.46
4	0.40	0.22	b	b
6	0.36	0.13	b	b

a) Data was collected at a current density of 1.0 mA/cm^2. b) The $-\dot{C}_4H_9$ and $-C_6H_{13}$ terminated surfaces decayed very rapidly under illumination and light limited curves (at 1.0 mA/cm^2) could not be recorded for them after 60 minutes.

follows. Physical characterization of the alkyl overlayers showed (see Chapter 3) that for the short chain lengths ($n \leq 6$) the thickness of the overlayer increased linearly with the alkyl chain length, with little or no change in the areal packing density. For longer chain lengths ($10 \leq n \leq 18$), however, the increase in chain length was accompanied by a non linear, and even non-monotonic, decrease in the areal packing density. This observation can be directly correlated with the observed resistance of the monolayers. For the same (areal density dependent) overlayer resistivity, thicker overlayers gave higher resistance to charge transfer. Therefore for short chains ($n \leq 6$), the overlayer resistance increased with the length of the alkyl moiety covering the surface. On the other hand, for longer chain lengths, ($10 \leq n \leq 18$), an increase in the thickness of the film was compensated by a decrease in the (areal density dependent) resistivity, which did not correlate with the length of the alkyl group. Correspondingly, the trend in the resistance of these long chain alkyl overlayers also did not correlate with the length of the alkyl moiety covering the surface.

The open circuit voltages for the alkyl-terminated surfaces showed that the chlorination/alkylation procedure did not degrade the quality of the silicon surface. Similar V_{oc}, J_0 and diode quality factors indicated that the alkylation procedure did not significantly increase the number of recombination centers at the silicon/alkyl group interface. This result was significant because it showed that this surface modification procedure provided improved chemical stability of the silicon surface without sacrificing the excellent electrical properties of the H-terminated silicon surface.

Capacitance-voltage measurements on the alkyl-terminated surfaces further supported the observation that the electrical characteristics of the derivatized surfaces were very similar to those of a H-terminated surface. For the chemically modified surfaces, the flat-band potentials and the barrier heights were very similar to those observed for the H-terminated n-Si(111) electrode under identical conditions. The barrier heights calculated in these experiments also agreed with recent determinations of barrier heights for n-Si(100) samples in contact with the same redox couple.[36,42,59,60] The invariance of the flat-band

potential upon alkylation was expected due to the neutral character of the adsorbate.[55-58] The results of the C-V measurements, taken together with the results from the I-V measurements described above, clearly indicated that the derivatization procedure enhanced the chemical stability of the silicon surface but did not degrade the electrical properties of the silicon electrode.

The similarity in the electrical properties of the alkyl-terminated and H-terminated silicon surface, and the resistive nature of the alkyl overlayer suggests that these overlayers can be tailored for possible applications in MIS devices. The excellent uniformity and reproducibility of the alkane films, and the ability to alter the thickness accurately down to atomic levels makes them ideal candidates as an alternative to the thin oxide layers used in the current MIS devices. Earlier experiments showed that while Si/metal junctions were pinned and gave low V_{oc}, introduction of thin, electrochemically grown oxide layers increased the V_{oc} by almost a factor of 2 for the same current density.[48] The results of Si/alkyl/Au MIS devices showed that the alkyl monolayers did not completely prevent the metal from reaching the silicon surface. A simple calculation showed that for the sample for which the highest V_{oc} was observed, at least 3% of the surface area was covered with the low barrier height Si/metal junction. This value for the Si/Au contact area is not surprising because it is known from physical studies (see Chapter 3) that the alkyl monolayers cover only 72% of the silicon surface. Therefore these films are currently unsuitable replacements for the insulator layer of an MIS device. However, in one particular case, where the surface was derivatized with $C_{10}H_{21}Li$ and the chain packing density was determined by XPS to be near-ideal, extremely high resistance to charge transfer was observed. This observation indicates that the thickness and areal density of the alkane chains on the silicon surface needs to be controlled accurately to achieve overlayers that can act as suitable replacements for the oxide in a MIS device. One suggestion for how this can be attempted is described in the section on Future Directions.

The most significant attribute of these films, however, is their ability to suppress photooxidation of silicon in the presence of water. Overcoming this obstacle has been one of the "holy grails" of semiconductor-liquid junction photoelectrochemistry. The interaction of photogenerated holes with an oxidizing media (e.g., water) at the silicon surface results in the formation of silicon oxide, which being an insulator, prevents further charge transfer across the Si/liquid junction. A number of strategies have been adopted in the past to prevent this photooxidation. A lot of effort has been focused on optimizing the "barrier" effect of the electro-inactive overlayers. Thin barrier layers of metal[61,62] or conducting polymer[33,63] or both,[64-66] have been applied on the silicon surface in an attempt to physically separate the two reacting components - water and silicon. Deposition of a thin metal layer on silicon surface and subsequent immersion of this surface in an electrolyte results in a Schottky junction that is simply in series with a metal/liquid junction.[64,67] The I-V characteristics of such a junction are determined solely by the metal semiconductor contact so although this strategy prevents oxide formation, the junctions exhibit Fermi level pinning characteristic of a Schottky contact.[64] In some cases, ultra-small metal islands have been deposited on the Si surface to stabilize it against oxidation but this strategy has also met with only partial success.[68-72] Conducting polymers have also been used as conductive barriers between the Si and the liquid but the polymer layers are prone to peeling off the surface and this procedure results in unstable junctions.[63] A second approach has involved attachment of redox active moieties to the silicon surface to remove holes rapidly from the silicon surface and to mediate charge transfer from the semiconductor to the liquid.[6,18-20] While this strategy has been generally successful in stabilizing the silicon surface towards *further* oxidation, it involves the use of a thin layer of oxide to anchor the protective layer onto the silicon surface and only works at low carrier densities. A third, totally different approach to semiconductor stabilization utilizes rigorously dried non-aqueous liquids containing the redox couples, thereby completely

removing water from the liquid.[32,38,44,73] However, trace amounts of water can destabilize the cell and can potentially make them unstable over extended periods.

On the other hand, scant attention has been focused on strengthening the bonding at the surface silicon atom in order to stabilize the surface against oxidation.[9,10,74,75] The results of the experiments outlined above show that formation of a stable covalent bond between the alkyl chains and the silicon surface can be used to impart stability against photooxidation even in a situation where the overlayer is significantly porous. While n-silicon is stable in the presence of CH_3OH-$Me_2Fc^{+/0}$ solution, addition of water to this solution induces oxide growth and ruins the I-V properties. However, as shown in Table II, the presence of a covalently attached alkane monolayer can reduce the oxidation rate of the surface by more than an order of magnitude. For identical operating conditions, a Si/alkyl/liquid junction lasted longer and exhibited lower oxide growth as compared to a Si-H/liquid junction.

Even more significant is the result that the alkyl monolayer can partially stabilize a silicon surface *in an aqueous electrolyte*. The data indicate that two factors contribute to the initial stability and the subsequent decay of the I-V characteristics of alkyl-terminated surface in contact with the $Fe(CN)_6^{3-/4-}$(aq) solution. The formation of a stable Si-C bond stabilizes the surface and reduces its propensity towards oxidation. This fact was borne out by the observation that alkyl-terminated surface was more resistant to oxidation than the H-terminated surface, when both of them were simply immersed in the $Fe(CN)_6^{3-/4-}$(aq) solution. On the other hand, the resistance to hole transfer, presented by the alkyl group, increased the propensity for the surface to oxidize. Thus surfaces derivatized with longer chains provided higher resistance to hole transfer and oxidized much more rapidly than surfaces derivatized with shorter chains. These arguments suggest that improvements in the surface quality and coverage of the shortest alkyl group should provide improved stability for the silicon surface in an aqueous environment.

V. CONCLUSIONS

In agreement with the general picture of the alkyl derivatized silicon surface developed in the previous chapter, the electrical properties indicate that the silicon surface is covered by a porous layer of covalently bound alkane molecules that only partially impedes charge transfer across the semiconductor/liquid interface. The resistance of the film is a function of its thickness and the areal density (packing) of the alkyl groups on the surface. The film thickness and the packing density are interrelated and are in turn determined by the length of the alkyl group and the tilt angle of the molecules on the surface. Furthermore, as expected for a neutral adsorbate, the alkyl overlayers do not shift the band edges of silicon. These observations imply that the electrical properties of the derivatized silicon surface can be tailored for electronic applications by choosing the right chain length and by controlling the density (and tilt) of the alkyl groups on the surface.

The partial stability of the silicon surface towards photooxidation, achieved by the alkylation procedure, is a significant step forward towards achieving the "holy grail". The importance of this achievement is underscored by the fact that the resistance to oxidation has been achieved without any significant compromise in the excellent electrical quality of the silicon surface. Furthermore, the alkyl-terminated surfaces used here have the potential for further improvement (see below) which suggests that even greater stabilization of silicon surface towards photooxidation in aqueous environments is achievable. For now, the experiments described above have provided the first direct evidence of stabilization of the silicon surface to photooxidation which does not involve any oxidized layer of silicon as the intermediate anchoring layer.

VI. FUTURE DIRECTIONS

It is indeed heartening to see that the chlorination/alkylation procedure can be used to prepare surfaces that are more resistant to oxidation and yet exhibit the excellent electrical characteristics of a hydrogen-terminated silicon surface. The partial stability of these

derivatized surfaces in aqueous solutions suggests that further improvements in the quality and nature of these surfaces can be expected to produce surfaces that should be even more stable in aqueous environments. Given below are some directions in which the work described in this chapter can be extended.

1. Variability of V_{oc} with Barrier Height

Although the experiments described above have shown that the band edge positions and the I-V characteristics of the alkyl-terminated surfaces are similar to those of a hydrogen-terminated surface, it is not clear if this similarity is fortuitous or not. In other words, while it is known that the Fermi level of H-terminated surface is not pinned, it is not clear whether the Fermi level of the alkyl-terminated surface is pinned or not. Evaluation of this issue is important because if the Fermi level of the derivatized surface is pinned, then the I-V properties of the system would be determined by the Si/alkane junction which would be in series with the alkane/liquid junction. This situation would be similar to a high barrier height, "buried" Schottky junction analyzed for in Chapter 2.[67] Under such conditions, the electrical contact to the solution would not be necessary for photovoltaic action, and the presence of the liquid phase would not influence the maximum attainable energy conversion efficiency of the device. Instead, the liquid would only complicate the system by adding possible corrosion pathways and increased ohmic losses to the cell. In contrast, a "hybrid" silicon/alkyl/liquid junction would be more amenable to variations in the properties of the liquid phase.[67] Such systems would be good candidates for fundamental studies of charge transfer across semiconductor/liquid interfaces in which the semiconductor and the redox couple are separated by a known distance.[12] In the past, such studies have been done on gold,[76-83] silver[84,85] and silicon electrodes,[56,86] to gain insight into the rate of heterogeneous charge transfer from the substrate to the solution.

2. Surface Attachment of Redox Active Groups

The idea of surface attachment of redox active groups to the silicon surface by

means of alkane chains of varying lengths is not new. While Wrighton et al. showed that this strategy was successful in stabilizing the silicon surface towards *further* oxidation,[6,18-20] it involved the use of an initial thin layer of oxide to anchor the protective redox-active alkyl layer onto the silicon surface. The work described above[8] as well as the work of Linford et al.[9,10] has shown that it is possible to attach molecules to the silicon surface *without* any concomitant oxidation, and Lewis et al. have recently proposed to use this strategy to derivatize silicon with surface bound redox couples.[87] Such redox-active silicon surfaces can be used to investigate quantitatively the distance dependence of charge transfer rate constants at semiconductor/liquid interfaces and thus compare them with theoretical expectations.[12]

Another application of these surfaces is in stabilization of silicon surfaces towards oxidation. A higher effective concentration can be achieved by binding the redox molecules to the surface than can be achieved by dissolving the redox couple in the solution phase. The surface-bound groups can act as an effective hole capture shuttles, catalyzing charge transfer from the silicon to the redox couple in solution, in competition with photocorrosion or photopassivation processes.[87] Higher effective concentrations and electrocatalytic effects of the redox couple can effectively remove holes from the silicon surface and stabilize it against oxidation.

3. Derivatization with Fluoroalkanes

As described at the end of the previous chapter, the two-step strategy of surface binding of alkyl groups can be extended to fluoroalkyl groups. While the fluorocarbon chains would bind the surface silicon atoms in a manner similar to the hydrocarbon chains, the "barrier" effect of the fluorocarbon chains is expected to be significantly higher than their hydrocarbon counterparts due to their lower porosity and higher hydrophobicity. In addition, the low porosity of fluorocarbon chains is also more likely to aid the formation of better insulator layers for MIS devices as compared to those formed from alkyl chains.

VII. REFERENCES

(1) Wolf, S.; Tauber, R. N. *Silicon Processing for the VLSI Era*; Lattice Press: Sunset Beach, 1986.

(2) Sze, S. M. *The Physics of Semiconductor Devices;* 2nd ed.; Wiley: New York, 1981.

(3) Hsu, J. W. P.; Bahr, C. C.; vom Felde, A.; Downey, S. W.; Higashi, G. S.; Cardillo, M. J. *J. Appl. Phys.* **1992**, *71*, 4983.

(4) Myamlin, V. A.; Pleskov, Y. V. *Electrochemistry of Semiconductors*; Plenum Press: New York, 1967.

(5) Brattain, W. H.; Garrett, C. G. B. *Bell Syst. Tech. J.* **1955**, *34*, 129.

(6) Bolts, J. M.; Bocarsly, A. B.; Palazzotto, M. C.; Walton, E. G.; Lewis, N. S.; Wrighton, M. S. *J. Am. Chem. Soc.* **1979**, *101*, 1378.

(7) Kumar, A.; Lewis, N. S. *J. Phys. Chem.* **1991**, *95*, 7021.

(8) Bansal, A.; Li, X.; Lauermann, I.; Lewis, N. S.; Yi, S. I.; Weinberg, W. H. *J. Am. Chem. Soc.* **1996**, *118*, 7225.

(9) Linford, M. R.; Chidsey, C. E. D. *J. Am. Chem. Soc.* **1993**, *115*, 12631.

(10) Linford, M. R.; Fenter, P.; Eisenberger, P. M.; Chidsey, C. E. D. *J. Am. Chem. Soc.* **1995**, *117*, 3145.

(11) Buczkowski, A.; Radzimski, Z. J.; Rozgonyi, G. A.; Shimura, F. *J. Appl. Phys.* **1991**, *69*, 6495.

(12) Lewis, N. S. *Ann. Rev. Phys. Chem.* **1991**, *42*, 543.

(13) Leyden, D. E.; Collinus, W. *Silylated Surfaces*; Gordon and Breach, Science Publishers Inc.: New York, 1980.

(14) *Silanes, Surfaces, and Interfaces*; Leyden, D. E., Ed.; Gordon, Breach and Harwood: Snowmass, Colorado, 1986; Vol. 1.

(15) Calvert, J. M. *Organic Thin Films and Surfaces*; Academic Press: San Diego, CA, 1993.

(16) Ulman, A. *An Introduction to Ultrathin Organic Films*; Academic: San Diego, CA, 1991.

(17) Roberts, G. *Langmuir-Blodgett Films*; Plenum Press: New York, 1990.

(18) Bocarsly, A. B.; Walton, E. G.; Bradley, M. G.; Wrighton, M. S. *J. Electroanal. Chem.* **1979**, *100*, 283.

(19) Bocarsly, A. B.; Walton, E. G.; Wrighton, M. S. *J. Am. Chem. Soc.* **1980**, *102*, 3390.

(20) Wrighton, M. S.; Austin, R. G.; Bocarsly, A. B.; Bolts, J. M.; Haas, O.; Legg, K. D.; Nadjo, L.; Palazzotto, M. C. *J. Am. Chem. Soc.* **1978**, *100*, 1602.

(21) Angst, D. L.; Simmons, G. W. *Langmuir* **1991**, *7*, 2236.

(22) Wasserman, S. R.; Tao, Y. T.; Whitesides, G. M. *Langmuir* **1989**, *5*, 1074.

(23) Wasserman, S. R.; Whitesides, G. M.; Tidswell, I. M.; Ocko, B. M.; Pershan, P. S.; Axe, J. D. *J. Am. Chem. Soc.* **1989**, *111*, 5852.

(24) Maoz, R.; Sagiv, J. *J. Colloid Interface Sci.* **1984**, *100*, 465.

(25) Pomerantz, M.; Segmuller, A.; Netzer, L.; Sagiv, J. *Thin Solid Films* **1985**, *132*, 153.

(26) Dulcey, C. S.; Georger, J. H.; Krauthamer, V.; Fare, T. L.; Stenger, D. A.; Calvert, J. M. *Science* **1991**, *252*, 551.

(27) Silberzan, P.; Leger, L.; Aussere, D.; Benattar, J. J. *Langmuir* **1991**, *7*, 1647.

(28) Kumar, A.; Lewis, N. S. *J. Phys. Chem.* **1990**, *94*, 6002.

(29) Forbes, M. D. E.; Lewis, N. S. *J. Am. Chem. Soc.* **1990**, *112*, 3682.

(30) Lewis, N. S.; Rosenbluth, M. L.; Casagrande, L. G.; Tufts, B. J. In *Homogeneous and Heterogeneous Photocatalysis* ; E. Pelizzetti and N. Serpone, Ed.; Reidel: Dordrecht, 1986; Vol. 174; pp 343.

(31) Rosenbluth, M. L.; Lewis, N. S. *J. Am. Chem. Soc.* **1986**, *108*, 4689.

(32) Gronet, C. M.; Lewis, N. S.; Cogan, G.; Gibbons, J. *Proc. Natl. Acad. Sci., USA* **1983**, *80*, 1152.

(33) Simon, R. A.; Wrighton, M. S. *Appl. Phys. Lett.* **1984**, *44*, 930.

(34) Bruce, J. A.; Wrighton, M. S. *J. Electroanal. Chem.* **1981**, *122*, 93.

(35) Fajardo, A. M.; Lewis, N. S. *Science* **1996**, *274*, 969.

(36) Pomykal, K. E.; Fajardo, A. M.; Lewis, N. S. *J. Phys. Chem.* **1996**, *100*, 3652.

(37) Lewis, N. S. *Solar Energy Mater. Solar Cells* **1995**, *38*, 323.

(38) Shreve, G. A.; Karp, C. D.; Pomykal, K. E.; Lewis, N. S. *J. Phys. Chem.* **1995**, *99*, 5575.

(39) Pomykal, K. E.; Fajardo, A. M.; Lewis, N. S. *J. Phys. Chem.* **1995**, *in press*,

(40) Shreve, G. A.; Lewis, N. S. *J. Electrochem. Soc.* **1995**, *142*, 112.

(41) Fajardo, A. M.; Karp, C. D.; Kenyon, C. N.; Pomykal, K. E.; Shreve, G. A.; Tan, M. X.; Lewis, N. S. *Solar Energy Mater. Solar Cells* **1995**, *38*, 279.

(42) Laibinis, P. E.; Stanton, C. E.; Lewis, N. S. *J. Phys. Chem.* **1994**, *98*, 8765.

(43) Tufts, B. J.; Kumar, A.; Bansal, A.; Lewis, N. S. *J. Phys. Chem.* **1992**, *96*, 4581.

(44) Rosenbluth, M. L.; Lieber, C. M.; Lewis, N. S. *Appl. Phys. Lett.* **1984**, *45*, 423.

(45) Rhoderick, E. H.; Williams, R. H. *Metal-Semiconductor Contacts;* 2nd ed.; Oxford University Press: New York, 1988.

(46) *Metal-Semiconductor Schottky Barrier Junctions and Their Applications*; Sharma, B. L., Ed.; Plenum: New York, 1984.

(47) Fahrenbruch, A. L.; Bube, R. H. *Fundamentals of Solar Cells: Photovoltaic Solar Energy Conversion*; Academic: New York, 1983.

(48) Kumar, A.; Rosenblum, M. D.; Gilmore, D. L.; Tufts, B. J.; Rosenbluth, M. L.; Lewis, N. S. *Appl. Phys. Lett.* **1990**, *56*, 1919.

(49) Blakers, A. W.; Wang, A.; Milene, A. M.; Zhao, J.; Green, M. A. *Appl. Phys. Lett.* **1989**, *55*, 1363.

(50) Green, M. A.; Blakers, A. W.; Shi, J.; Keller, E. M.; Wenham, S. R. *Appl. Phys. Lett.* **1984**, *44*, 1163.

(51) Fonash, S. J. *Solar Cell Device Physics*; Academic: New York, 1981.

(52) Bard, A. J.; Faulkner, L. R. *Electrochemical Methods: Fundamentals and Applications*; John Wiley & Sons: New York, 1980, pp 629.

(53) Rosenbluth, M. L. Ph. D. Thesis, Stanford University, 1988.

(54) Seah, M. P. In *Practical Surface Analysis ;* 2nd ed.; D. Briggs and M. P. Seah, Ed.; John Wiley & Sons: Chichester, 1990; Vol. 1; pp 201.

(55) Morrison, S. R. *Electrochemistry at Semiconductor and Oxidized Metal Electrodes*; Plenum: New York, 1980.

(56) Gu, Y.; Waldeck, D. H. *J. Phys. Chem.* **1996**, *100*, 9573.

(57) Gu, Y.; Lin, Z.; Butera, R. A.; Smentkowski, V. S.; Waldeck, D. H. *Langmuir* **1995**, *11*, 1849.

(58) Nakagawa, O. S.; Ashok, S.; Sheen, C. W.; Märtensson, J.; Allara, D. L. *Jpn. J. Appl. Phys.* **1991**, *30*, 3759.

(59) Tomkiewicz, M. *Electrochimica Acta* **1990**, *35*, 1631.

(60) Kobayashi, H.; Takeda, N.; Sugahara, H.; Tsubomura, H. *J. Phys. Chem.* **1991**, *95*, 813.

(61) Fan, F. R. F.; Keil, G.; Bard, A. J. *J. Am. Chem. Soc.* **1983**, *105*, 220.

(62) Fan, F. R. F.; Shea, T. V.; Bard, A. J. *J. Electrochem. Soc.* **1984**, *131*, 828.

(63) Noufi, R.; Frank, A. J.; Nozik, A. J. *J. Am. Chem. Soc.* **1981**, *103*, 1849.

(64) Skotheim, T.; Petersson, L. G.; Inganaes, O.; Lundstrom, I. *J. Electrochem. Soc.* **1982**, *129*, 1737.

(65) Fan, F.-R. F.; Wheeler, B. L.; Bard, A. J.; Noufi, R. N. *J. Electrochem. Soc.* **1981**, *128*, 2042.

(66) Skotheim, T.; Lundstrom, I.; Prejza, J. *J. Electrochem. Soc.* **1981**, *128*, 1625.

(67) Bansal, A.; Tan, M. X.; Tufts, B. J.; Lewis, N. S. *J. Phys. Chem.* **1993**, *97*, 7309.

(68) Nakato, Y.; Yano, H.; Tsubomura, H. *Chem. Lett.* **1986**, 987.

(69) Nakato, Y.; Tsubomura, H. *Ber. Bunsenges Phys. Chem.* **1987**, *91*, 405.

(70) Nakato, Y.; Ueda, K.; Yano, H.; Tsubomura, H. *J. Phys. Chem.* **1988**, *92*, 2316.

(71) Kobayashi, H.; Tsubomura, H. *J. Electroanal. Chem.* **1989**, *272*, 37.

(72) Kobayashi, H.; Chigami, A.; Takeda, N.; Tsubomura, H. *J. Electroanal. Chem.* **1990**, *287*, 239.

(73) Gibbons, J. F.; Cogan, G. W.; Gronet, C. M.; Lewis, N. S. *Appl. Phys. Lett.* **1984**, *45*, 1095.

(74) Bansal, A.; Li, X. L.; Lieberman, M.; Lewis, N. S.; Yi, S. I.; Weinberg, W. H. *188th Meeting of the Electrochemical Society* **1995**, abstract No. 605.

(75) Bansal, A. "Research Proposal: Modification of Silicon Surface by Covalently Attached Langmuir-Blodgett Film," California Institute of Technology, 1996.

(76) Terrettaz, S.; Becka, A. M.; Traub, M. J.; Fettinger, J. C.; Miller, C. J. *J. Phys. Chem.* **1995**, *99*, 11216.

(77) Miller, C.; Cundet, P.; Graetzel, M. *J. Phys. Chem.* **1991**, *95*, 877.

(78) Becka, A. M.; Miller, C. J. *J. Phys. Chem.* **1992**, *96*, 2657.

(79) Becka, A. M.; Miller, C. J. *J. Phys. Chem.* **1993**, *97*, 6233.

(80) Finklea, H. O.; Hanshew, D. D. *J. Am. Chem. Soc.* **1992**, *114*, 3173.

(81) Chidsey, C. E. D. *Science* **1991**, *251*, 919.

(82) Guo, L. H.; Facci, J. S.; McLendon, G. *J. Phys. Chem.* **1995**, *99*, 8458.

(83) Smalley, J. F.; Feldberg, S. W.; Chidsey, C. E. D.; Linford, M. R.; Newton, M. D.; Liu, Y. *J. Phys. Chem.* **1995**, *99*, 13141.

(84) Kadyshevitch, A.; Naaman, R. *Phys. Rev. Lett.* **1995**, *75*, 2905.

(85) Kadyshevitch, A.; Naaman, R. *Phys. Rev. Lett.* **1995**, *74*, 3443.

(86) Haran, A.; Waldeck, D. H.; Naaman, R.; Moons, E.; Cahen, D. *Science* **1994**, *263*, 948.

(87) Lewis, N. S. Personal Communication.